DESIGN AND ANALYSIS OF AN ELLIPSOIDAL MIRROR REFLECTOMETER

By

STUART THOMAS DUNN

Bachelor of Science
University of Missouri at Rolla
Rolla, Missouri
1962

Master of Science
Oklahoma State University
Stillwater, Oklahoma
1963

Submitted to the Faculty of the Graduate School of
the Oklahoma State University
in partial fulfillment of the requirements
for the degree of
DOCTOR OF PHILOSOPHY
May 1965

DESIGN AND ANALYSIS OF AN ELLIPSOIDAL MIRROR REFLECTOMETER

Thesis Approved:

J. A. Wickett
Thesis Adviser

Joseph C. McClymond
Research Adviser

D. R. Haworth

Paul E. Long

J. W. Bruce
Dean of the Graduate School

ACKNOWLEDGMENTS

In works of this nature the author becomes indebted to many people. In sincere appreciation of the support and help that these people and organizations have given me, I wish to acknowledge my indebtedness to: Professors J. A. Wiebelt, D. R. Haworth, P. E. Long, and J. H. Boggs; D. G. Moore and J. C. Richmond, of the National Bureau of Standards, for the facilities, equipment, and suggestions that made this thesis possible; the National Defense Education Act for my financial support; to the National Aeronautics and Space Administration and the U. S. Air Force for funding this research; to John Anderson for his excellent work on the development of the sulfur sphere coatings; to John Perone for ably taking part of the data and for contribution of useful suggestions; to Leota Hafner for many helpful improvements in the manuscript and its typing; and most of all to my wife, Barbara, and to little Paul and Lorri Dunn, for their patience and understanding.

TABLE OF CONTENTS

TABLE OF CONTENTS (Cont'd)

LIST OF TABLES

LIST OF FIGURES

LIST OF FIGURES (Cont'd)

LIST OF FIGURES (Cont'd)

CHAPTER I

INTRODUCTION

Motivation

This dissertation is concerned with the development of a new means of measuring the reflectance of engineering materials for eventual use in heat transfer calculations. Further, it is anticipated that this instrumentation will aid experimental studies of the effect of various surface parameters on reflectance. The demand for accurate and well-defined reflectance data is relatively new and intimately tied to the space exploration program of this country, where the basic problem of satellite temperature control has not been adequately solved. The most important controllable parameters in the solution of this problem are the thermal radiation properties of the satellite's surface. Engineering heat transfer calculations in this field are, at best, estimates, since existing reflectance data are generally considered to have ten percent accuracy, and little or nothing is known about the goniometric distribution of the reflected or emitted flux from common engineering materials. Further, the effect on reflectance of roughness, surface contamination, surface damage, and surface temperature cannot be predicted from existing experimental data.

Because of a lack of this kind of information, the heat transfer engineer usually assumes perfectly diffuse reflection or emission (i.e., equal intensity in all directions), or, in a limited number of

calculations [1,2,3]*, the analyst has assumed specular reflection. However, the most useful approach of assuming that the surface is partially specular and partially diffuse cannot be used, since data of this nature are limited.

Aside from the demands of spacecraft temperature control, there is a continuing demand for accurate experimental verification of existing theories concerning the relations between surface parameters and reflectance (including a need for the goniometric distribution of the reflected flux). To date, the directional hemispherical reflectance (see definition, page 3) measured to test existing theories has often had uncertainties exceeding five percent, and goniometric (bi-directional) data off the specular direction have uncertainties easily exceeding ten percent. With these magnitudes of uncertainty, it is extremely difficult for the designer or the theoretician to arrive at reasonable conclusions from the experimental data.

Types of Reflectances

Given the above motivation, it is then necessary to ascertain the types of reflectance that are needed by the heat transfer analyst and the theorist. Keeping in mind the diverse definitions presently in use, the author has attempted to use the definitions which best suit this dissertation. Further, all terms and definitions used in this dissertation are assumed to refer to monochromatic flux, except where otherwise noted.

---

*Numbers in brackets refer to the bibliography.

Figures 1 and 2 illustrate the general terms to be used throughout this dissertation. Figure 1, part A, illustrates the bi-directional reflectance, which is defined as

$$\rho[\varphi,\theta,\varphi',\theta'] = \frac{I'(\varphi',\theta')\cos\phi'(\Delta\omega)'}{I_{\varphi,\theta}\cos\varphi(\Delta\omega)} \tag{1}$$

where $I_{\varphi,\theta}$ is the unidirectional intensity over a small solid angle $\Delta\omega$ about the particular direction φ,θ and $I'(\varphi',\theta')$ is the functional description of the reflected intensity $[0 \le \varphi \le \frac{\pi}{2},\ 0 \le \varphi' \le \frac{\pi}{2},$ $0 \le \theta \le 2\pi$, and $0 \le \theta' \le 2\pi]$. The intensity is described as power per unit solid angle per unit projected area of the reflector [4].

Part B of figure 1 illustrates the direction hemispherical reflectance, which is defined as

$$\rho(\varphi,\theta) = \frac{\int_0^{2\pi} I'(\varphi',\theta')\cos\varphi'\, d\omega'}{I_{\varphi,\theta}\cos\varphi(\Delta\omega)} \tag{2}$$

which is the ratio of the flux reflected into a hemisphere above the surface to that incident at φ,θ in a small solid angle $\Delta\omega$, where $0 \le \varphi \le \frac{\pi}{2}$ and $0 \le \theta \le 2\pi$. Another term for this concept is hemispherical reflectance of the second kind.

Part C of figure 1 illustrates the diffuse directional reflectance, which is defined as

$$\bar{\rho}(\varphi',\theta') = \frac{I'(\varphi',\theta')}{I_b'(\varphi',\theta')} \tag{3}$$

which is the ratio of the flux per unit solid angle reflected into the φ',θ' direction (for conditions of diffuse illumination) to the flux per unit solid angle that is reflected by the diffuse complete reflector into the φ',θ' direction (for the same conditions of diffuse illumination).

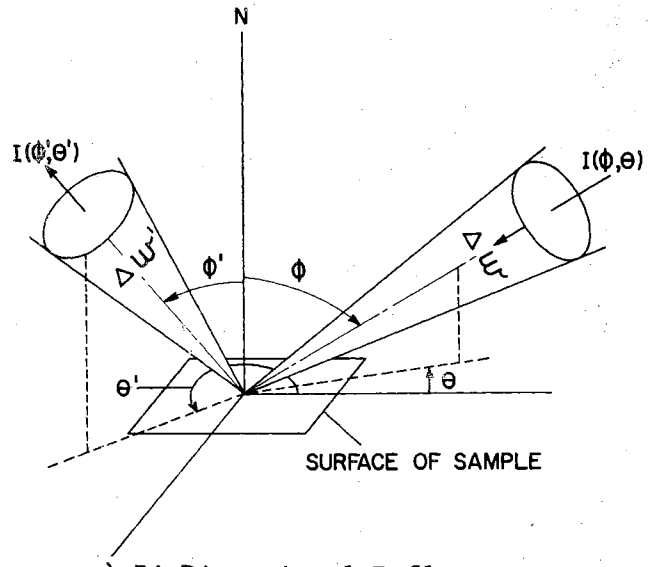

a) Bi-Directional Reflectance

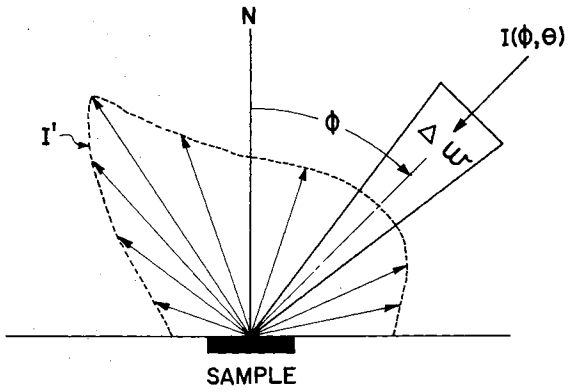

b) Directional Hemisperical Reflectance

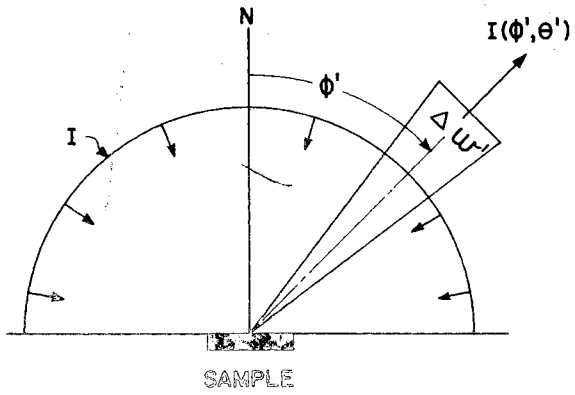

c) Diffuse Directional Reflectance

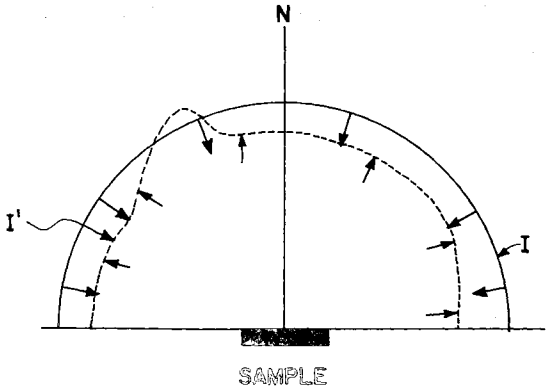

d) Hemispherical Reflectance

Figure 1. Reflectance Terminology (A)

The hemispherical reflectance (Part D, figure 1) is defined as

$$\rho_H = \frac{\int_0^{2\pi} I'(\varphi',\theta')\cos\varphi' \, d\omega'}{\int_0^{2\pi} I(\varphi,\theta)\cos\varphi \, d\omega} \tag{4}$$

which is the ratio of flux reflected into the hemisphere to that which is incident over the hemisphere. Note that this equation is considerably more general than the others, since nothing is specified about the incoming or outgoing energy; further, this term probably has the least use in accurate heat transfer calculations and only limited use to the theoretical investigator. However, it is useful in that $1 - \rho_H$ is the fraction of the incident energy absorbed for the given illumination conditions.

Further, the diffuse-hemispherical reflectance is defined as

$$\rho(\text{diffuse hemispherical}) = \frac{\int_0^{2\pi} I'(\varphi',\theta')\cos\varphi' \, d\omega'}{\pi I} \tag{5}$$

that is the ratio of flux reflected into the hemisphere above the surface to the incident flux, which is perfectly diffuse over the hemisphere.

The foregoing definitions of reflectance provide a basis for defining and discussing some additional terms, which facilitate the remaining discussions in this dissertation. For a more complete discussion of reflectance terms and other related ways of defining these terms, see references 4 and 5. The first is the specular reflectance, which is defined as

$$\rho(\text{specular}) = \frac{\int_{\Delta w'} I'(\varphi,\theta + 180^\circ)\cos\varphi \, d\omega'}{I_{\varphi\theta}\cos\varphi(\Delta\omega)} \tag{6}$$

and is illustrated in part A of figure 2. In the case of a perfect mirror reflection, the specular component would be defined on the same size solid angle as the incident flux; however, in this case, it appears useful to leave the outgoing solid angle unspecified, as it will be desirable to measure and use different size solid angles for different calculations and for different surfaces. For instance, the heat transfer analyst is primarily interested in the flux grouped around the specular direction, so that he knows, fairly accurately, the amount of flux that is reflected in the primary direction of specular reflectance. At this time, the heat transfer literature provides no study of the size of solid angle of interest; however, the extensive studies on gloss measurement may be of use [34]. Further, note that this term, as defined (which is the experimentally measured parameter) contains part of the diffuse component of the reflectance. Thus, when ρ(specular) is used for heat transfer calculations of the specular-diffuse type, the diffuse component should be subtracted from ρ(specular) to give an estimate of the additional energy (over and above the diffuse component) that is grouped around the specular direction.

For this work, the non-specular reflection is defined as

$$\rho(\text{non-specular}) = \frac{\int_0^{2\pi} I'(\varphi,\theta)\cos\varphi' \, d\omega'}{I_{\varphi\theta}\cos\varphi(\Delta\omega)} - \rho(\text{specular}) \qquad (7)$$

This is illustrated in part B of figure 2. Note that this is not the true diffuse component of reflectance, since the diffuse component of the flux in the specular direction is not accounted for.

One remaining term seems advisable to define; the directional annular cone reflectance is

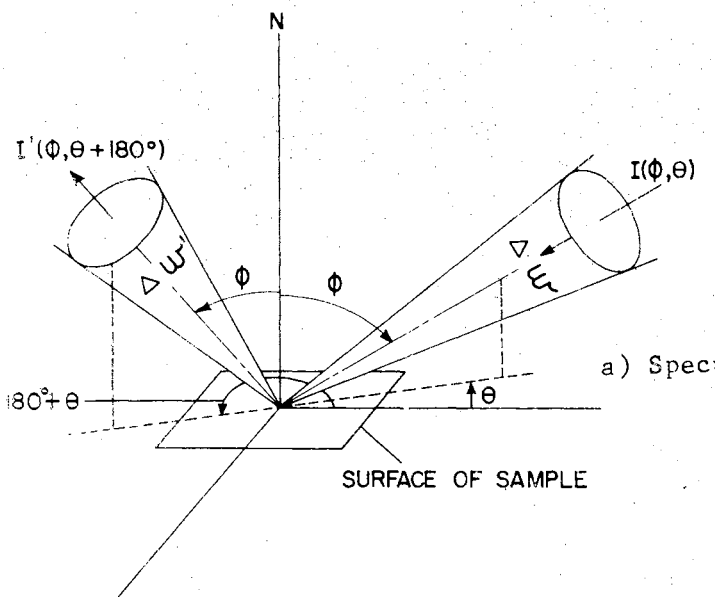

a) Specular Reflectance

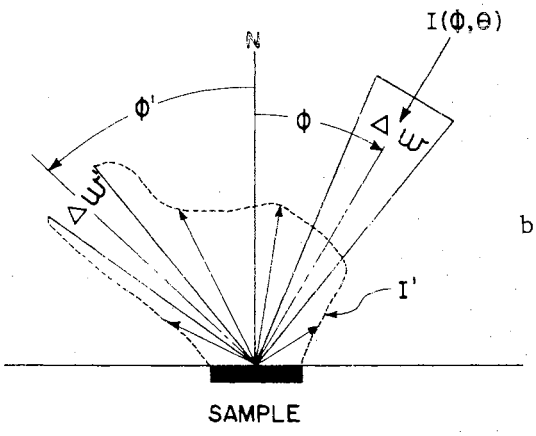

b) Non-Specular Reflectance

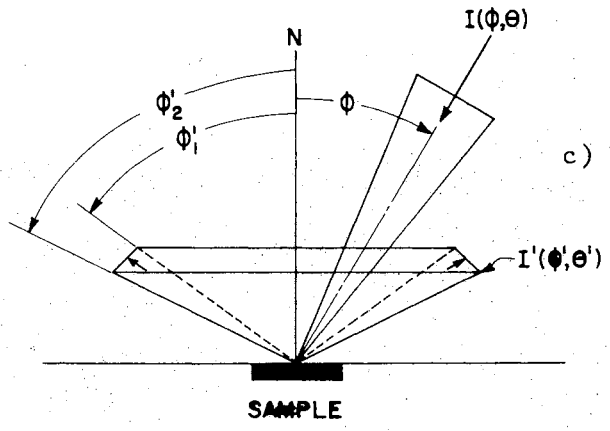

c) Directional Annular Cone Reflectance

Figure 2. Reflectance Terminology(B)

$$\rho(\text{directional annular cone}) = \frac{\int_{\varphi_1}^{\varphi_2} \int_0^{2\pi} I'(\varphi',\theta')\cos\varphi'\sin\varphi' d\varphi' d\theta'}{I_{\varphi,\theta}\cos\varphi(\Delta\omega)} \qquad (8)$$

which is the ratio of the flux leaving the surface in an annular cone to that incident at φ,θ in solid angle $(\Delta\omega)$. This is illustrated in part C of figure 2.

It is hoped that the author has not defined terms solely for the sake of defining, but rather as a basis for further discussion. With the above types of reflectances defined on a monochromatic basis, as previously stated, it is necessary to know the wavelengths at which these reflectances should be measured. If one considers the problems of heat transfer, it is apparent that the wavelengths of interest for a reflectance messurement are those at which the principal amount of energy is transmitted. The cross-hatched areas of figures 3 and 4 indicate the wavelength band encompassing 99 percent of the flux emitted by a blackbody source at the indicated temperature. This graph indicates that for high temperatures the band is very small and centered near the visible (0.4 to 0.7 μ); as the temperature decreases, the center of the band shifts to longer wavelengths and becomes much wider, so that at very low temperatures it is extremely wide and centered far out in the infrared. Thus, the wavelength of interest varies with application; the space program of satellite temperature control is primarily concerned with the 0.35 to 35 μ region, which encompasses the principal flux from the sun, that emitted and reflected by the earth, and that emitted by the spacecraft. The theorist for most studies is not too concerned with the wavelengths measured, but mostly with having a very wide band of wavelengths to choose from.

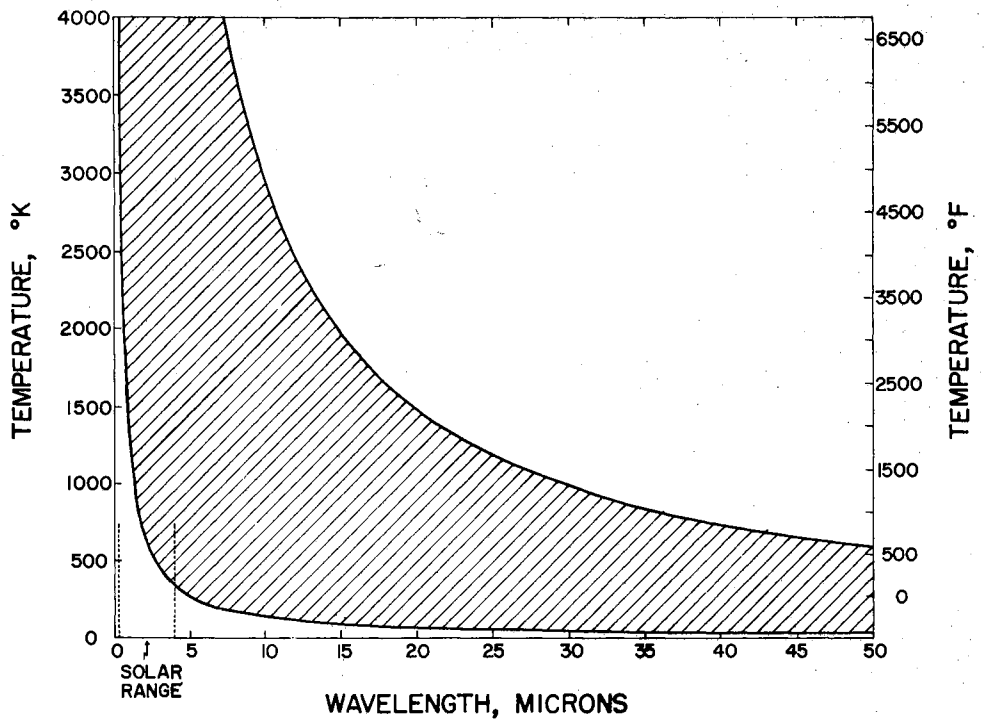

Figure 3. Ninety-Nine Percent Energy Bands for High Temperatures

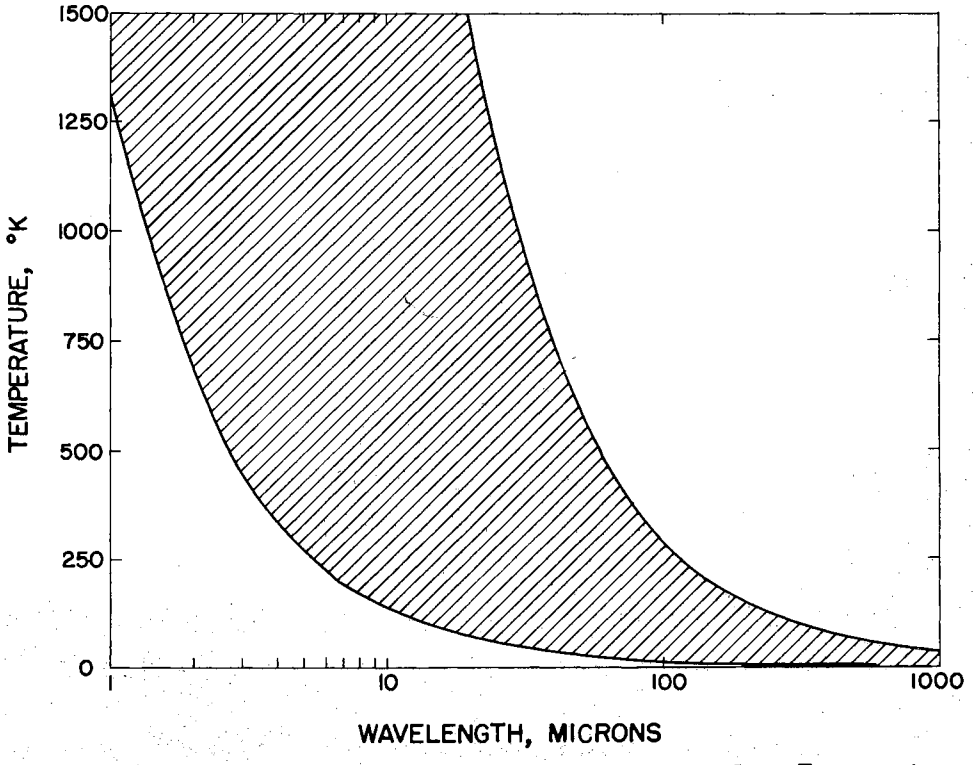

Figure 4. Ninety-Nine Percent Energy Bands for Low Temperatures

Methods of Measurement

The directional hemispherical reflectance from 0.4 to 2.1 μ is accurately measured by use of integrating spheres. From 2.1 to 35 μ there exist many instruments which measure $\overline{\rho}(\varphi'\theta')$ and $\rho(\varphi,\theta)$ and a few instruments which measure the reflectance with and without the specular component, which are essentially the reflectances defined in equations (6) and (7). This section contains a review of the existing instrumentation, with a discussion of main sources of error, accuracy, wavelength range, types of reflectances measured, and limitations.

Due to the present lack of proven integrating sphere coatings for the infrared, this approach will not be discussed (for further information on the operation and theory of integrating spheres, see references 1, 6, and 7). Further, the measurement of true specular reflectance of mirrors or other highly specular surfaces is not reviewed; the reader is referred to references 8, 9, 10, and 11, for detailed information. Thus, the following review concerns itself with the measurement of the previously defined reflectances in the wavelength range of 2.0 to 35 μ, where reliable data are not generally available. There exist two basic methods of measurement of reflectance in this range: (a) Coblentz hemisphere type instruments [12], and (b) Gier-Dunkle heated cavity reflectometers [13]. These two instruments, with individual variations, are presented in chronological order of development.

A. Coblentz Hemisphere:

Around 1910, several investigators [12,14,15, & 16] measured $\rho(\varphi,\theta)$ by use of what has become known in this country as the Coblentz hemisphere reflectometer. Figure 5 illustrates the basic configuration

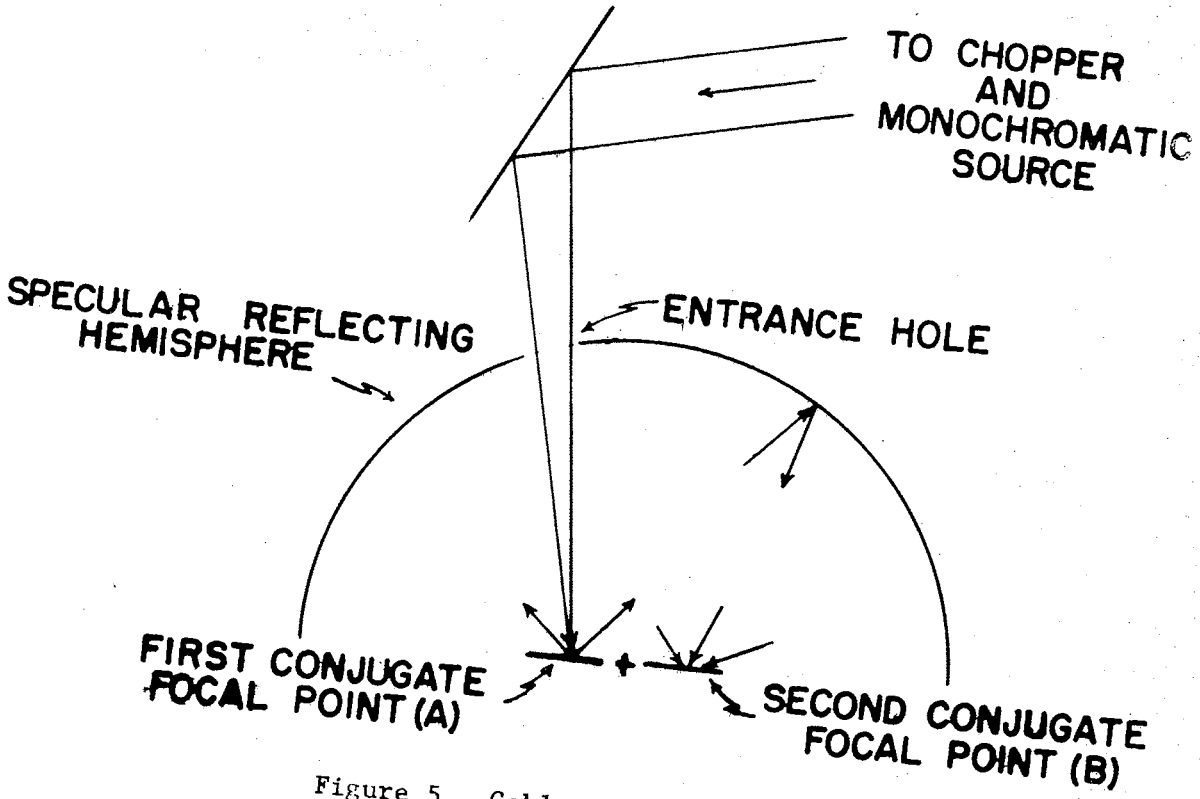

Figure 5. Coblentz Hemisphere

of this instrument. The basic optical principle involved in the use of this instrument is the concept of conjugate focal points existing about the center of curvature of a hemisphere; thus, if a light source is moved to the right of the center of curvature, its image appears to the left of the center of curvature. This image is very much blurred due to spherical aberrations which increase with distance from the center [17]. Also, the "image," because of the blurring, is smeared out, and, hence, enlarged.

Thus, if a sample is placed at the first conjugate focal point in figure 5, then an enlarged image of the illuminated area appears at the second conjugate point. This instrument is used to obtain both absolute data and relative data (i.e., absolute data are taken by directly measuring the incident flux and the reflected flux and calculating reflectance from a knowledge of system losses; relative data are taken by measuring the reflected flux from a standard of known reflectance and then measuring the reflected flux from the sample and calculating the reflectance of the sample from knowledge of relevant system losses and the reflectance of the standard). The operation of the Coblentz hemisphere in the absolute mode is as follows: first, the detector is placed at the first conjugate focal point to read the incident flux, and then the sample is placed at the first conjugate focal point and the detector at the second conjugate to measure the reflected flux. The ratio of these two fluxes, corrected for system losses, is then $\rho(\varphi,\theta)$, where generally φ is close to the normal. In the comparison mode, two measurements are made with the detector at the second conjugate focal point, one with a sample at the first conjugate focal point, and the other with the standard at the first conjugate focal point.

Major flux losses in this system are due to atmospheric absorption, losses out the entrance hole, mirror absorption (which may vary with position on the mirror), and the inability of the detector to sense equally the reflected flux from all directions over the hemisphere. Because of the spherical aberrations, a large image is formed at the second conjugate focal point, which requires the use of a large detector (such as a ten junction thermopile). Thus, large errors due to detector spatial sensitivity are probable (chapter III and reference 18). In the relative mode of operation, it is possible to minimize all of the above mentioned effects if the distribution of the reflected flux from the sample and from the standard are similar.

If the sample and standard differ in distribution of reflected flux, losses due to detector angular and spatial sensitivity, hole losses, and mirror absorption are not proportional. Especially the hole loss, which is very dependent on the distribution of reflected flux (i.e., for a specular surface there is no hole loss; while for a perfectly diffuse reflection, the hole loss is identical to the diffuse configuration factor between the image and the hole, and for the distribution of reflected flux between perfectly specular and perfectly diffuse reflection, the correction can be almost any fraction up to 100 percent for a perfect back scatterer). Further, the detector is more sensitive to energy from the top of the hemisphere than to energy from the edges. An additional problem is the criticality of sample and detector elevations, which, if they are not both in the focal plane, will yield large errors, since much of the energy will miss the detector entirely.

With large unknown errors, and the experience of more recent investigators, it is impossible to accept Coblentz's stated accuracy of 1 part

in 400 [10]. The wavelength range of this instrument is normally 0.5 to 15 μ, with a probable accuracy for any general engineering surface of, at best, ten percent. During the 50-year history of this instrument, many innovations have been made. The most prominent of these are:

(1). Janssen and Torborg modified the original concept of the Coblentz hemisphere to measure $\bar{\rho}(\varphi;\theta')$, as shown in figure 6 [19]. This modification allows sample heating and relative reflectance measurements from 0.4 to 20 μ, with probable accuracy of five percent for general engineering materials. This modification essentially eliminated the detector problem, doubled the hole correction problem, introduced the problem of getting a good infrared diffuser, introduced the effect of sample-diffuser interreflection, and did not affect the other principal errors. For accurate use of this instrument, the sample and standard must both be either perfectly diffuse or specular, or they must have the same distribution of reflected flux; under these specific conditions, it is probable that an accuracy on the order of two percent is obtainable. Further, $\bar{\rho}(\varphi;\theta') \equiv \rho(\varphi;\theta')$ only if a perfect diffuser is used in the first conjugate focal point and an accurate correction can be made for the hole losses.

(2). J. U. White built, in 1964, an automatic recording Coblentz-type instrument for the National Bureau of Standards [20]. The instrument requires the use of a specular standard and a diffuse standard, and makes relative measurements over the 2.5 to 22.5 μ range of $\bar{\rho}(\varphi;\theta')$ with no estimated accuracy. It appears that this instrument has an accuracy of the order of ten percent. It is questionable whether this instrument illuminates the sample diffusely, so that it is doubtful that data from this instrument can be used in the reciprocity relations to yield $\rho(\varphi;\theta')$.

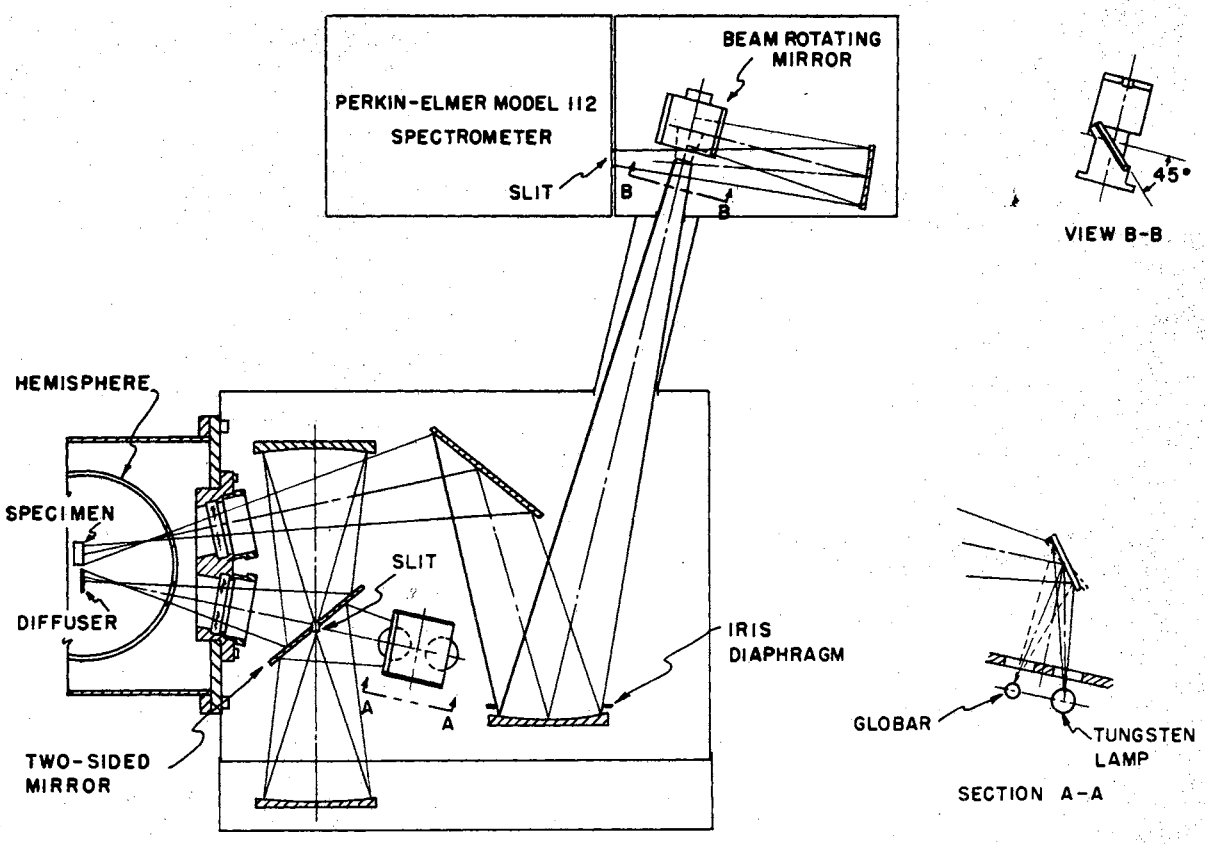

Figure 6. An illustration of the optical system of the Janssen-Torborg hemispherical reflectometer. Reprinted from reference 19 by permission of the Editor, J. C. Richmond.

The main innovation with the instrument was placing the source at the first conjugate focal point and viewing the source and sample through a very large hole in the hemisphere.

(3). Birkebak and Hartnett, utilizing the basic Coblentz concept, extended the hemisphere to about $\frac{3}{4}$ the size of a sphere, which allowed the sample and detector to be tilted so φ was no longer restricted to near normal illumination [21].

(4). Kozyrev and Vershinin, utilizing the basic Coblentz concept, extended the use of the instrument to a directional annular cone reflectance measurement by use of carefully constructed baffles [22].

(5). References 23, 24, 25, and 26 illustrate some of the many other varied applications of this instrument.

Further, it should be noted that all of the above instruments, with proper procedures, are able to measure the reflectance (either $\rho(\varphi,\theta)$ or $\bar{\rho}(\varphi',\theta')$) with and without the specular component; however, they are all very restricted in the size of solid angle that can be eliminated as the specular component.

B. Heated Cavity Reflectometer:

In the late 1940's, the heated cavity reflectometer, conceptually illustrated in figure 7, was developed, which offered a means of measuring $\bar{\rho}(\varphi',\theta')$ from 1 to 35 μ, with a probable accuracy of five percent for general engineering materials [13,27,28, and 29]. The principle of this system is to place the sample in a blackbody cavity (i.e., equal intensity from all directions) and thus illuminate it diffusely. The sample and a spot on the wall are viewed alternately through a small hole in the cavity, and thus a measure of the incident and reflected flux is obtained to enable absolute reflectance measurement. By mounting

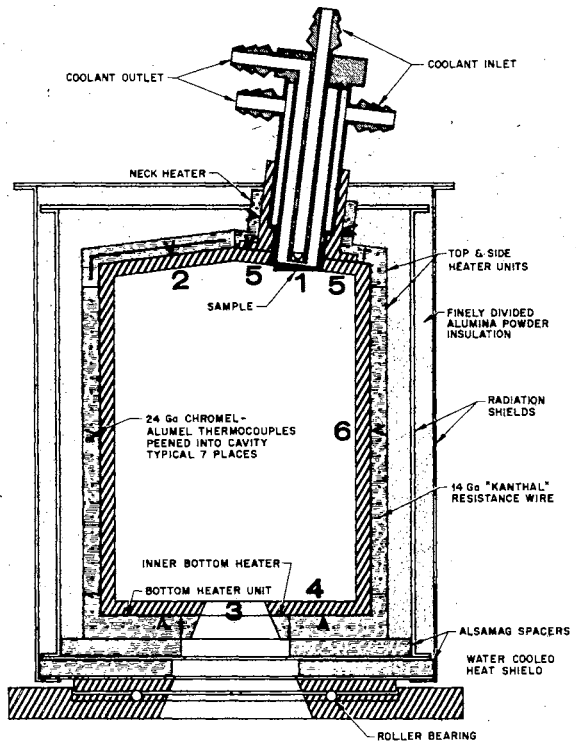

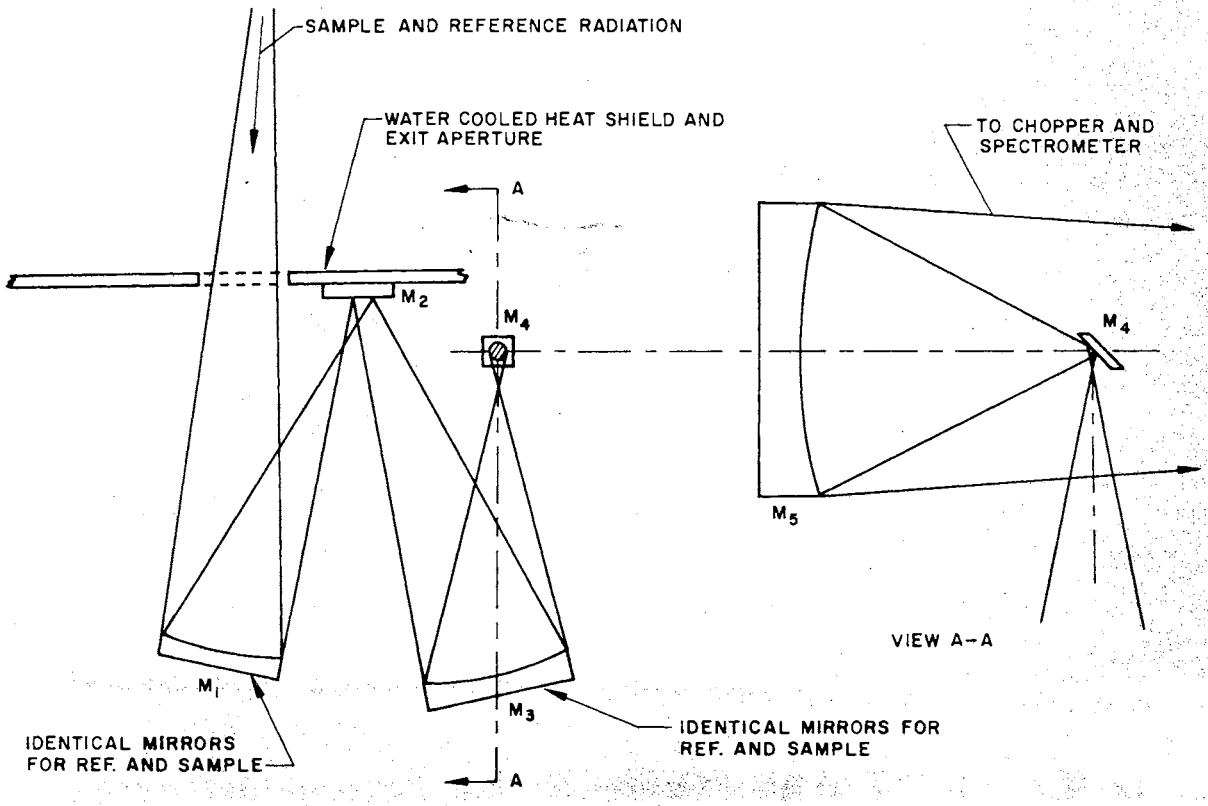

Figure 7. A typical heated cavity reflectometer with associated optics. Reprinted from reference 19 by permission of the Editor, J. C. Richmond.

the sample in the middle of the cavity, the angle of viewing (φ') for relative measurements of $\rho(\varphi',\theta')$ can be varied by tilting the sample. The major unique problems with this instrument are eliminating the temperature gradients and hole effects in the cavity so that it is indeed a blackbody cavity, and accounting for the energy emitted by the sample. In the Coblentz-type instruments, the incident energy is chopped so that its a-c signal can be distinguished from the d-c signal of the sample emitted energy, whereas in the heated cavity, no distinction can be made between the two. Also, in the heated cavity, the sample must be water-cooled and its temperature is quite hard to control, except for samples of high thermal conductivity.

The remaining problems occurring with the heated cavity are analogous in nature to those in the Coblentz-type reflectometers, that is, the effect of the hole loss is similarly dependent (through the reciprocity relations) on distribution of the reflected flux. This instrument is also capable of eliminating the specular component by viewing at $\varphi' = 0$, then the specular component would come from the hole, which emits no energy into the cavity. Again, however, the solid angle for the specular component is limited by the hole size and its distance from the sample.

Summary

From the brief foregoing discussion, it seems apparent that the heated cavity reflectometer offers the largest wavelength range and the highest accuracy for use in infrared reflectance measurements. However, it is restricted to the measurement of $\bar{\rho}(\varphi',\theta')$ for limited values of φ',θ'.

It is also apparent that several problems are common to most of the investigators and have yet to be eliminated. They are:

(1) The effect of the entrance or exit hole on the measurement,

(2) The lack of versatility in the instruments which restricts them to very special measurements,

(3) The inability to define specifically the accuracy of measured reflectance,

(4) The necessity for a calibrated reflectance standard of known goniometric distribution of reflected flux, and

(5) Spherical aberrations and/or detector spatial sensitivity problems.

It should be noted that reflectance measurements with the above instruments are still an art and the estimated accuracy as given herein for each instrument is intended to imply the use of the best possible measurement procedures for surfaces of unknown distribution of reflected flux. Further, it is felt that the general literature data, much of it going back to the work of Coblentz in 1913, do not reflect the best measurement procedures available today and may be in error on the order of 30 percent. References 30, 31, 32, and 33 give or review other methods of measuring infrared reflectance. One reflectometer that was not discussed above is the parboloid reflectometer [30]. This reflectometer appears to have many of the advantages of the ellipsoidal reflectometer discussed in this work, and is considered in chapter V. Table I is a summary of the previously defined reflectances.

TABLE I

REFLECTANCE TERMINOLOGY

Reflectance Measurements	Definition	Figure	Remarks
Bi-directional Reflectance	$\frac{I'(\varphi',\theta')\cos\phi'(\Delta\omega)'}{I_{\varphi,\theta}\cos\varphi(\Delta\omega)}$	1a	Yields complete description of surface's reflection characteristics. Very few measurements available.
Directional Hemispherical	$\frac{\int_0^{2\pi} I'(\varphi'\theta')\cos\varphi'\,d\omega'}{I_{\varphi,\theta}\cos\varphi(\Delta\omega)}$	1b	Measured by Coblentz, paraboloidal, and ellipsoidal reflectometer.
Diffuse Directional	$\frac{I'(\varphi',\theta')}{I_b'(\varphi',\theta')}$	1c	Measured by heated cavity and recent modifications of integrating hemispheres and spheres.
Hemispherical	$\frac{\int_0^{2\pi} I'(\varphi',\theta')\cos\varphi'\,d\omega'}{\int_0^{2\pi} I(\varphi,\theta)\cos\varphi\,d\omega}$	1d	Very general and is seldom useful.
Specular Component	$\frac{\int_{\Delta w} I'(\varphi,\theta+180^\circ)\cos\varphi\,d\omega'}{I_{\varphi,\theta}\cos\varphi(\Delta\omega)}$	2a	Of interest in heat transfer calculations. Has not been extensively measured. Should become important.
Non-specular Component	$\frac{\int_0^{2\pi} I'(\varphi',\theta')\cos\varphi'd\omega'}{I_{\varphi,\theta}\cos\varphi(\Delta\omega)} - \rho(\text{specular})$	2b	Complimentary to specular component measurement.
Directional Annular Cone	$\frac{\int_{\varphi_1}^{\varphi_2}\int_0^{2\pi} I'(\varphi',\theta')\cos\varphi'\sin\varphi'd\varphi'd\theta'}{I\varphi,\theta\cos\varphi(\Delta\omega)}$	2c	Appears that this type of reflectance would be useful for specific heat transfer configurations.

CHAPTER II

AN ELLIPSOIDAL MIRROR REFLECTOMETER

This chapter describes the conceptual design and operation of an ellipsoidal mirror reflectometer, which was developed to minimize the problems experienced during previous attempts to measure accurately infrared reflectance. Further, during the development of this instrument, the versatility of measurement was stressed to enable absolute or relative measurement of $\rho(\varphi,\theta)$, $\rho(\varphi,\theta,\varphi',\theta')$, ρ(specular), ρ(non-specular), and ρ(directional annular cone). Initially, the instrument is intended for use in the near infrared, where sufficient energy is available from a Globar to activate thermopile detectors. Eventually, the instrument will be utilized throughout the 0.4 to 15 μ range.

Figure 8, which illustrates the basic design of this instrument, shows a Globar as the source. The flux from the Globar is chopped by a 11.3 cps chopper before entering a Perkin-Elmer Model 83 monochromator; the monochromatic beam is then refocused (by two mirrors, one an optically flat, front surface, aluminum mirror with no overcoat, and the other a 36-inch radius of curvature, front surface, spherical mirror) through a small entrance hole onto the first focal point of an ellipsoidal mirror.* The ellipsoidal mirror is 12¼ inches in diameter and 3$\frac{9}{16}$ inches high, the first focal point is in the plane of the edges of the

* Purchased from Strong Electric Corporation, City Park Avenue, Toledo 1, Ohio.

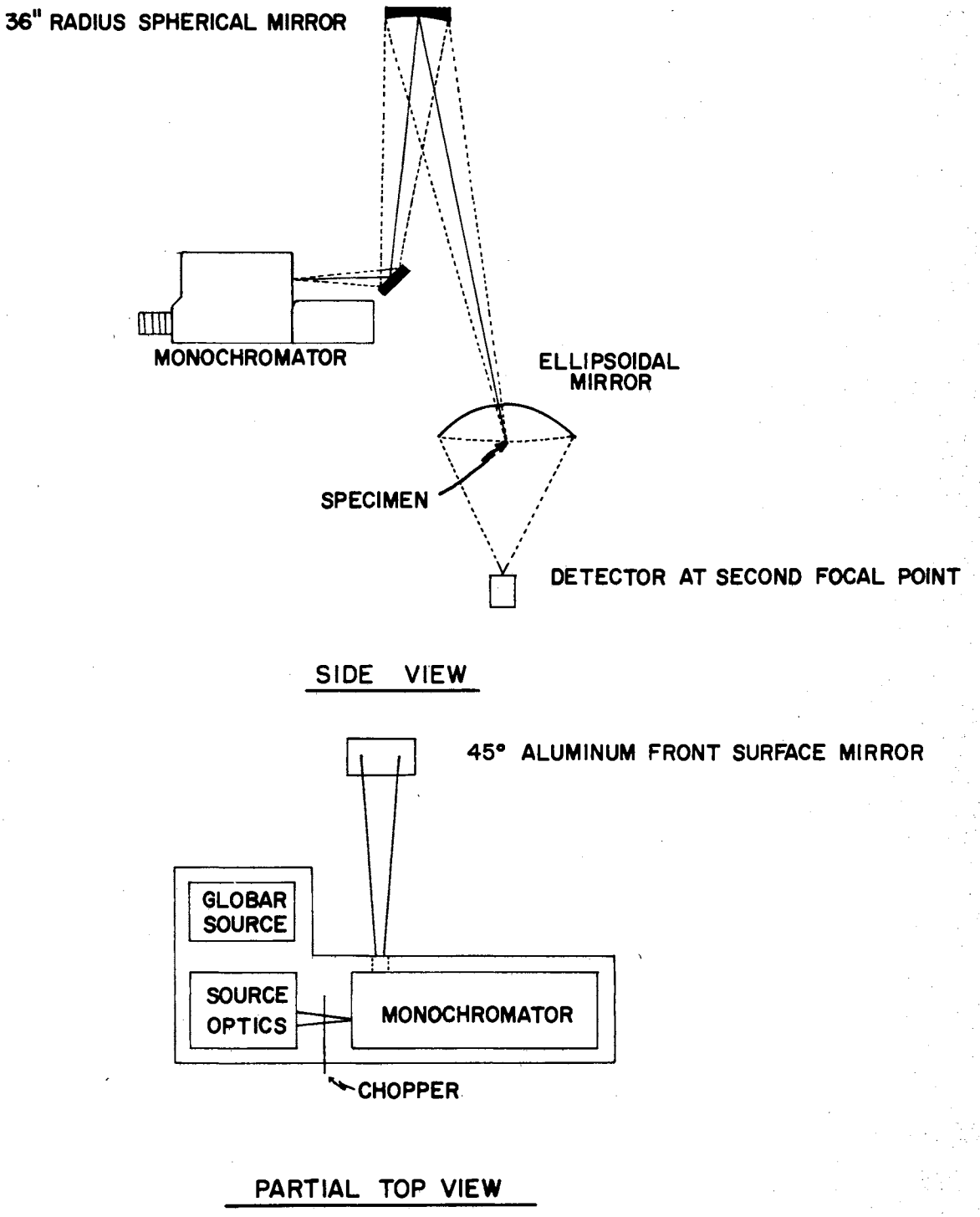

Figure 8. General Optical System of the Ellipsoidal Mirror Reflectometer

mirror, and the second focal point is 17 inches below the first focal point. The detector signal is amplified by a Brower Model 129 thermocouple synchronous amplifier.* To measure the incident flux, the detector is placed at the first focal point (see figure 9). The reflected flux is measured by placing the detector at the second focal point and the sample at the first focal point; the reflected flux leaves the sample and is reflected by the ellipsoidal mirror to the detector at the second focal point. Thus, after correcting for system losses (qualitatively described on page 26), the absolute directional diffuse reflectance is measured for $\varphi = 7°$. When the instrument is operated in the relative mode, the detector is always at the second focal point and two measurements are made, one with a sample at the first focal point, the other with a reflectance standard at the first focal point. As in other methods of reflectance measurement, the relative measurement tends to eliminate the effects of atmospheric absorption and reduce the effect of the other corrections; however, it also requires the use of nonexistent reflectance standards.

This instrument has the same inherent losses as the other systems, with the following exceptions:

(1). Aberrations are reduced to a minimum, since all measurements are centered around true focal points rather than conjugate focal points [17].

(2). The reflected energy is now concentrated in a small cone (24° half-angle), instead of over the entire hemisphere, which reduces errors due to angular sensitivity (chapter III).

---

* Brower Laboratories, Inc., Turnpike Road, Westboro, Massachusetts.

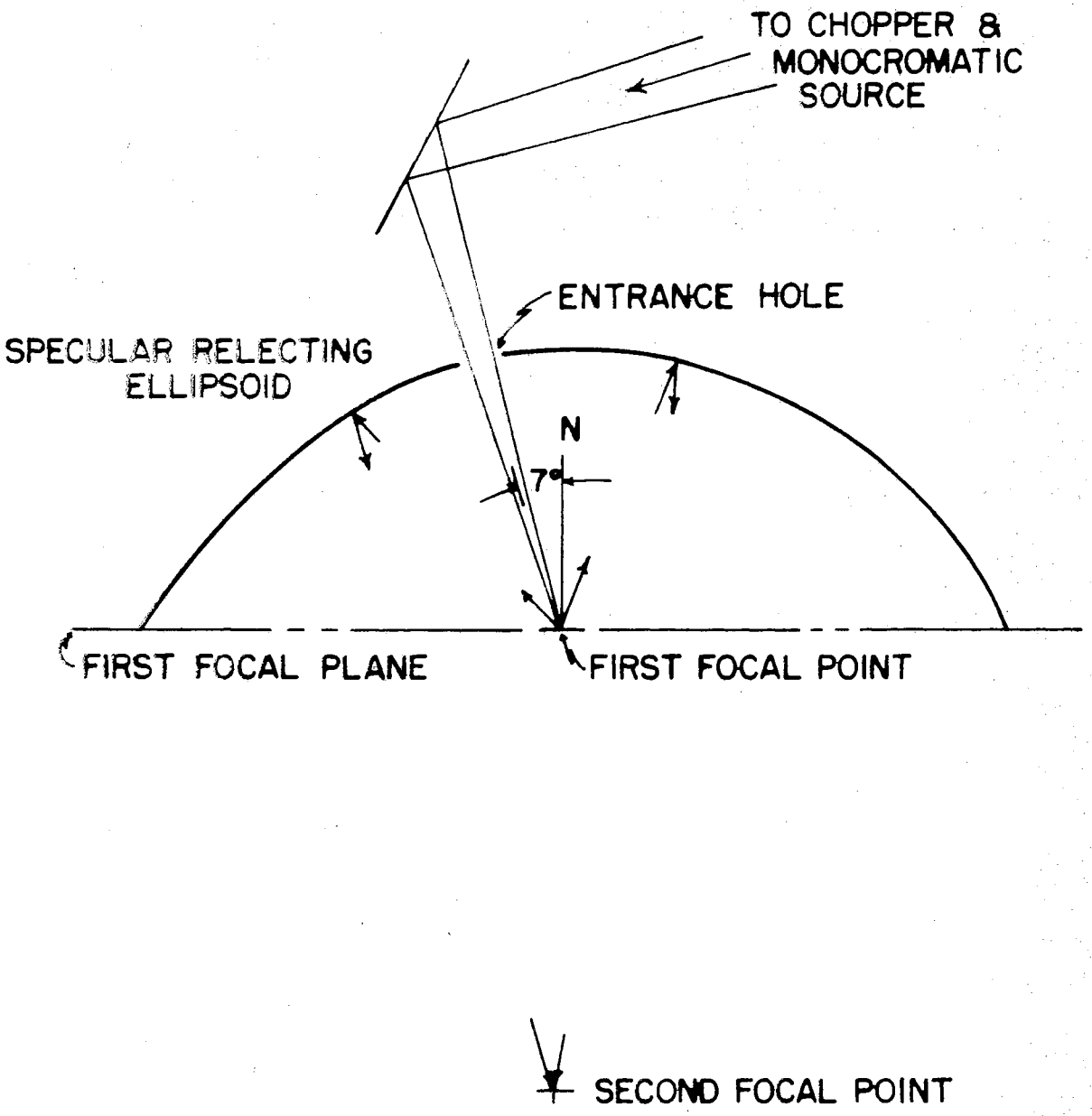

Figure 9. Optics of the Ellipsoidal Mirror.

(3). The detector and sample are widely separated (17 inches), which will allow heating and cooling of the sample over large temperature ranges. (This is also an advantage of the Janssen-Torborg system.)

(4). Further, the unique optics involved in the use of the ellipsoidal mirror will allow accurate calibration of mirror and hole losses for all but the most radically distributed reflected flux (such as a diffraction grating).

Measurement Capabilities

This thesis is primarily concerned with the measurement of $\rho(\varphi,\theta)$; however, the unique optics of the ellipsoidal mirror allow accurate description of the distribution of the reflected flux, because the spatial distribution of the reflected energy crossing the first focal plane is related precisely to the goniometric distribution of the reflected flux. That is, every direction φ',θ' in the hemisphere above the surface is represented by a point P in the first focal plane, and every solid angle centered in the direction φ',θ' is represented by an area about P. This implies the ability to select the energy that the detector views by blanking out the unwanted energy with a shield placed in the first focal plane. With this procedure, a specular component can be measured which has a solid angle determined by the open area of the shield placed at the first focal point. Similarly, the bi-directional reflectance (i.e., $\rho(7°,\theta,\varphi',\theta')$) could be measured by the same procedure (i.e., by varying the position of the hole in the shield). Measurement of the directional annular cone reflectance is accomplished through use of a set of circular disks centered on the sample, which allows sufficient data for calculation of this reflectance. Further, this ability to measure

the distribution of the reflected flux will aid greatly in making precise corrections for the system losses.

Due to energy limiting factors presented in chapter III, the instrument is initially used in the 1.5 to 7.0 μ region. Further, since absolute measurements are taken in the laboratory atmosphere, eight wavelengths and corresponding band passes have been chosen which do not include the absorption bands of water and CO_2. These wavelengths are 1.5, 2.0, 2.5, 3.5, 4.5, 5.5, 6.5, and 7.0 microns. The width of the band passes varies from about 0.2 μ for the shorter wavelengths to about 0.4 μ for the longest wavelength setting. These large band passes will not in general be a hindrance, since the materials studied do not have absorption bands or radical changes of reflectance in the wavelength range, 1.5 to 7.0 μ.

Description of System Losses

In order to attain a high degree of accuracy, the flux losses in the system must be accounted for precisely. Thus, this section qualitatively describes these losses for future use in a flux balance of the system.

(1). Ellipsoidal Mirror Losses ($F\alpha$):

Energy is absorbed by the ellipsoidal mirror; therefore the reflectance of the mirror coating must be known. This reflectance may vary with angle of incidence on the mirror, and, hence, position on the mirror. The angle of incidence varies from 0° at the apex to 35° at the edge of the mirror. There also will be losses from scattering due to scratches, dust, and other imperfections of the mirror surface.

(2). Hole Losses (F_H):

Some of the reflected flux will escape through the hole in the mirror which admits the incident beam. This loss varies with the geometric distribution of the reflected flux. Previous instruments have been unable to establish accurately this loss, which does not necessarily lie between the condition of no loss for a specular sample and a loss based on a diffuse configuration factor from the sample to the entrance hole. For most engineering surfaces, this loss will be higher, since they reflect a predominant amount of flux about the specular component, which will include the direction of the hole.

(3). Sample Shielding (F_{SP}-F_{SR}):

Flux leaving the sample normal to its surface will be re-reflected to the sample, and, hence, be blocked from reaching the detector. Most of this will be lost, but some may be multiply reflected by the sample and reach the detector.

(4). Sample Holder Losses (F_W):

Those parts of the sample holder and its supports (not shaded by the sample) will shade the detector and cause a loss of flux.

(5). Atmospheric Absorption:

The path lengths for incident and reflected energy will be different; hence, atmospheric absorption will introduce errors in the absolute measurement. These errors can be minimized in a comparison measurement.

(6). Edge Losses:

If the sample is not properly aligned in the first focal plane of the ellipsoid, some of the flux reflected by the specimen will miss the lower edge of the ellipsoidal mirror and be lost. Again, the amount depends on the geometric distribution of the reflected flux.

(7). Detector Related Problems:

A problem common to most previous reflectance measurement methods has been the need for large area detectors to accept the large images. Large area thermopiles, in particular, always have a non-uniform spatial sensitivity (i.e., they do not sense flux equally well if the illuminated area of the detector is changed) and angular sensitivity (i.e., as the angle of the incidence gets further from the normal, the detector is much less sensitive to the flux, due in part to shading by the housing of the thermopile, and because the absorbing blacks on the detector become specularly reflecting at grazing incidence).

Chapter III deals with the problems of detectors in detail, while chapter IV describes the analysis used to ascertain the magnitude of the above listed losses, and appendices F and G discuss the calibration techniques and the probable magnitudes of the losses.

CHAPTER III

DETECTOR PROBLEMS

In this chapter the problems of detector spatial and angular sensitivity are investigated and corrective measures described. Spatial sensitivity is defined as the variation in response of the detector with changes in the illuminated portion on the sensitive area of the detector. This leads to errors in the comparison between measurements of (1) two small area beams that are not incident on identical portions of the sensitive area, and (2) a small area beam and a much larger area beam. Angular sensitivity is defined as the variation in response of the detector with angle of incidence of the measured flux.

(A). Detector Spatial and Angular Sensitivity.

As previously stated, a large area detector is required in the ellipsoidal mirror reflectometer, because the incident image (2mm x 2mm) is magnified about 25 times to a size of 1cm by 1cm at the second focal point. Hence, when the instrument is used in the absolute mode, it is necessary for the detector to sense flux incident in a cone of 4° half angle centered around a direction 7° from the normal over a 2mm by 2mm area equally, as well as flux from a cone about the normal having a 24° half angle and an image area of 1cm by 1cm. When the instrument is used in the relative mode this is not as critical since the reflected beams are similar.

Two detectors were considered for use in the instrument: (1) A Golay cell, and (2) a Reeder ten junction thermopile. The Golay cell has a sensing area 1 cm in diameter and the Reeder thermopile has a sensing area 1 cm square. The Golay detector was discarded early in the effort as being too microphonic. The microphonic noise was accentuated by operation of the detector with its sensitive diaphragm in a horizontal position, rather than the more usual vertical position [31]. Because of these difficulties, the ten junction thermopile was selected for the measurements reported herein. The first attempts to obtain absolute measurements of selected samples with the equipment resulted in errors of reflectance in excess of 40 percent. It was felt that the spatial and angular sensitivity of the thermopile might well contribute errors of this magnitude. The spatial sensitivity was measured by W. Schneider, National Bureau of Standards [18], and the angular sensitivity was measured with an attachment to the reflectometer instrument. These measurements are described below.

(A.1). Detector Spatial Sensitivity:

The thermopile was mounted on an automatically driven micrometer head that could move it horizontally in the plane of the sensitive area at a rate of about 0.08 inch per minute. A stationary aperture stop, having a circular opening $\frac{1}{16}$ inch in diameter, was mounted directly in front of the detector. The detector was illuminated through the aperture stop by radiation from a tungsten lamp.

The thermopile consists of ten plates, each approximately 2mm by 5mm in size, arranged in two columns of five rows each to form a sensitive area 1 cm square. A thermocouple was attached to the back of each plate, and the ten thermocouples were connected in series to form the thermopile.

The scans in th A-A′ direction were made across the center of the sensitive area, along the line between the two columns. The scans in the B-B′ direction were made across the center of the sensitive area along the long axis of the two plates in the third row. In both cases scans were made (1) using incident radiation chopped at 13 cycles per second with the amplifier tuned to 13 cps, and (2) using unchopped incident radiation with a d-c amplifier. Results are shown in figure 10 for the a-c scans, and in figure 11 for the d-c scans. For some of the runs, a screen holder was placed over the thermopile; this was used to hold the roughened NaCl window described in appendix C. This screen holder was an attachment to the thermopile which should not have obstructed the incident flux.

In figure 10 for the A-A′ scans, it can be seen that, with the screen holder only, there are three distinct peaks, with some indication of two others, corresponding to the positions of the five rows of plates. In the B-B′ scan, without the screen holder, it is apparent that the plate on the right had greater sensitivity than that on the left. The screen holder alone had very little effect, as would be expected.

In figure 11, the d-c scans in the B-B′ direction are somewhat similar to the equivalent a-c scans for the screen holder only; however, with no screen holder, the curve is relatively smooth and shows that the plate on the left has greater sensitivity than that on the right. The scans in the A-A′ direction show five distinct peaks with no screen holder. The curve with the screen holder only is qualitatively similar to the equivalent a-c scan.

At this same time, W. Schneider also measured the spatial sensitivity of the Golay cell in a similar manner. In this case, a Globar-filter arrangement provided the different wavelengths. The results are contained in figures 12 and 13.

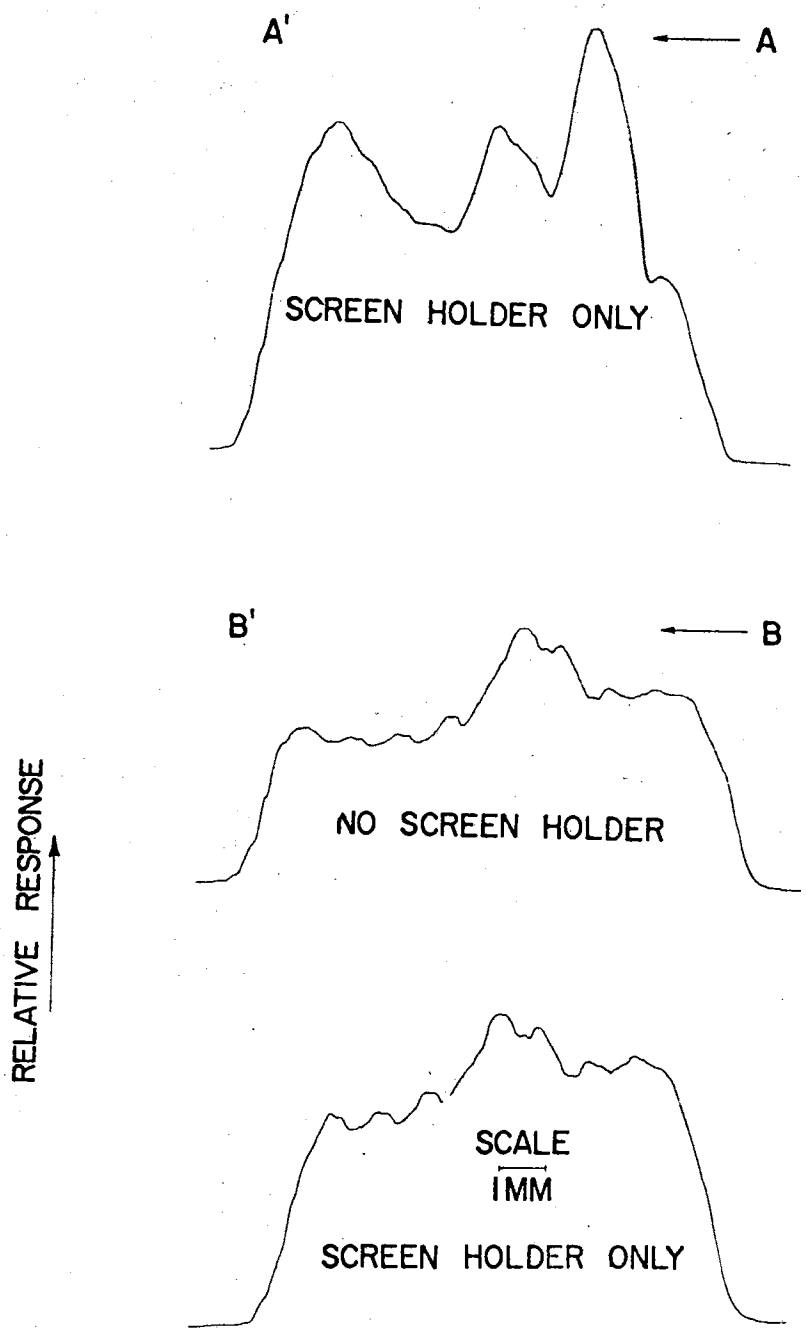

Results of scans across the sensitive area of the thermopile detector in the A-A' and B-B' directions, with chopped tungsten incident flux. The A-A' direction is across five rows of plates, and the B-B' direction is across two columns of plates.

Figure 10

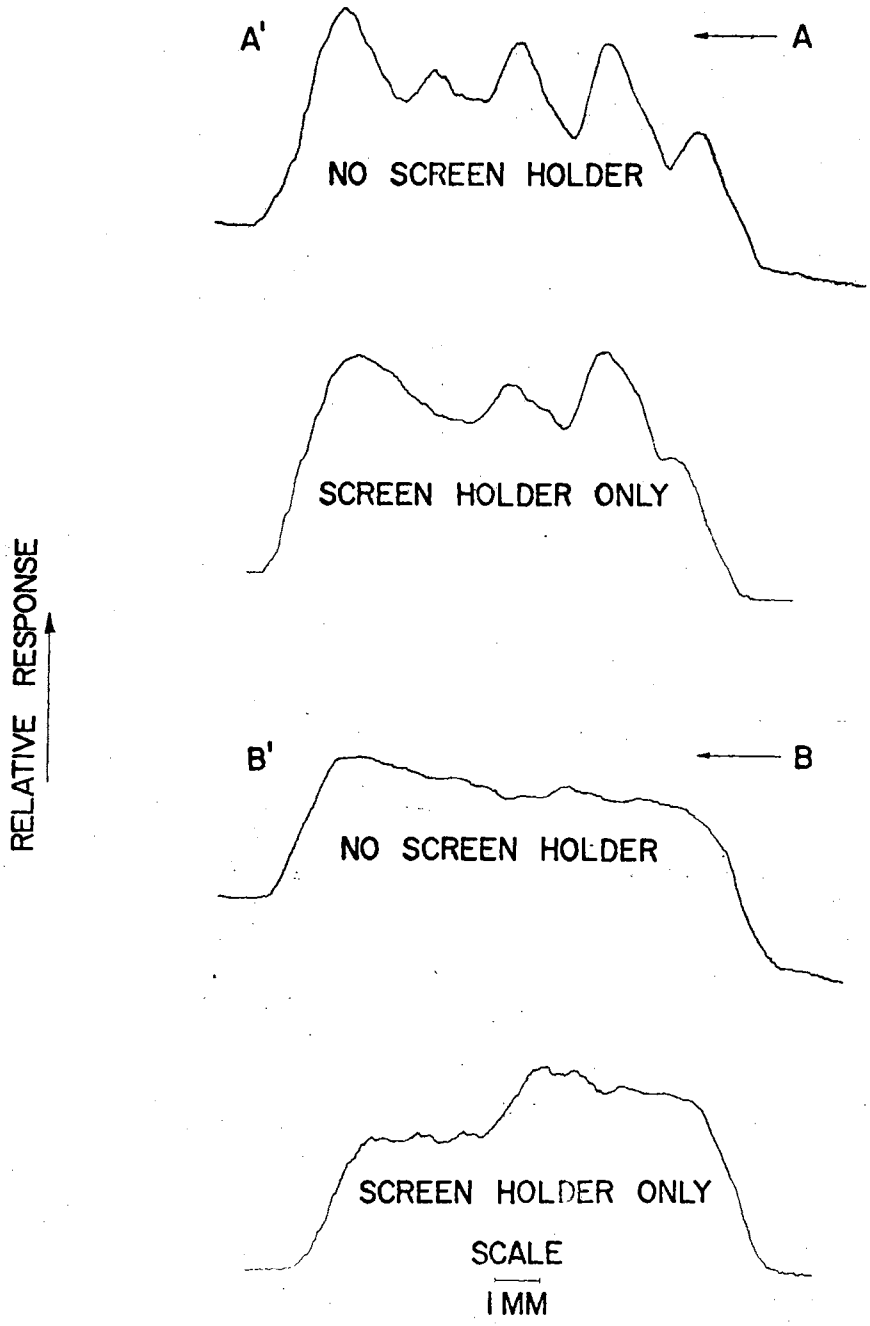

Results of scans across the sensitive area of the thermopile detector in the A-A' and B-B' directions, with unchopped tungsten incident flux. The A-A' direction is across five rows of plates, and the B-B' direction is across two columns of plates.

Figure 11

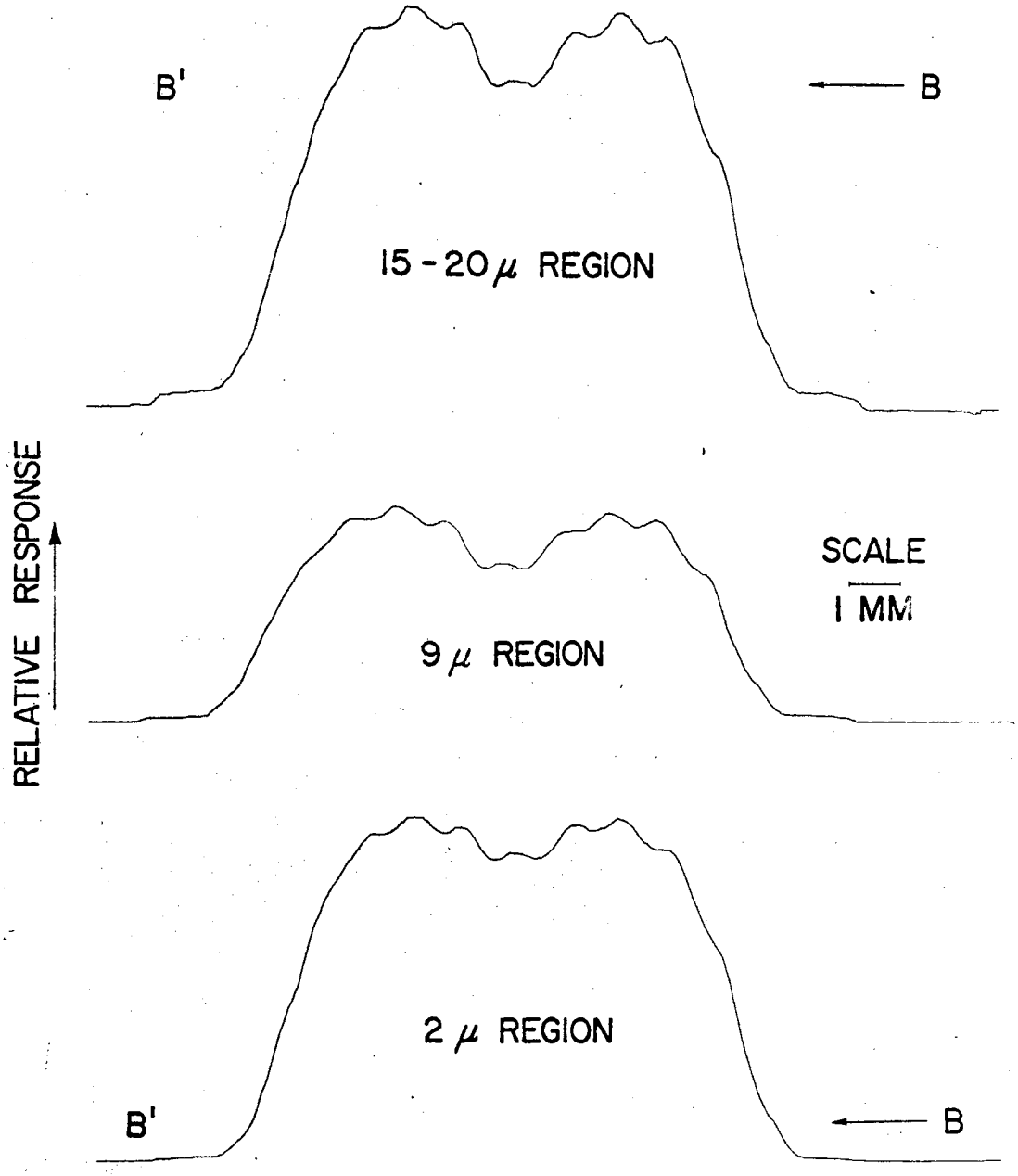

Results of scan across the sensitive area of the Golay cell detector in the B-B' direction, with incident flux in three different wavelength regions as indicated

Figure 12

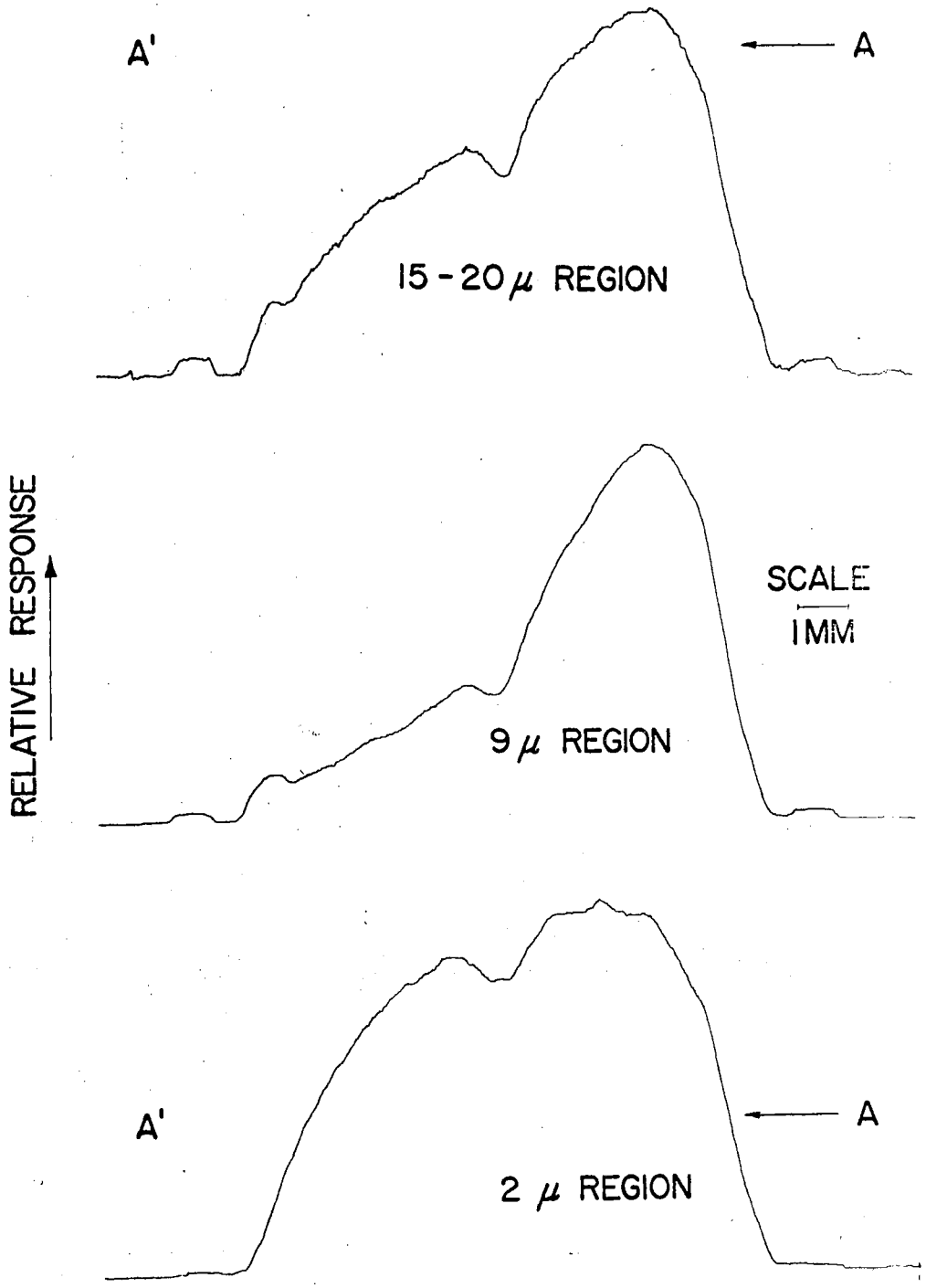

Results of scan across the sensitive area of the Golay cell detector in the A-A' direction, with incident flux in three different wavelength regions as indicated.

Figure 13

(A.2). Detector Angular Sensitivity:

Since a detector was required that was equally sensitive to radiation striking at any angle from 0 to 24°, the angular sensitivity of the thermopile detector was measured. To make this measurement, the detector was mounted on a milling head (figure 16) with its sensitive area in a vertical plane and with the two columns of plates vertical, in a position such that the center line of the sensitive area coincided with the vertical axis of rotation of the milling head. An image of the exit slit of the monochromator, 3mm by 3mm in size, was focused on the center of the sensitive area from a direction normal to it, by means of a 6-inch diameter spherical mirror having a 49-inch radius of curvature. The cone of rays thus had a half-angle width of about $3\frac{1}{2}°$. The monochromator was adjusted to give a band of radiation centered at 2.2 μ. The response of the detector was recorded as R_n when the axial ray of the incident beam was normal to the sensitive area. The milling head was then rotated to give incident angles of 5, 10, 15, 20, 25, 30, 40, 50, 60, and 70° to the normal, and the response of the detector was recorded at each setting as R_θ, θ being the angle of incidence. The data were normalized by dividing each reading by the reading at normal incidence, and plotted as a function of angle of incidence to produce the curve shown in figure 14. Similar measurements were made with a cover plate 0.15 inch in thickness with a 1 cm by 1 cm hole mounted over the sensitive area. The entire procedure was repeated with a band of radiation centered at 8 μ.

The experimental curves are compared in figure 14 with two computed theoretical curves. The top curve, in which $R_n/R_\theta = 1$ at all angles would be obtained if the detector were equally sensitive to flux striking it at all angles, and if all of the incident flux struck the sensitive

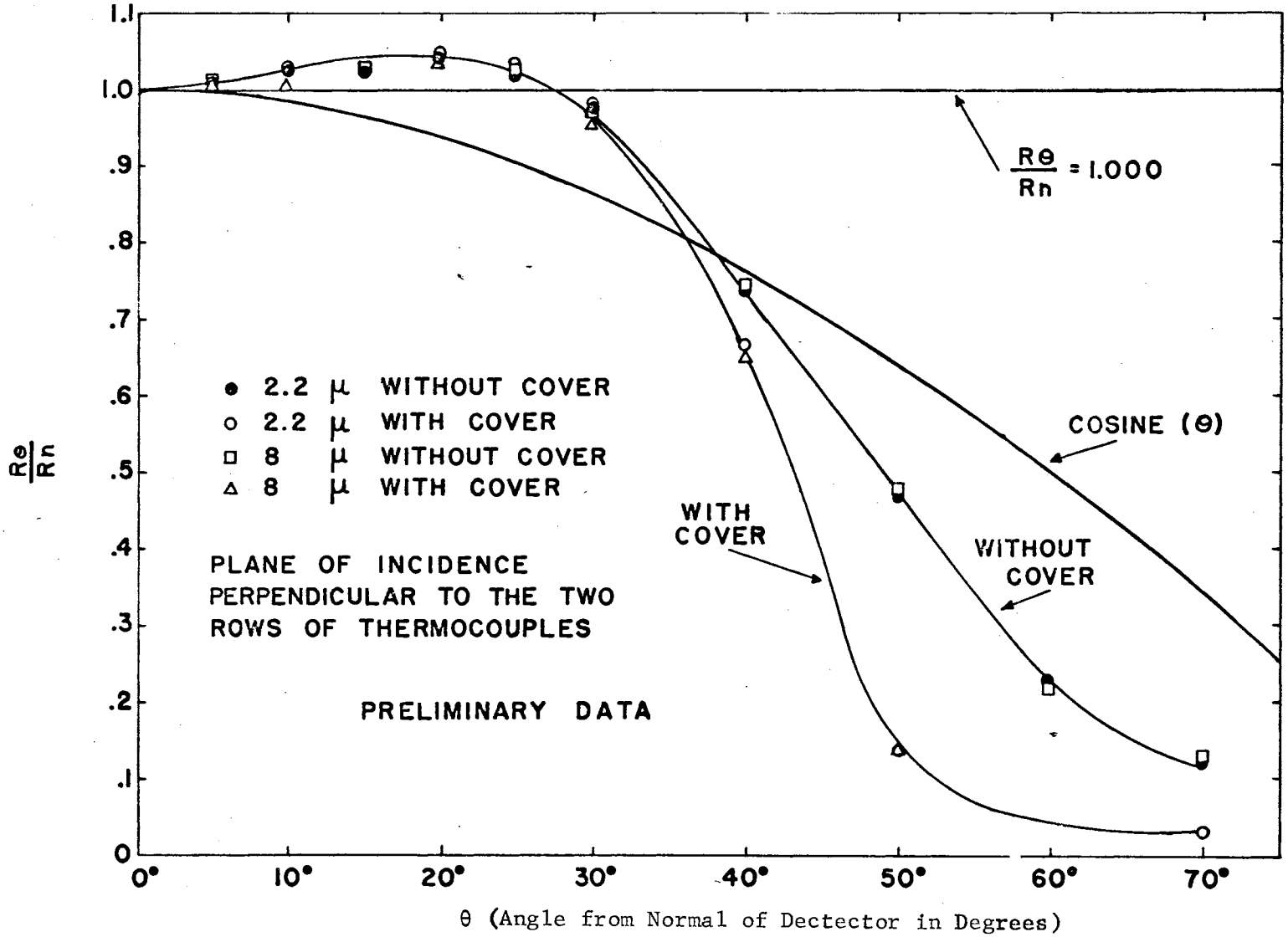

Figure 14. Angular sensitivity of Reeder thermopile across the two rows of thermocouples.

area. The lower curve, in which $R_n/R_\theta = \cos \theta$, would be obtained if the detector were equally sensitive to flux striking it at all angles, and were completely filled at normal incidence.

From the experimental curves in figure 14 it can be seen that the sensitivity increases slightly from normal to 20°, then decreases. The increase is undoubtedly due to the fact that as the illuminated area of the detector increases, the more sensitive areas, as shown in the previous section, become illuminated. The sharp drop in response beginning at about 30° is due to some of the flux being lost; either not admitted through the window or not striking the sensitive area if admitted. The presence of the cover plate increases the rate of fall-off in this range, as might be expected.

Similar tests were made with the detector mounted with the five rows of plates vertical. The results shown in figure 14 are similar to those in figure 9, except that the increase in signal from 0 to 20° was not observed. This is undoubtedly due to the fact that as the angle was increased, more plates were illuminated, but in the same relative areas, hence, the signal remained constant.

The curves plotted in figures 14 and 15 show no significant differences for flux of 2.2 and 8 μ, respectively. The fact that the curves are nearly flat from 0 to 25° indicates that variation in angular sensitivity will be only a minor problem with the ellipsoidal reflectometer, since the marginal rays strike the detector at an angle of approximately 24°.

From these measurements it is apparent that spatial sensitivity of the detector could cause errors in excess of 30 percent, since the reading with the detector at the first focal point is dependent on where

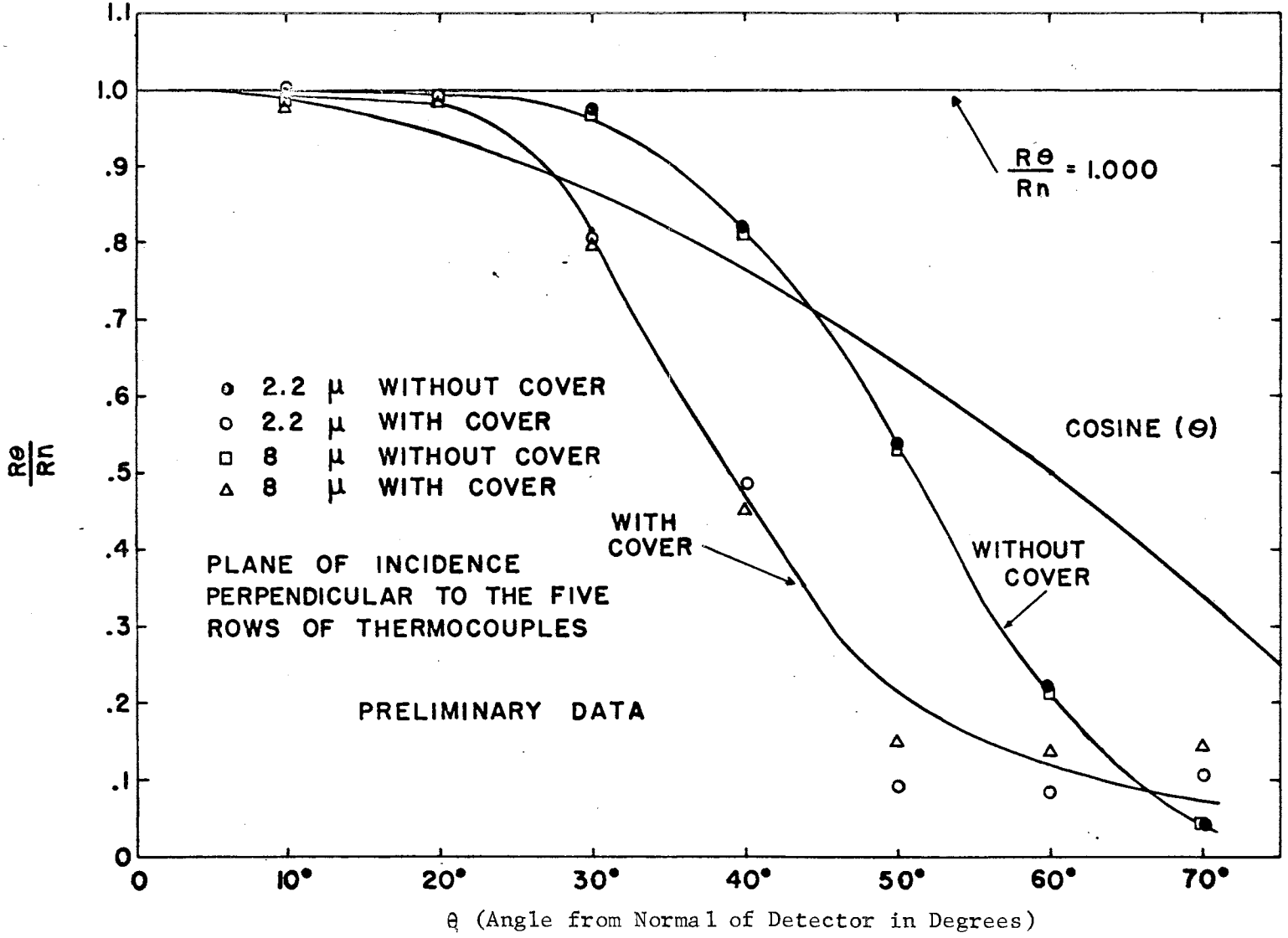

Figure 15. Angular sensitivity of Reeder thermopile across the five rows of thermocouples.

the small image is placed on the detector. Further, the image at the second focal point slightly overfills the detector sensing area due to aberrations and any slight misalignment of the optical components. Hence, if reliable measurements are to be obtained, it is first necessary to eliminate the problems of spatial sensitivity, angular sensitivity, and failure to collect all of the reflected flux.

(B). Flux Averaging Devices.

The data on the variation in spatial and angular sensitivity of the detector indicated that a flux-averaging device would be required for use with any of the available large-area infrared detectors. The function of such a device is to spread the available flux uniformly over the sensitive area of the detector, regardless of image size, shape, or intensity distribution. Any averaging device will, of course, reduce the efficiency of a detector system, because some of the incident flux in absorbed by the diffuser, and some is scattered away from the sensitive area of the detector and is lost. In general, the losses in the diffuser tend to increase with an increase in its efficiency as a diffuser.

The literature provides several references to this problem. One is the work of Bennett and Koehler [9], who used a small integrating sphere to average out the signal over a photomultiplier detector. Another is the work of Ronzhin [39], who tried light ducts and integrating spheres to average the signal over the sensitive area of a photomultiplier. However, these references offer solutions only in the ultraviolet and visible portions of the spectrum, where good integrating sphere coatings are available. In the infrared, the spectral region for which the

reflectometer was specifically designed, no one has yet shown that satisfactory integrating sphere coatings exist for use beyond 4 μ.

Three different types of diffusing devices were investigated. They are listed in estimated order of increasing efficiency of diffusion as: (1) A diffusing screen placed directly over the detector, (2) a light duct with diffusing walls or a diffusing surface in the system, and (3) an integrating sphere coated with a material having high reflectance in the infrared and sufficient diffusing power to permit it to be used as an averaging device.

The results of the tests with the diffusing screen and with the various light ducts are presented in appendix C of this dissertation. Neither of these approaches yielded satisfactory answers for this work.

Initial results using a 2-inch diameter sphere with a 3M white diffusing paint indicated that this approach seemed feasible, at least at short wavelengths where known diffusers are available. It is known from the theory of integrating spheres [7] that for sphere efficiency to be high, it is necessary for (1) the wall reflectance to be close to unity, (2) the diameter of the sphere to be a minimum, (3) the area of the entrance and exit ports to be a minimum, and (4) the detector to view the entire sphere. Further, it is important that the sphere wall be a diffusing surface if a constant intensity across the detector port is to be expected.

High sphere efficiency is required in this application, because the amount of flux available for measurement is near the lower limit of the useful range of the detector, particularly at the longer and shorter wavelengths, near 1.5 and 7.0 μ. Certain white paints, MgO, and $BaSO_4$, are good sphere coatings in the visible and near infrared, but they have low reflectance beyond 4 or 5 μ and are not suitable for use

at the longer wavelengths. Birkebak [36] shows that sulfur is both a good diffuser and reflector at 2 μ and at 4 μ, and assumes that it is usable out to 10 μ. However, he does not mention the specific form of sulfur that was used for his measurements, or his method of applying it to the sphere wall. Kronstein, et al. [38], report that mu sulfur is a good reflector out to 15 μ, and give a spectral reflectance curve, but did not use it as a sphere coating. Further, Agnew and McQuistan [40] show that sulfur is a diffuse reflector to the flux from a Globar with wavelengths shorter than and longer than 4 μ. Polished metals have high reflectance at all wavelengths from the visible to the far infrared, but they are not suitable for use in integrating spheres, since they reflect specularly. Roughening the surface of a polished metal, however, will diffuse the reflected beam. Hence, it may be possible to produce a usable sphere coating by first suitably contouring a metal surface, and then applying a vacuum-deposited metal to increase the surface reflectances. In the present work, two general types of surfaces were considered for use as a diffusing sphere coating for use in the infrared: (1) A roughened gold-plated surface, and (2) a sulfur coating.

Many spheres were built and coated. The following is a list of those tested:

(1). A 4-in. diameter aluminum sphere coated with smoked MgO. The entrance and detector port areas were 0.188 sq. in. and 0.875 sq. in., respectively.

(2). A 2-in. diameter sphere that was roughened by "roto-blasting" with spherical glass shot.* The sphere was then vapor plated with an

*The Roto-blast process is a trade name used by Pangborn Corp. to describe the blasting of surfaces, in this case with spherical shot. Both glass and steel spherical shot are available from this company. The roughened spheres used in this investigation were Roto-blasted by Mr. Mann of Pangborn Corp., Hagerstown, Maryland.

opaque coating of gold. Entrance and exit port areas for all the 2-in. spheres utilized in this chapter are 0.444 sq. in. and 0.515 sq. in., respectively.

(3). A 2-in. diameter sphere, which had a sulfur* wall coating. The sulfur was hand pressed onto a roughened sphere wall.

(4). The roughened, gold-plated sphere wall of sphere 2, above, was over-coated with a very thin coat of sulfur. The sulfur was suspended in alcohol and sprayed with an ordinary paint sprayer.

(5). A 2-in. diameter sphere was coated with a $\frac{1}{8}$-in. thick coating of sulfur, which had been sprayed from a suspension of alcohol.

(6). A 2-in. diameter sphere was coated with a $\frac{1}{8}$-in. thick coating of sulfur, which was sprayed from a benzene suspension.

Appendices C, D, and E give additional information concerning these and other sphere coatings. Appendix E specifically deals with the methods of coating or preparing the sphere walls.

To examine these spheres for their ability to collect energy from small and large areas and to be insensitive to small changes in image position, two tests were utilized. The general optical system for these tests is shown schematically in figure 16. A 6-inch diameter spherical mirror of 49-inch radius was used to focus the beam from the exit slit of the monochromator onto the entrance port of the sphere. The sphere was mounted in a milling head, so that it could be moved 8 inches in the x and y directions, and rotated 360° in the x-y plane.

---

*The sulfur used in this investigation was Crystex brand sulfur and was supplied by Mr. A. Blackwell, Manager, Technical Service Dept., Stauffer Chemical Co., 380 Madison Ave., New York, N. Y. The analysis given by the supplier is 99.5% Elemental Sulfur, 90% mu (insoluble sulfur), 0.10% ash, and the acidity is 0.05%. Mu (insoluble) sulfur comprises 90% of elemental sulfur.

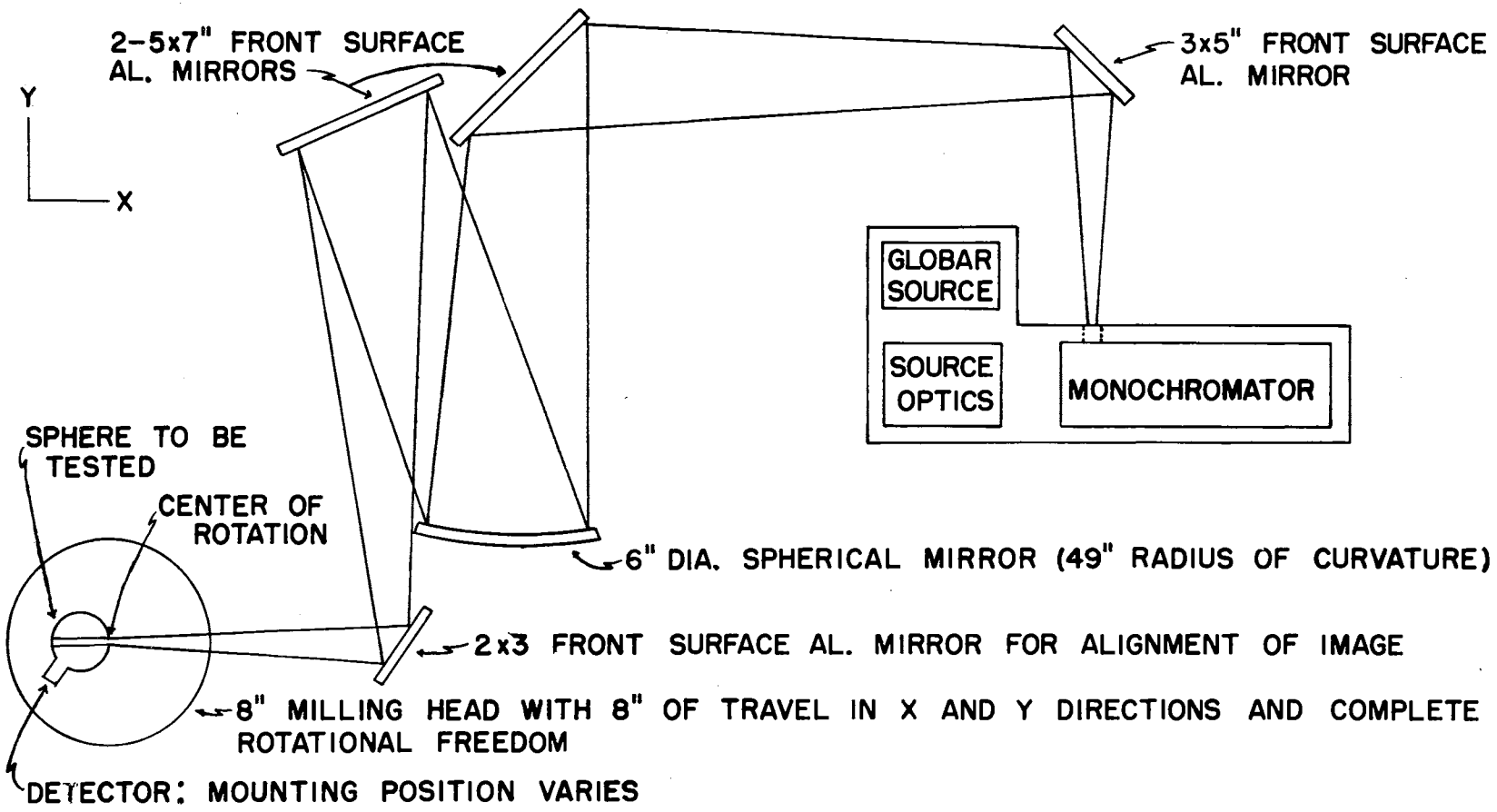

Figure 16. Spatial and Angular Sensitivity Test Apparatus

In the first test, the sphere was mounted with its entrance port at the center of rotation of the milling head, and the incident beam was centered on the entrance port. The sphere was moved along the axial ray of the divergent incident beam, and the detector response was recorded as a function of sphere position.

In the second test, the sphere was mounted as before, but in this case, it was moved across the axial ray of the incident beam, which was focused on the entrance to the sphere, and the detector response was recorded as a function of sphere position.

(B.1). Area Sensitivity (Test No. 1):

This series of tests was performed in an effort to establish which of the various coated spheres was the most suitable for use with the ellipsoidal mirror reflectometer. In these tests, the detector port and entrance port were centered on radii of the sphere 135° apart, as indicated in figure 16. The sphere was mounted on the milling head (figure 16) with the axial ray of the incident beam centered on and normal to the entrance port. The sphere was moved along the axial ray of the incident beam, and the detector response was recorded as a function of sphere position. This test was designed to evaluate the variation in detection response with the size of the illuminated area on the sphere wall, when the total flux is held constant. Since the incident beam is diverging from a focus, the size of the illuminated area could be varied from minimum size when the beam was focused on the sphere wall (or inside the sphere for the 4-inch diameter sphere) to a maximum size when the marginal rays fell just inside the entrance port. The maximum area ratio was 12.25 to 1 for the 2-inch diameter sphere and about 2.36 to 1 for the 4-inch diameter sphere. The measured sphere position was experimentally

correlated to the area of sphere wall illuminated by the incident beam, and each area was divided by the cross-sectional area of the beam at the focal point of the spherical mirror to obtain the area ratio for each position. The detector response at each position was divided by the response at the position where the beam was focused on the sphere wall, to obtain the response ratio R/R_o. Response ratio was then plotted as a function of area ratio to obtain the curves shown in figures 17, 19, and 20.

This test simulates the conditions that exist when the detector is moved from the first to the second focal point of the ellipsoidal mirror. Since the sphere wall is behind the first focal point when the incident flux is measured, the illuminated area on the sphere wall will be on the order of 10 mm by 12 mm; hence, the test conditions fully cover the range of areas that will be encountered in service.

The test was applied to all the spheres considered for use with the ellipsoidal reflectometer. The data at the top of figure 17 represent the results for MgO at 1.5 μ, where it is a known diffuser. R/R_o varied by 0.8 percent for an area ratio of 2.36 to 1. Since the sphere was 4 inches instead of 2 inches in diameter, as all the others tested, the optics of the test system limited the area changes of the image on the sphere wall to a smaller value than for the 2-inch spheres. The results from this test indicate that the sphere does indeed reduce the effect of spatial sensitivity of the detector. However, it is not possible to use MgO as a coating in the infrared.

The second curve in figure 17 represents the results for a roughened sphere, which has been vapor-plated with gold; the roughness of the sphere wall was of the order of 25 μ inches rms. The change in R/R_o was 2 percent, indicating poorer diffuseness than for the MgO. Further, the

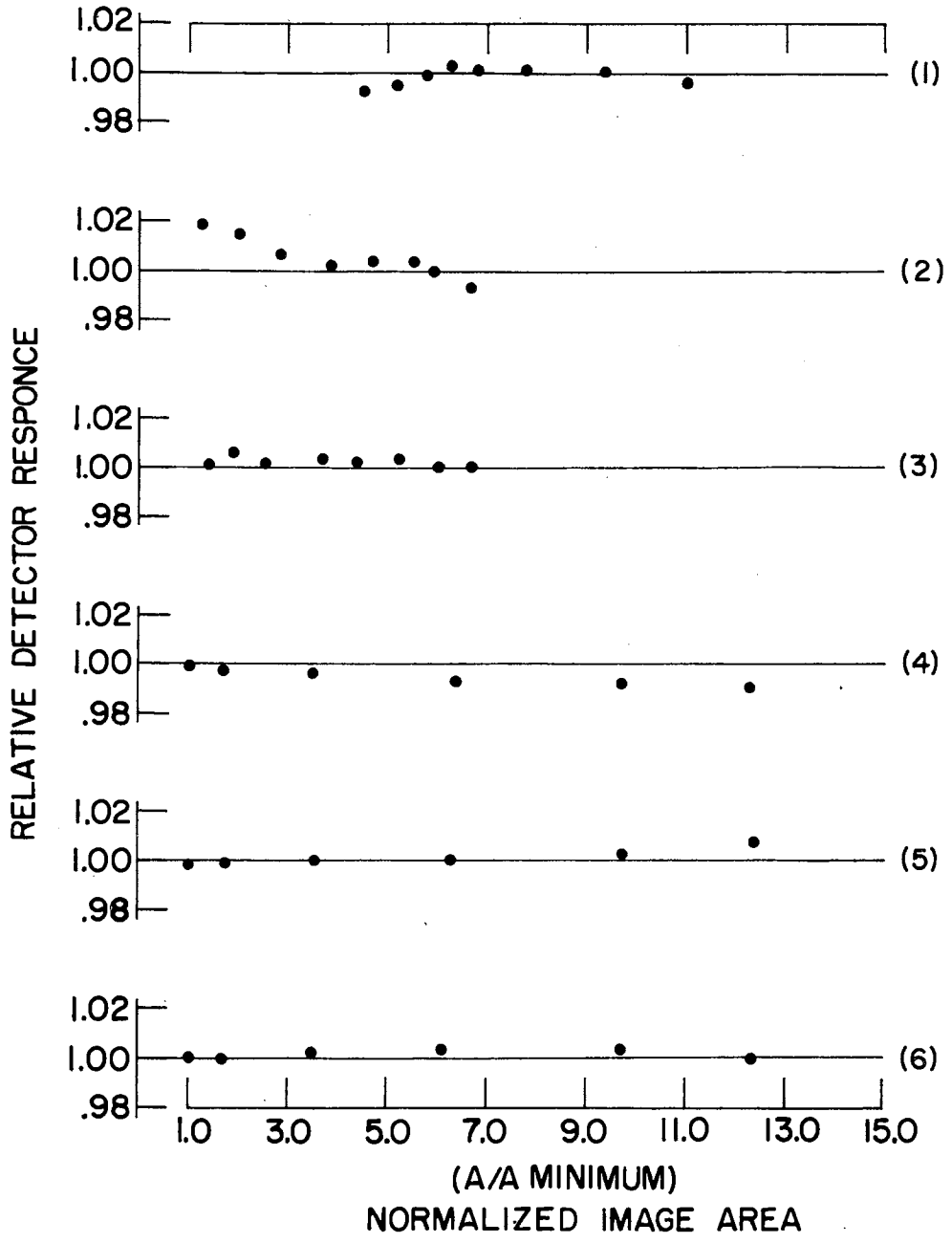

(1) 4" MgO SPHERE a 1.5μ
(2) 2" L-SHOT GOLD SPHERE a 2.4μ
(3) 2" HAND PRESSED SULFUR SPHERE a 2.4μ
(4) 2" GOLD SULFUR SPHERE a 2.4μ
(5) 2" SULFUR SPHERE a 2.4μ SHIELD #1
(6) 2" SULFUR SPHERE a 2.4μ SHIELD #2

Figure 17. Results of Area Sensitivity Test for Various Sphere Coatings

efficiency of this sphere is almost identical to the other spheres tested despite the very high reflectance of gold. This is due to the fact that in this design there is a large specular component of flux that passes out the entrance of the sphere on the first reflection from the sphere wall. Thus, to increase the efficiency of this sphere, the specular component of the first reflection must be kept in the sphere; on the other hand, it must be kept away from the detector's sensitive area, since slight variations in image placement would yield large changes in detector response. Appendix C considers this device further.

Next, figure 17 shows the data for Crystex brand sulfur, which was hand pressed onto the sphere wall. These data have a spread of 0.6 percent in R/R_o and illustrate the usefulness of sulfur for an averaging sphere coating; however, the application technique yielded a surface that was extremely fragile and whose reflectance probably varied significantly over the sphere wall. Thus, other methods were tried to obtain a more uniform and mechanically durable surface. First, the gold sphere previously tested above was coated with a very thin coat of Crystex sulfur, which was applied by suspending the sulfur in alcohol and spraying it on with a paint spray gun. The results of the area sensitivity test indicate a change in R/R_o of 1.1 percent. Further, the efficiency of this sphere was nearly the same as the hand-pressed sulfur sphere. Since the efficiency was the same, and R/R_o showed a greater change than the hand-pressed sulfur sphere, it was decided to try spraying on a $\frac{1}{8}$-inch thick coat of sulfur on the sphere wall. This sphere exhibited the same change in R/R_o as the hand-pressed sphere and was less fragile. To further reduce changes in R/R_o, two different methods of shielding the detector viewing area were tried. This is useful, because the detector does not

view the entire sphere equally well, as illustrated by its angular sensitivity in figures 14 and 15. The primary function of a shield is to prevent the detector from viewing the first reflection of the incident energy on the sphere wall for all image configurations. The first shield, which is illustrated in figure 18a, was a 0.15-inch thick disk placed over the detector with a $\frac{1}{2}$-inch diameter hole centered over the detector sensing area. The sides of this hole were coated with Parson's black and thus restricted the detector's field of view. The results are presented in the second to last graph in figure 17 and indicate an over-all range in R/R_o of 0.6 percent for an area ratio spread twice as large as for the hand-pressed sphere.

The second shield tested is shown in figure 18b. This shield was tried because it yields a higher detection efficiency, since it only restricts the detector viewing field in the direction of the image on the sphere wall. The shield was constructed of 0.005-inch thick polished platinum. The data for this sphere are plotted in the last graph of figure 17 and show a 0.4 percent variation in R/R_o.

Thus, this test indicates that either of the spheres with detector shields are usable at 2.4 μ.

These two spheres were then tested at the wavelengths at which the ellipsoidal mirror takes data. The results for the platinum shield (shield 2) are given in figure 19. Note that the scale of the graphs for the longer wavelengths is smaller. This figure shows that at the longer wavelengths, where sulfur's reflectance is lower, R/R_o decreases by as much as 2.8 percent. This could be caused by (1) by the incident flux becoming trapped between the platinum shield and the sulfur wall (this would be more pronounced at the longer wavelengths, because the

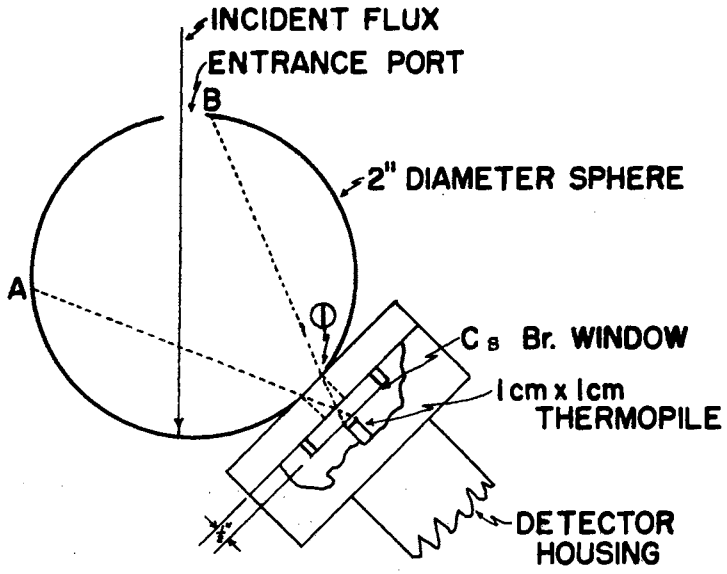

A-B IS FIELD OF VIEW FOR THE DETECTOR

① BLACKENED .15" SHIELD

a) EXTERNAL SHIELD

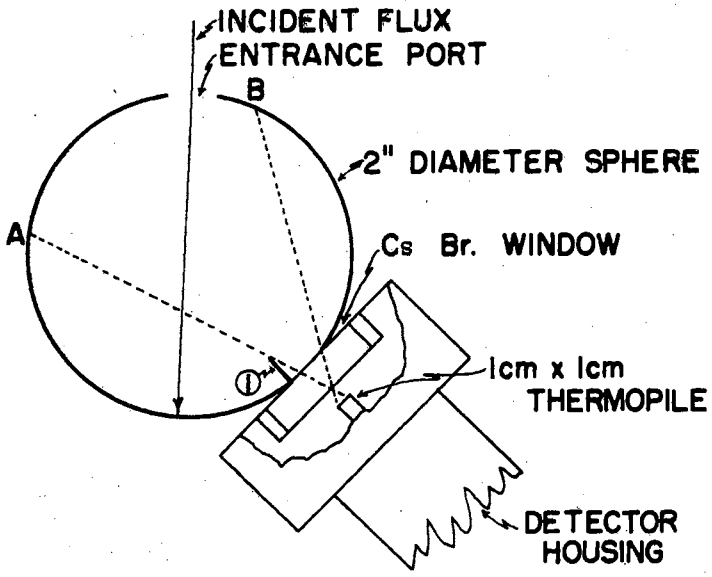

A-B IS FIELD OF VIEW FOR THE DETECTOR

① POLISHED PLATINUM SHIELD

b) INTERNAL SHIELD

Figure 18. Shield Configurations for Averaging Spheres

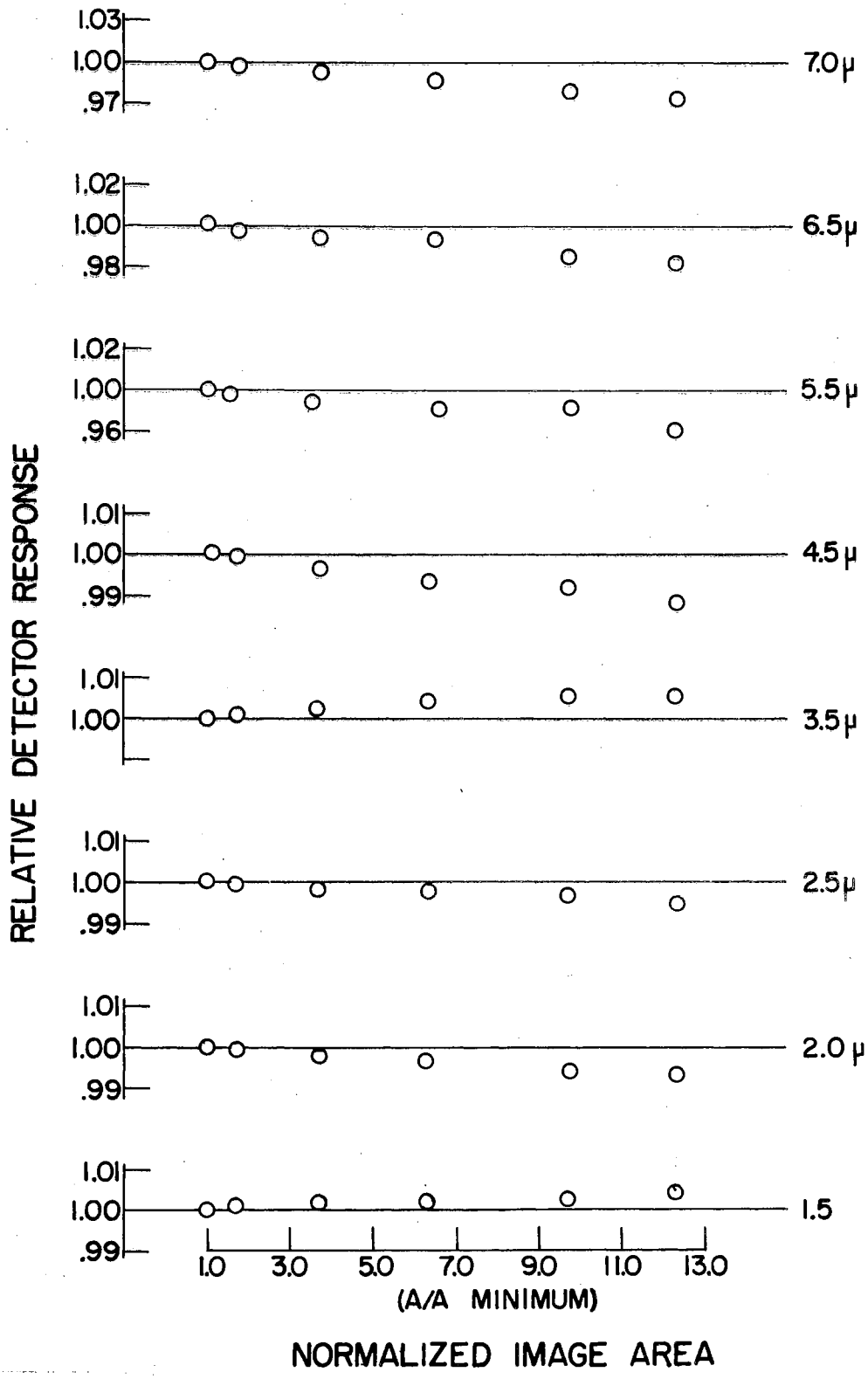

Figure 19. Area Sensitivity Test Results for the Internal Shield

reflectance of the sulfur wall is lower), or (2) by atmospheric absorption in the increased path length due to water and CO_2 in the atmosphere. Such atmospheric absorption is not probable, since the wavelengths used were between the absorption bands (the results in figure 20 for the sphere with the circular disk shield substantiate this conclusion).

Since the change in R/R_o for the sphere with the platinum shield was quite large at the longer wavelengths, the sphere configuration using the circular disk was also tested at these wavelengths.* The results of the tests for variation of response with image size are given in figure 20. These results show an increase in detector sensitivity with image size, indicating that part of the flux is still reaching the detector on the first reflection for large images. However, the change in R/R_o is limited to 1.5 percent for the longest wavelength. The reason that the change of R/R_o varies with wavelength is that the reflectance of sulfur varies with wavelength. At low sphere wall reflectance (i.e., long wavelengths for sulfur), the flux from the first reflection is a major portion of the flux in the sphere, and if the detector views even a very small amount of this flux (which is the case for large images on the sphere wall), there is a significant increase in detector response. This can be eliminated by increasing the thickness of the shield in figure 18a; however, this will reduce the efficiency of the sphere, which is intolerable, since the detection electronics are already at their limits for accurate readings at 6.5 and 7.0 μ.

---

*Since the previous tests, this sphere had been recoated with sulfur sprayed from a benzene suspension, which yielded a surface that was more mechanically stable than the alcohol suspension sprayed surfaces.

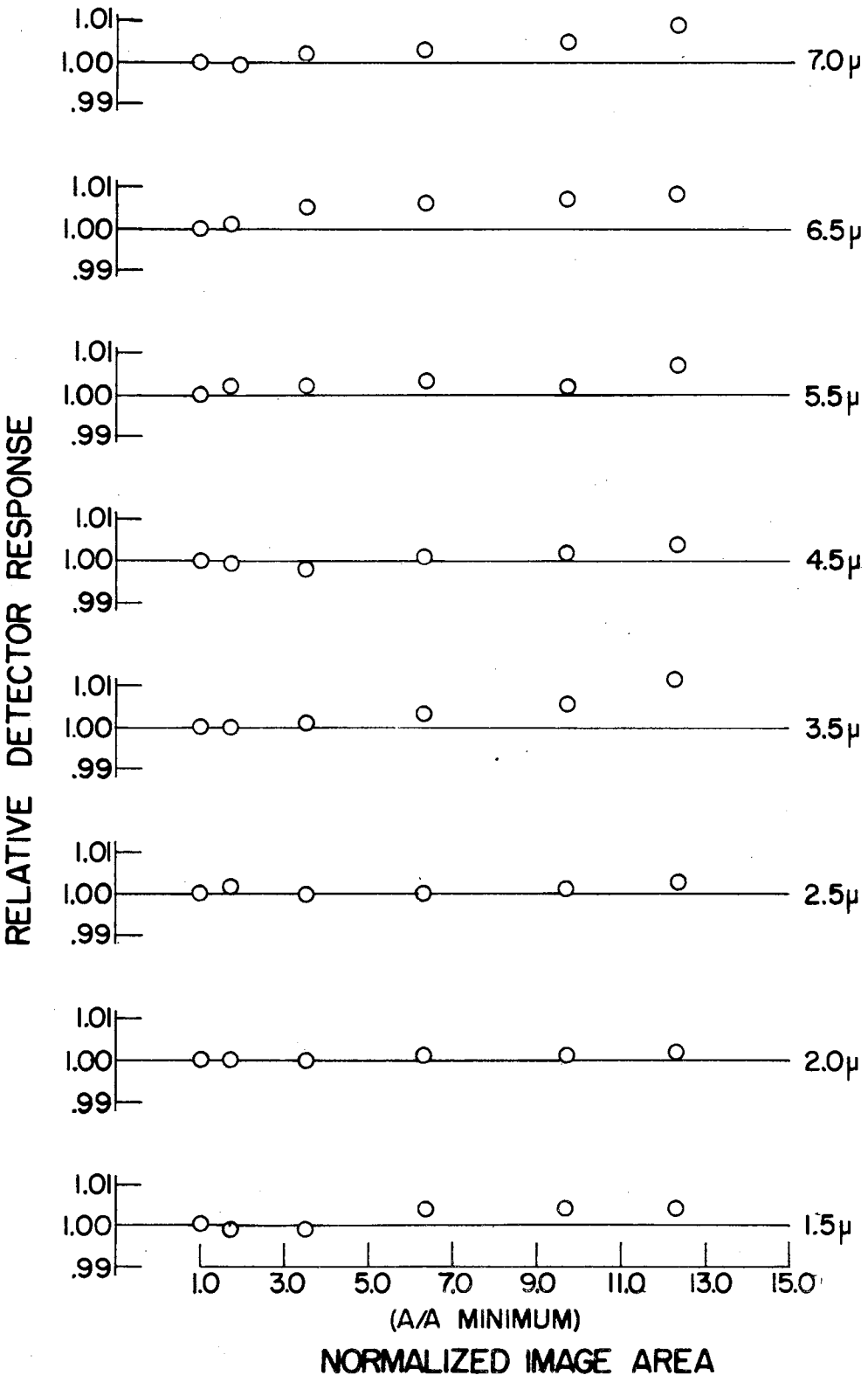

Figure 20. Results of Area Sensitivity Test for External Shield

The conclusions from this series of tests are that a sulfur sphere with the circular disk shield provides a good averaging device for signals of varying image size.

Further, the results of figure 20 illustrate that path length changes of 7 inches do not affect the readings, thus it can be assumed that the selected wavelengths and corresponding band passes can be utilized for taking absolute data with the ellipsoidal reflectometer.

(B.2). Spatial Sensitivity (Test No. 2):

This test was designed to illustrate required precision of incident image placement for comparing two signals of nearly the same image area. The sphere entrance was traversed across the incident beam, which was focused on the sphere entrance.

The results for the sulfur sphere with the platinum shield are presented in figure 21. The data are arbitrarily normalized to one of the central readings and plotted versus position on the entrance hole to the sphere as measured from one edge. These data show variations exceeding 2 percent for the longer wavelengths.

Results for the sphere with the circular disk shield show variations of less than 0.4 percent for the wavelengths below 5.5 μ and variations of about 0.8 percent for the longer wavelengths (figure 22). This again illustrates the effect of the first reflected flux, since at the long wavelengths, where the reflectance of sulfur is lower, the detector signal is higher for images between positions 0.4 and 0.6 on the entrance port of the sphere, which is where more of the first reflection could reach the detector (left hand side of sphere opening in figure 18a).

The results of these tests indicate that for short wavelengths, the position of the incident flux on the entrance to the sphere is not too critical, while at longer wavelengths, more care must be taken in

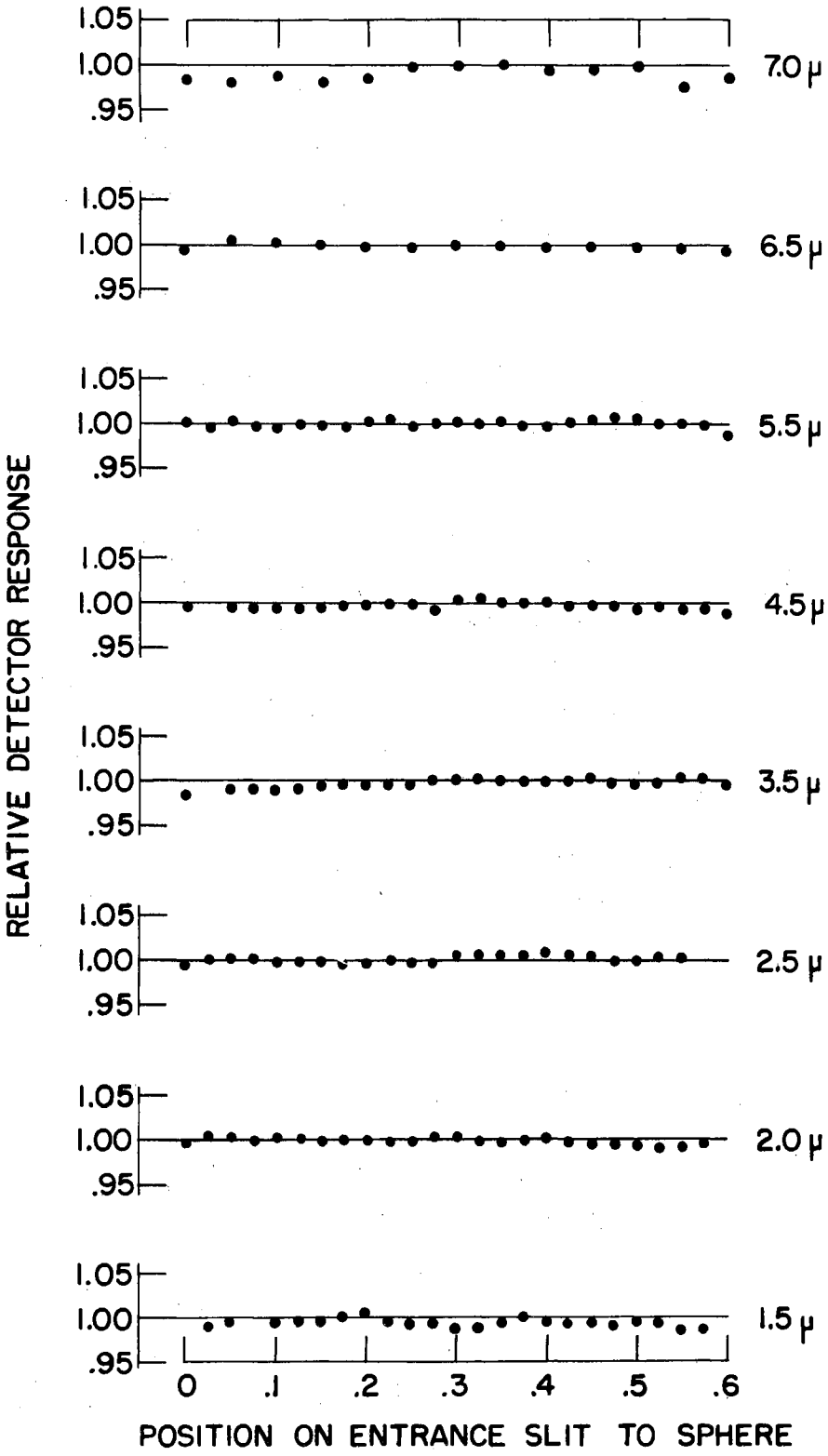

Figure 21. Results of Spatial Sensitivity Test for the Internal Shield

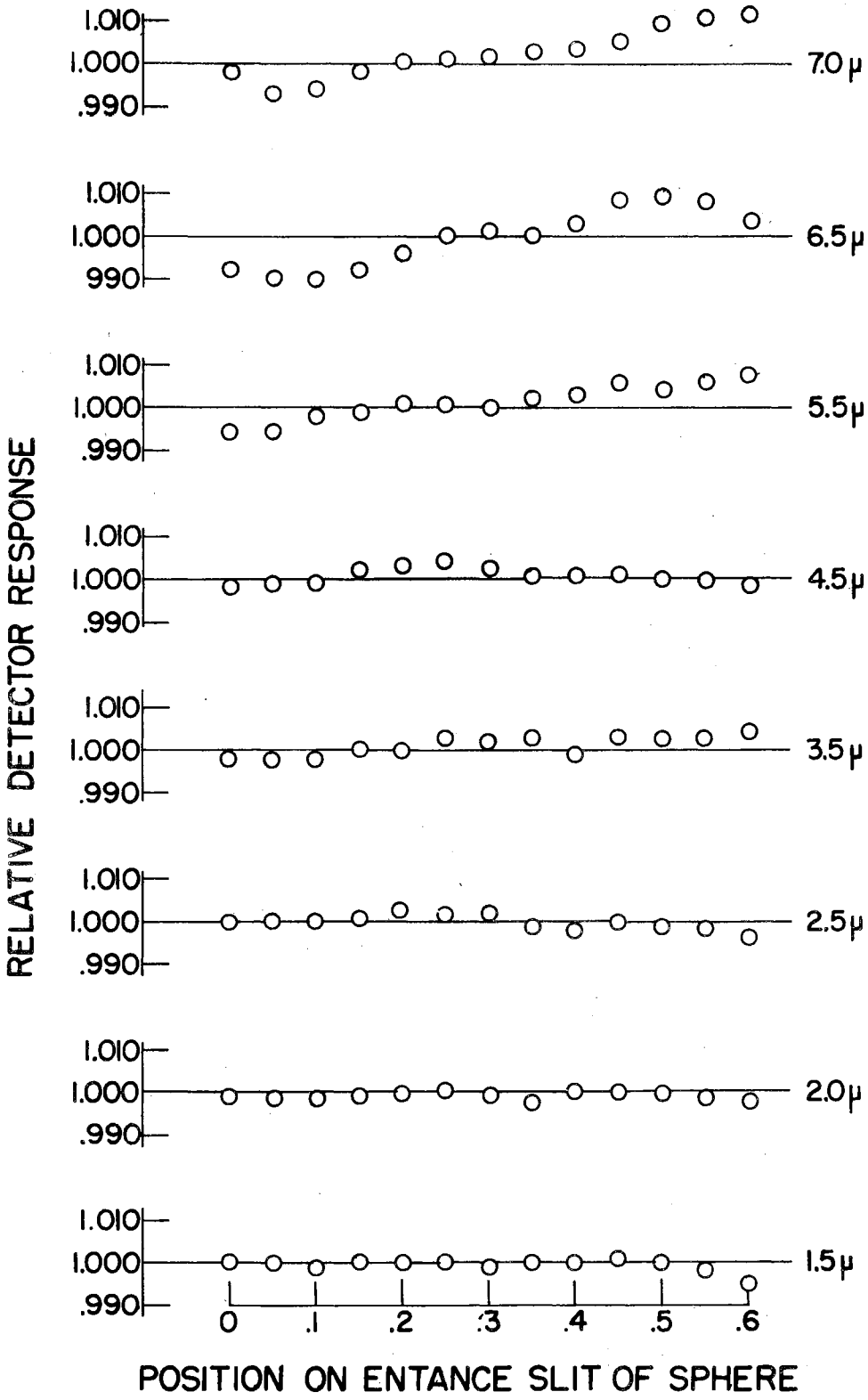

Figure 22. Results of Spatial Sensitivity Test for the External Shield

positioning the incident beam. Further, the results of these measurements were utilized in the design of a simple infrared specular reflectance instrument (appendix B).

SUMMARY

From the results established in this chapter, it can be stated that the use of an averaging sphere can be extended at least to 7 microns by use of sulfur as a sphere wall coating. Further, the inherent advantages of this approach are (1) the ability to accept images of varying size by use of a large entrance port and to measure accurately the total flux contained in the various incident fluxes, (2) the ability to collect the aberrant portions of the image that would miss even large area detectors, and (3) a reduction in the required precision of optical alignment of the instrument. In addition, the use of this device will increase the accuracy of the ellipsoidal reflectometer. The major disadvantage is the reduction (by about 90 percent) of the flux that reaches the detector.

CHAPTER IV

ANALYSIS OF AN ELLIPSOIDAL MIRROR REFLECTOMETER*

The results reported in chapter III indicate that the use of a sulfur coated averaging sphere with the detector will allow precise measurement of all the fluxes needed to accurately establish reflectance with the ellipsoidal mirror reflectometer. This chapter deals with the analysis of an ellipsoidal mirror reflectometer for both absolute and relative spectral reflectance measurements. The derivations of the reflectance equations in this chapter are, for the most part, applicable to any ellipsoidal mirror reflectometer. A few of the simplifying assumptions are based on experimental measurements with the particular ellipsoidal mirror used in this work. However, these assumptions appear to be very general in nature.

Two related analyses of the reflectometer are presented in this chapter: (1) The analysis of the absolute measurement of the reflectance $\rho(7°,\theta)$ by directly measuring the incident flux and the reflected flux, and (2) the analysis of the relative (or comparison) reflectance measurement, where a calibrated mirror is used as the reflectance standard (see appendix B).

In the derivations for both absolute and relative reflectances, two types of flux quantities are considered: (1) Primary and (2) secondary.

---

*A detailed list of terms used throughout this chapter is included at the end of this chapter.

The primary fluxes are those fluxes that comprise the largest portions of the incident or reflected flux, while the secondary fluxes are very small fluxes compared to the incident or reflected flux (usually less than 1 percent). The purpose of this distinction is to allow for very accurate correction of the large fluxes with the best possible techniques, and to allow simplified (although only moderately accurate) corrections to be made to the secondary fluxes. This is based on the fact that corrections to terms comprising only 1 percent of the total flux can be in error by 50 percent and cause only a ½ percent error in the total flux, while corrections to the primary fluxes must be more accurate that the desired accuracy of the final answer. There are some intermediate fluxes lying between these two extremes which should be corrected on the basis of their maximum possible effect on the final answer. Throughout the following derivation only the secondary fluxes will be specifically denoted, all other fluxes are considered to be primary or intermediate Further, it should be noted that the approach outlined in this chapter is designed to obtain systematic information about the distribution of the flux in the reflectometer. Since the distribution obtained in this manner is dependent on tacit assumptions about the distribution of flux reflected from the sample, it is apparent that any analysis of errors will have to deal with the most probable maximum deviations from the assumptions used in these derivations. Appendix G provides this type of error analysis for the particular reflectometer configuration utilized in this work. Appendices F and H provide system calibration techniques and experimental reflectance data.

Absolute Measurement of Reflectance

An absolute reflectance measurement is made by making two basic measurements; one of the incident flux F_I, and the other of the reflected flux F_R. Since neither of these measurements is as straightforward as would be desired, they will be discussed separately.

Incident Flux (F_I): To measure the incident flux, the detector is placed at (or near) the first focal point of the ellipsoidal mirror (figure 23). A major problem with this measurement is that some flux is back-reflected by the entrance port of the averaging sphere; some of this flux returns to the ellipsoidal mirror and is again reflected into the sphere, thus increasing the flux in the sphere that is read by the detector. This interchange was eliminated by placing a black shield 1½ inches above the sphere port, with a hole just large enough to admit the incident beam. With this procedure the flux incident on the detector is

$$F_{ID} = F_I \eta \tag{9}$$

where η if the efficiency of the averaging sphere, which for a given sphere configuration is a function only of the sphere coating's reflectance.

Reflected Flux (F_R): Figure 24 illustrates the flux balance for the flux reflected by the sample. The flux absorbed by the mirror is denoted by F_α, the flux lost through the entrance hole is denoted by F_H. The flux scattered by the wire sample supports is $(\overline{\rho}_\epsilon)_W F_W$*, while the flux lost due

*$(\overline{\rho}_\epsilon)_X$ is the average effective reflectance of the ellipsoidal mirror for the given distribution of F_X on the mirror.

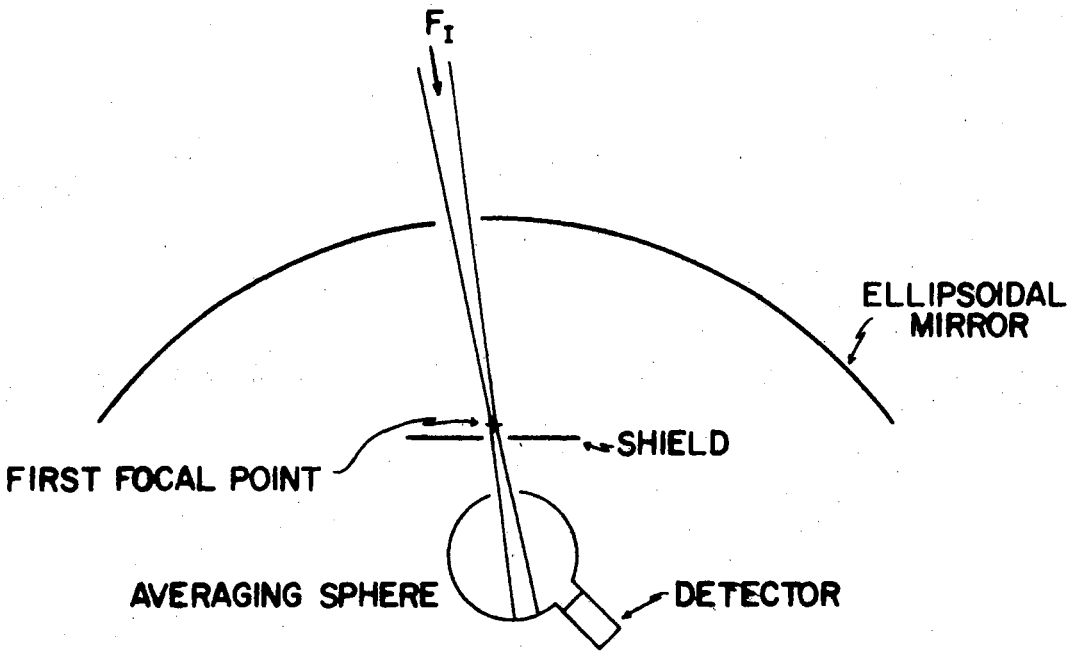

Figure 23. Direct Measurement of the Incident Flux

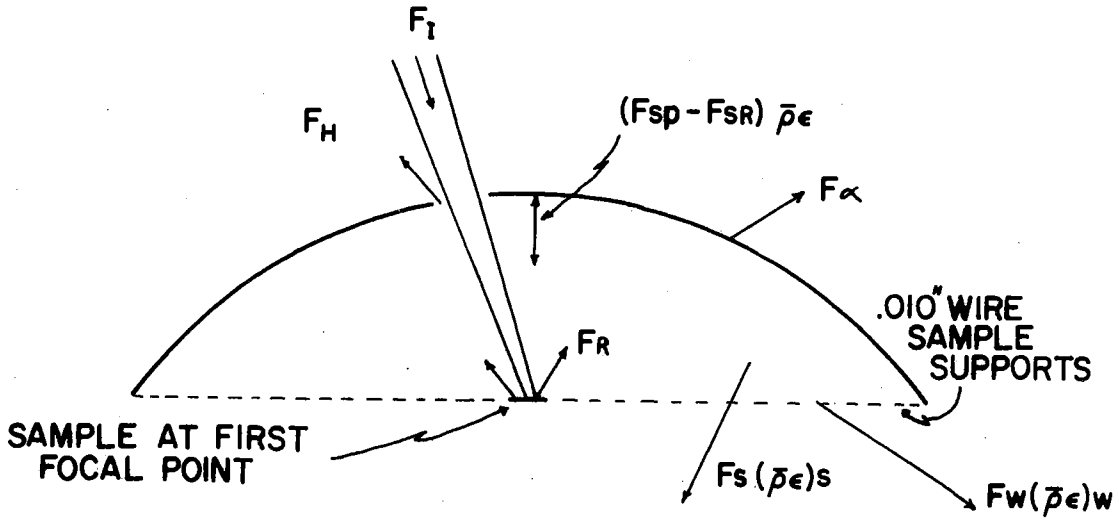

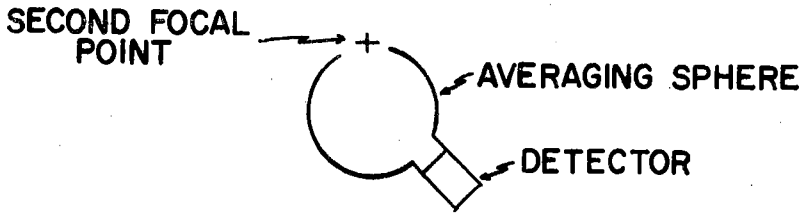

Figure 24. Measurement of the Reflected Flux and Definition of the Four Basic Fluxes

to shading of the detector by the sample is $\overline{\rho}_e[F_{SP} - F_{SR}]$.* The flux crossing the first focal plane is $(\overline{\rho}_e)_S F_S$. Thus, the total flux reflected by the sample is:

$$F_R = F_S + F_W + [F_{SP} - F_{SR}] + F_H \tag{10}$$

where F_W and F_{SR} are secondary fluxes. Depending on the distribution of the reflected radiation, the fluxes F_H and F_{SP} may be secondary fluxes; however, they will be treated as intermediate fluxes, since, in general, they are considerably larger than fluxes F_W and F_{SR}. All the fluxes in equation (10) are defined on the basis of the flux leaving the sample.

To aid in establishing the quantities in equation (10), the following fluxes are defined (figure 25):

(1). F_S is defined, as above, as being the flux crossing the first focal plane divided by the ellipsoidal mirror's average effective reflectance for the particular distribution of F_S on the mirror $(\overline{\rho}_e)_S$.

(2). F_{S1} is defined as the flux crossing the first focal plane divided by the mirror's average effective reflectance $(\overline{\rho}_e)_{S1}$ for the case when the A_{SH} shield is placed in the first focal plane.

(3). F_{S2} is defined as the flux crossing the first focal plane divided by the average effective reflectance $(\overline{\rho}_e)_{S2}$ of the outer edges of the ellipsoidal mirror for the case where shield S2 is in the first focal plane.

(4). F_D is defined as the flux crossing the first focal plane divided by the mirror's average effective reflectance $(\overline{\rho}_e)_D$ when shield D is in place.

---

*$\overline{\rho}_e$ is the average effective reflectance of the central part of the ellipsoidal mirror, which varies by less than 0.2 percent as given in appendix F. The effective reflectance is defined in appendix F.

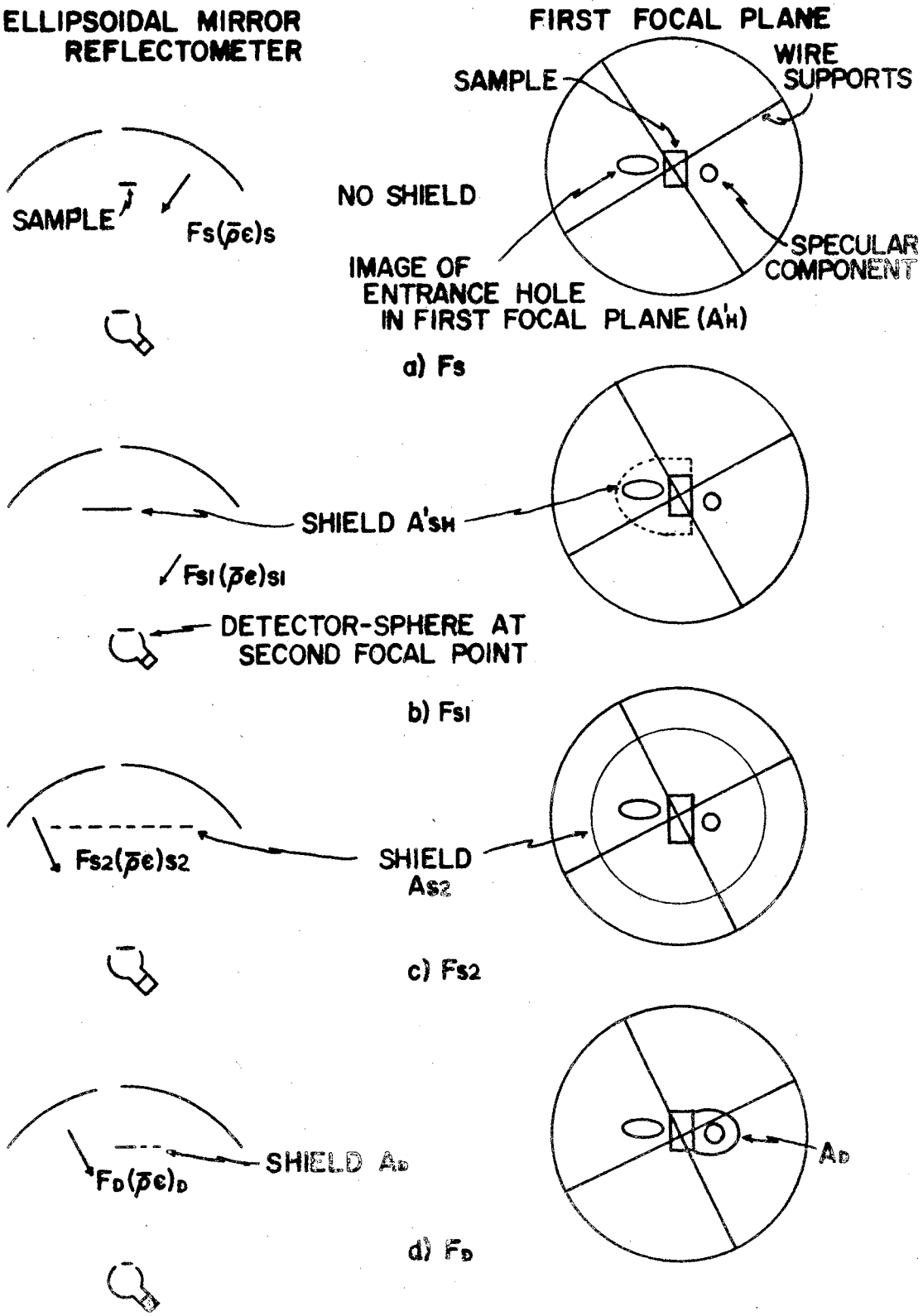

Figure 25. System Configuration for Definition of the Basic Fluxes F_S, F_{S1}, F_{S2}, and F_D.

It is possible to establish all the defined fluxes one by one and then complete the flux balance for the reflected flux. After that it is then necessary to relate the defined fluxes (F_S, F_{S1}, F_{S2}, F_D) to those fluxes viewed by the detector (F_{SD}, F_{S1D}, F_{S2D}, and F_{DD}), which views a portion of the averaging sphere.

Mirror Loss (F_α): The ellipsoidal mirror will absorb some of the reflected flux F_R. Further, if the ellipsoidal mirror has a poor surface finish and/or a partially transmitting mirror coating, the mirror may transmit some of F_R and/or scatter some of the reflected flux (i.e., $F_R\rho_e$, where ρ_e is the true reflectance of the coating) away from the second focal point. Thus, it is necessary to know the effective reflectance ρ_e' of the ellipsoidal mirror. The effective reflectance of the ellipsoidal mirror is defined as the ratio of the flux that reaches a predefined area (i.e., the entrance port to the averaging sphere) at the second focal plane to the flux incident on the ellipsoidal mirror from a defined area in the first focal plane (i.e., the illuminated area of the specimen). By this definition, the absorbed flux, $(1 - \rho_e')$, includes flux lost by scattering of the ellipsoid, absorption by the ellipsoid, transmission by the ellipsoid, and any optical aberrations in the ellipsoidal mirror. This reflectance was measured for the particular ellipsoid used in this work, and the effective reflectances of the mirror as a function of position on the mirror are reported in Appendix F. These values indicate that the mirror reflects better (by about 1.5 percent) near its edges than at the apex of the ellipsoid. Thus, the portion of flux reflected by this part of the mirror should be individually corrected for mirror reflectance. The use of the previously defined flux F_{S2} allows this individual correction to be made, since this is the flux

that is incident on the higher reflecting edges of the ellipsoidal mirror. The average effective reflectance for each of the four defined fluxes is

$$(\overline{\rho}_e)_S = \frac{(F_S - F_{S2})\overline{\rho}_e + F_{S2}(1.015)\overline{\rho}_e}{F_S} \tag{11}$$

$$(\overline{\rho}_e)_S = \overline{\rho}_e\left(1 + \frac{F_{S2}}{F_S}(0.015)\right) \tag{11a}$$

$$(\overline{\rho}_e)_{S1} = \frac{(F_{S1} - F_{S2})\overline{\rho}_e + F_{S2}(1.015)\overline{\rho}_e}{F_{S1}} \tag{12}$$

$$(\overline{\rho}_e)_{S1} = \overline{\rho}_e\left(1 + \frac{F_{S2}}{F_{S1}}(0.015)\right) \tag{12a}$$

$$(\rho_e)_D = \frac{(F_D - F_{S2})\rho_e + F_{S2}(1.015)\rho_e}{F_D} \tag{13}$$

$$(\overline{\rho}_e)_D = \overline{\rho}_e\left(1 + \frac{F_{S2}}{F_D}(0.015)\right) \tag{13a}$$

and from appendix F (14)

$$(\overline{\rho}_e)_{S2} = 1.015\ \overline{\rho}_e$$

where $\overline{\rho}_e$ is the average effective reflectance of the central part of the ellipsoidal mirror (i.e., assumed to be the effective reflectance of point 3 in figure 44).

Since F_{S2} is the only flux corrected for changes in the reflectance of the ellipsoidal mirror with positions of incidence on the mirror, the approximate magnitude of F_α is

$$F_\alpha = [F_S - F_{S2}](1 - \overline{\rho}_e) + F_{S2}(1 - \overline{\rho}_e(1.015)) \tag{15}$$

$$F_\alpha = F_S[1 - \overline{\rho}_e] - F_{S2}(0.015)\overline{\rho}_e \tag{15a}$$

Note that the mirror actually absorbs slightly more flux than is indicated in equation (15), but these additional amounts are accounted for in the wire loss correction and the sample shading correction.

Hole Loss (F_H): The use of the defined fluxes F_S and F_{S1}, as shown in figure 26, allows the flux density around the entrance hole on the ellipsoidal mirror to be calculated, where

$$F_{SH} = F_S - F_{S1} \tag{16}$$

is the flux incident on the area A_{SH}, where A_{SH} is the area on the ellipsoidal mirror projected from the second focal point of A'_{SH} in the first focal plane. Thus, the average flux density around the entrance hole is

$$\frac{F_{SH}}{A_{SH} - A_H} \tag{17}$$

A good assumption about the flux on the area $A_{SH} - A_H$ is that its distribution is sufficiently uniform that the correction for the flux lost through the entrance hole A_H, which is centered on the area A_{SH}, can be made on the basis that the average flux density over A_H is the same as the average flux density over $A_{SH} - A_H$. With this assumption, the hole loss is

$$F_H = \frac{A_H F_{SH}}{A_{SH} - A_H} \tag{18}$$

or in terms of the defined fluxes, the hole loss is

$$F_H = \frac{A_H(F_S - F_{S1})}{A_{SH} - A_H} \tag{19}$$

The assumption of uniform intensity over the small solid angle subtended by A_{SH} is more accurate and reasonable than the assumption of uniform intensity over the hemisphere made in almost all the methods reviewed in chapter I. A specific surface for which this correction F_H would be seriously in error is the diffraction grating with a reflection lobe directly out the hole.

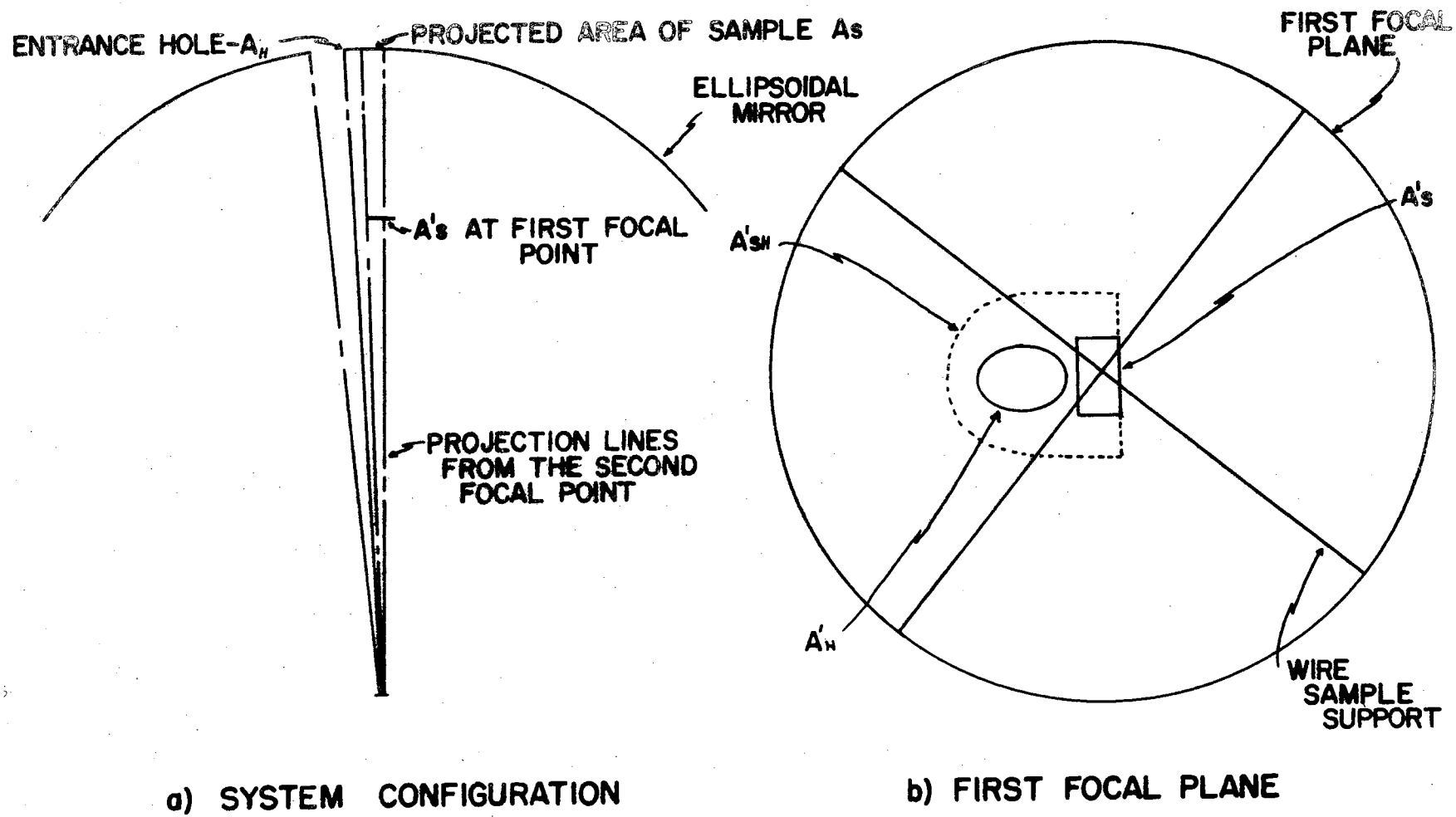

Figure 26. Illustration of Shields and Areas Involved in the Correction for the Hole Loss (F_H).

Wire Loss (F_W): Some of the flux reflected by the sample and re-imaged by the ellipsoidal mirror toward the second focal point is absorbed by the wire sample supports. The amount absorbed by the wire ($F_W(\overline{\rho}_\epsilon)_W$) can be established in the following manner. First, it should be noted that the sample is oriented so that the specular component of reflection does not hit any of the wire supports. That is, only a part of the nonspecular component of the reflected flux is blocked by the wires. Therefore, if a shield (of area A_D) were constructed to block out the flux about the specular component, then one could measure the non-specularly reflected flux. This may be assumed to be uniformly distributed over the area (A_ϵ) of the first focal plane of the ellipsoidal mirror. Then a knowledge of the area A_ϵ over which the energy is distributed and the cross-sectional area of the wires allows the calculation of F_W.

$$(\overline{\rho}_\epsilon)\ F_W = F_D \frac{A_W}{A_\epsilon}(\overline{\rho}_\epsilon)_D \tag{20}$$

where

$$A_\epsilon = \frac{\pi D_\epsilon^2}{4} - A_D \tag{20a}$$

where D_ϵ is the diameter of the opening of the ellipsoidal mirror in the first focal plane, and A_D is the area of the shield used to eliminate the specular component. This equation reduces to

$$F_W = F_D \frac{A_W}{A_\epsilon} \tag{21}$$

since $(\overline{\rho}_\epsilon)_W \equiv (\overline{\rho}_\epsilon)_D$ when F_D is evenly distributed over the area A_ϵ.

It should be noted that the absorptance of the wire supports was not included in equation (21); this is because the wires are specular reflectors and any flux striking them is reflected out of the optical path between the first and second fical points and therefore is entirely lost to the system. Since F_W is a secondary correction, it is apparent that the assumption that average flux density over the first focal plane is intercepted by wire supports (except at the specular peak) is sufficiently accurate, especially since the wire supports comprise two diameters of the circle D_e and the wire loss is distributed about the area A_e rather than at one specific point, as is the case for the hole loss.

Sample Loss (F_{SP} and F_{SR}): Some of the reflected flux is shielded by the sample from the detector at the second focal point (figure 27); however, not all of this flux that strikes the sample is completely prevented from reaching the detector, since any of the reflected flux incident on the specimen in the area A'_{S1} (the image on the first focal plane of the sphere entrance port at the second focal point) may be multiply reflected by the sample and ellipsoidal mirror to the second focal point and into the averaging sphere. To make the correction for these losses, the three defined fluxes F_D, F_S, and F_{S1} will be needed. The flux that is involved in these losses is that which strikes the ellipsoidal mirror on the projected area of the sample A_S. (This area is projected from the second focal point.) From figure 26 it is seen that A_S is partially surrounded by the shield A_{SH}, and will have approximately the same flux density as that on A_{SH}. Therefore, the total flux loss would be (from equation 17)

$$F_{SP} = \frac{A_S F_{SH}}{A_{SH} - A_H} \tag{22}$$

if all of the flux within the area A_S on the ellipsoidal mirror were lost.

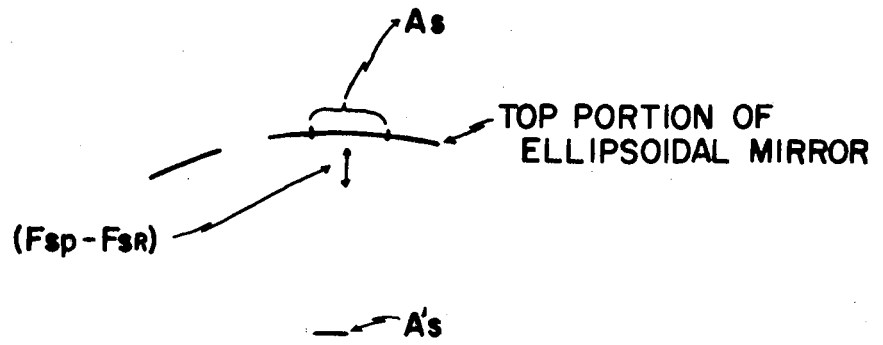

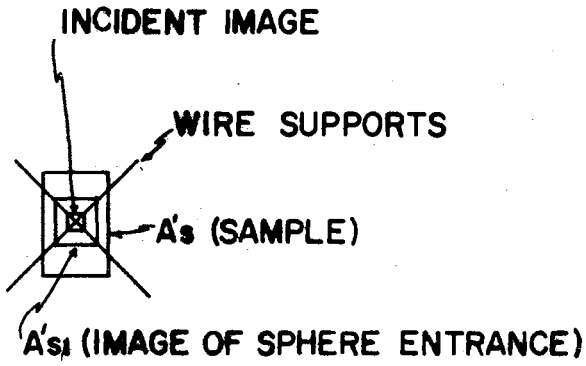

Figure 27. Illustration of Sample Loss Terminology.

However, of the flux F_{SP}, a portion A_{S1}/A_S (where A_{S1} is projected area on the ellipsoid of A'_{S1}) is reflected from the sample so that it could reach the detector, since any flux leaving the sample from the area A'_{S1} can reach the detector. The question is how much of this reflected flux reaches the detector. It is reasonable to assume that the sample has the same non-specular component for flux incident from 7° to the normal as for normally incident flux. Further, it is this non-specular component of the flux reflected from the area A'_{S1} which will reach the detector; thus, it is apparent that of the flux striking the sample for the second time, the amount

$$\frac{A_S F_{SH}}{A_{SH} - A_H}\left[\frac{A_{S1}}{A_S}\right]\left[\frac{F_D}{F_S}\right]\rho_S \bar{\rho}_\epsilon^2\left[\frac{A_\epsilon - A_W}{A_\epsilon}\right] \tag{23}$$

reaches the detector. The amount

$$\left[\frac{A_S F_{SH}}{A_{SH} - A_H}\right]\left[\frac{F_S - F_D}{F_S}\right]\rho_S \bar{\rho}_\epsilon \tag{24}$$

is reflected back into the area A_S on the ellipsoidal mirror. This flux is then reflected back to the sample, where again part of the flux $[A_{S1}/A_S]$ is reflected toward the detector. The amount that reaches the detector on the third reflection from the sample is

$$\left[\frac{F_{SH}(A_S)}{A_{SH} - A_H}\right]\left[\frac{A_{S1}}{A_S}\right]\left[\frac{A_\epsilon - A_W}{A_\epsilon}\right]\left[\frac{F_S - F_D}{F_S}\right]\rho_S^2 \bar{\rho}_\epsilon^3\left[\frac{F_D}{F_S}\right] \tag{25}$$

Further, the amount of flux reaching the detector after the "nth" reflection from the sample is

$$\left[\frac{(A_S) F_{SH}}{A_{SH} - A_H}\right]\left[\frac{A_{S1}}{A_S}\right]\left[\frac{F_D}{F_S}\rho_S \bar{\rho}_\epsilon^2\right]\left[\frac{A_\epsilon - A_W}{A_\epsilon}\right]\left[\rho_S \bar{\rho}_\epsilon\left(\frac{F_S - F_D}{F_S}\right)\right]^{n-1} \tag{26}$$

Therefore, F_{SR} of the flux F_{SP} in equation (22) reaches the sphere port where

$$F_{SR} = \sum_{n=1}^{\infty} \left[\frac{F_{SH}(A_{S1})}{A_{SH} - A_H}\right]\left[\frac{F_D}{F_S}\rho_S\bar{\rho}_\epsilon^{\,2}\right]\left[\frac{A_\epsilon - A_W}{A_\epsilon}\right]\left[\rho_S\bar{\rho}_\epsilon\frac{F_S - F_D}{F_S}\right]^{n-1} \tag{27}$$

which sums to

$$F_{SR} = \left[\frac{F_{SH}(A_{S1})}{A_{SH} - A_H}\right]\left[\frac{F_D}{F_S}\rho_S\bar{\rho}_\epsilon\left(\frac{A_\epsilon - A_W}{A\epsilon}\right)\right]\frac{1}{1 - \rho_S\bar{\rho}_\epsilon\left(\frac{F_S - F_D}{F_S}\right)} \tag{28}$$

Thus, the total effect of the sample shielding the detector is

$$F_{SP} - F_{SR} = \frac{F_S - F_{S1}}{A_{SH} - A_H}\left[A_S - A_{S1}\left(\frac{F_D}{F_S}\rho_S\bar{\rho}_\epsilon^{\,2}\right)\left(\frac{A_\epsilon - A}{A_\epsilon}\right)\left(\frac{1}{1 - \rho_S\bar{\rho}_\epsilon\left(\frac{F_S - F_D}{F_S}\right)}\right)\right]$$

This completes the calculation of the individual losses. The foregoing provide a basis for calculating F_R as given in equation (10).

$$F_R = F_S + F_H + F_W + (F_{SP} - F_{SR}) \tag{30}$$

Upon substitution of equations (15), (19), (21), and (29) into equation (30), F_R, in terms of the defined fluxes, sample reflectance and system constants, is given by

$$\begin{aligned} F_R = {} & F_S + \left(\frac{F_S - F_{S1}}{A_{SH} - A_H}\right)A_H \\ & + \frac{F_D A_W}{A_\epsilon} + \frac{F_S - F_{S1}}{A_{SH} - A_H}\left[A_S - A_{S1}\left(\frac{F_D}{F_S}\rho_S\bar{\rho}_\epsilon^{\,2}\left[\frac{A_\epsilon - A_W}{A_\epsilon}\right]\left[\frac{1}{1 - \rho_S\bar{\rho}_\epsilon\left(\frac{F_S - F_D}{F_S}\right)}\right]\right)\right] \end{aligned} \tag{31}$$

Measurement of Fluxes

Now the defined fluxes F_S, F_{S1}, F_{S2}, and F_D must be evaluated in terms of the flux that the detector views. First F_S will be considered. The measurement of these quantities is complicated because the "detector"

is not black; that is, the sphere entrance port back-reflects flux into the optical path, which gets back into the sphere and increases the flux sensed by the detector. Specifically for the F_S measurement, the flux $(\overline{\rho}_\epsilon)_S F_S$ is the desired quantity entering the sphere port. However, some η' of this flux is reflected out of the sphere entrance port where η' is the ratio of F_1 (the back-reflected flux) to $(\overline{\rho}_\epsilon)_S F_S$. This flux is reflected nearly diffusely so that $f_{S-\epsilon}\ \eta' F_S (\overline{\rho}_\epsilon)_S$ is intercepted by the ellipsoidal mirror and refocused on the sample at the first focal point.* The sample then reflects this flux back to the ellipsoidal mirror, which then refocuses it onto the sphere entrance. Thus, an amount F_S' is added to the flux $F_S(\overline{\rho}_\epsilon)_S$ that was originally incident on the sphere port

$$F_S' = \rho_{HS}\ \overline{\rho}_{\epsilon D}^{\,2}\ \eta'\ f_{S-\epsilon}\ [\ F_S(\overline{\rho}_\epsilon)_S\ ] \tag{32}$$

where $\overline{\rho}_{\epsilon D}$ is the average effective reflectance of the ellipsoidal mirror for flux coming diffusely from the sphere entrance at the second focal point and ρ_{HS} is the hemispherical reflectance of the sample (chapter I). Further, of the flux F_S' that reaches the sphere entrance on the second pass, the amount

$$F_S'' = \rho_{HS}\ \overline{\rho}_{\epsilon D}^{\,2}\ \eta'\ f_{S-\epsilon}\ F_S' \tag{33}$$

is added to the flux in the sphere in the same manner as F_S' was added. This continues until the total flux in the sphere is

$$F_{SS} = (\overline{\rho}_\epsilon)_S F_S[1 + \rho_{HS}\overline{\rho}_{\epsilon D}^{\,2}\eta' f_{S-\epsilon} + [\rho_{HS}\overline{\rho}_{\epsilon D}^{\,2}\eta' f_{S-\epsilon}]^2 . . . . .] \tag{34}$$

which, since $\rho_{HS}\ \overline{\rho}_{\epsilon D}^{\,2}\ \eta'\ f_{S-\epsilon} < 1$ sums to

---

*$f_{S-\epsilon}$ is the standard diffuse configuration factor as defined in reference 4.

$$F_{SS} = (\overline{\rho}_\epsilon)_S F_S \left[\frac{1}{1 - \rho_{HS}\, \overline{\rho}_{\epsilon D}{}^2\, \eta'\, f_{S-\epsilon}} \right] \tag{35}$$

Thus, the flux viewed by the detector is

$$F_{SD} = \eta(\overline{\rho}_\epsilon)_S\, F_S \left[\frac{1}{1 - \rho_{HS}\, \overline{\rho}_{\epsilon D}{}^2\, \eta'\, f_{S-\epsilon}} \right] \tag{36}$$

Several simplifying assumptions are made in the foregoing discussion:

(1). $\overline{\rho}_{\epsilon D}$ is the same for the flux leaving the second focal point and going to the first focal point as for the flux leaving the first focal point and going to the second focal point. Further it is logical to assume that $\overline{\rho}_{\epsilon D} = (\overline{\rho}_\epsilon)_D$.

(2). The loss of flux due to the shading of the ellipsoidal mirror by the sample and sample holder is accounted for in the calculation of $f_{S-\epsilon}$. Further, the loss due to the entrance hole is also taken into account during the calculation $f_{S-\epsilon}$.

(3). After the energy is re-reflected by the sample back to the ellipsoid, the losses due to shading of the sphere port by the sample, sample holder, and entrance hole are neglected.

Assumption (2) involves no error, since it just specifies the method of calculation for $f_{S-\epsilon}$. Assumptions (1) and (3) yield only extremely small errors, since the corrections, in general, are very small corrections to a quantity which in itself is already very small compared to F_S.

Thus, F_S is related to the flux striking the detector in the following manner

$$\frac{F_{SD}[1 - \rho_{HS}\, \overline{\rho}_{\epsilon D}{}^2\, \eta'(f_{S-\epsilon})]}{\eta(\overline{\rho}_\epsilon)_S} = F_S \tag{37}$$

The effect on the F_S measurement given by equation (37) is also present in the other three measurements (F_{S1}, F_{S2}, F_D). The effect on each of these measurements is similar. The major changes arise in the calculation of $f_{S-\epsilon}$ and in the reflectance of the sample. The changes in $f_{S-\epsilon}$ are caused by the shields (S1 and S2) shading the ellipsoid from the detector. The calculation of $f_{S-\epsilon}$ can easily be corrected for this shading. However, the change in reflectance (due to the types of reflectances involved) is not so easily established. The best assumption for F_S, F_{S1}, and F_D is to assume that the surface's hemispherical reflectance remains the same for these measurements. This is a very good approximation, since the introduction of the small shields A_{S1} and A_D into the first focal plane does not markedly change the condition of hemispherical illumination and hemispherical viewing. However, the F_{S2} measurement presents an entirely different problem, since the A_{S2} shield does not allow either hemispherical illumination or hemispherical viewing. An approximation to the differences between ρ_{HS} and the ρ_{HS2} could be

$$\rho_{HS2} = \rho_{HS}\left[\frac{F_S - F_{S2}}{F_S}\right] \tag{38}$$

No effort is made to defend this approximation, except to say that for a specular sample, equation (38) results in $\rho_{HS2} = \rho_{HS}$, which is approximately true (except for the effects of Fresnel's law); and for the diffuse reflector, equation (38) results in the sample reflecting the same amount of flux onto the lower edge of the ellipsoidal mirror for illumination conditions of 7° to normal as for near grazing illumination conditions. This yields a low value for ρ_{HS2} since most surfaces tend to become specular at grazing incidence. It is felt that equation (38), although a guess at best, is better than no correction at all.

From these assumptions, then, the flux that the detector views for measurement of the remaining fluxes F_{S1}, F_{S2}, and F_D is

$$F_{S1D} = \eta\, F_{S1}(\bar{\rho}_\epsilon)_{S1}\left[\frac{1}{1 - \rho_{HS}\bar{\rho}_{\epsilon D}{}^2\eta'(f_{S-\epsilon})_{S1}}\right] \tag{39}$$

$$F_{S2D} = \eta\, F_{S2}(\bar{\rho}_\epsilon)_{S2}\left[\frac{1}{1 - (\frac{F_S - F_{S2}}{F_S})\rho_{HS}\bar{\rho}_{\epsilon D}{}^2\eta'(f_{S-\epsilon})_{S2}}\right] \tag{40}$$

$$F_{DD} = \eta\, F_D(\bar{\rho}_\epsilon)_D\left[\frac{1}{1 - \rho_{HS}\bar{\rho}_{\epsilon D}{}^2\eta'(f_{S-\epsilon})_D}\right] \tag{41}$$

Equations 39 through 41 can be rewritten to give F_{S1}, F_{S2}, and F_D as functions of the system and the flux that the detector views.

$$F_{S1} = \frac{F_{S1D}(1 - \rho_{HS}\bar{\rho}_{\epsilon D}{}^2\eta'(f_{S-\epsilon})_{S1})}{\eta\,(\bar{\rho}_\epsilon)_{S1}} \tag{42}$$

$$F_{S2} = \frac{F_{S2D}(1 - \frac{F_{SD} - F_{S2D}}{F_{SD}}\,\rho_{HS}\bar{\rho}_{\epsilon D}{}^2\eta'(f_{S-\epsilon})_{S2})}{\eta\,(\bar{\rho}_\epsilon)_{S1}} \tag{43}$$

$$F_D = \frac{F_{DD}(1 - \rho_{HS}\bar{\rho}_{\epsilon D}{}^2\eta'(f_{S-\epsilon})_D)}{\eta\,(\bar{\rho}_\epsilon)_D} \tag{44}$$

In equation (40) the term $(F_S - F_{S2})/F_S$ occurs, which, as shown later, is closely approximated by $(F_{SD} - F_{S2D})/F_{SD}$, which has been substituted in equation (43).

It is now possible to find F_R in terms of measured quantities and system parameters by use of equation (31) with equations (37), (42), (43), and (44). First, however, some simplifying assumptions will be made about the terms composed of ratios of fluxes in the last term of

equation (31). The ratios F_D/F_S and $(F_S - F_D)/F_S$ both appear. The ratios are equal to

$$\frac{F_D}{F_S} = \frac{F_{DD}(1 - \rho_{HS}\bar{\rho}_{\epsilon D}{}^2\eta'(f_{(S-\epsilon)})_D)\eta(\bar{\rho}_\epsilon)_S}{F_{SD}(1 - \rho_{HS}\bar{\rho}_{\epsilon D}{}^2\eta'(f_{S-\epsilon})_S)\eta(\bar{\rho}_\epsilon)_D} \tag{45}$$

and

$$\frac{F_S - F_D}{F_S} = 1 - \frac{F_{DD}(1 - \rho_{HS}\bar{\rho}_{\epsilon D}{}^2\eta'(f_{S-\epsilon})_D)\eta(\bar{\rho}_\epsilon)_S}{F_{SD}(1 - \rho_{HS}\bar{\rho}_{\epsilon D}{}^2\eta'(f_{S-\epsilon})_S)\eta(\bar{\rho}\ )_D} \tag{46}$$

In equations (45) and (46), all corresponding terms are equal or have been previously assumed equal without introducing significant errors. Thus,

$$\frac{F_D}{F_S} = \frac{F_{DD}}{F_{SD}} \text{ and } \frac{F_S - F_D}{F_S} = \frac{F_{SD} - F_{DD}}{F_{SD}} \tag{47}$$

Further, equations (11a), (12a), and (13a) can be converted to functions of F_{S2D}, F_{SD}, and F_{S1D} in the same manner.

Substituting equations (37), (42), (43), (44), and (47) into equation (31), and combining terms, yields

$$F_R = \frac{F_{SD}[1 - \rho_{HS}\bar{\rho}_{\epsilon D}{}^2\eta'(f_{S-\epsilon})_S]}{\eta(\bar{\rho}_\epsilon)(1 + \frac{F_{S2D}}{F_{SD}}(0.015))}\left[1 + \frac{A_H + A_S}{A_{SH} - A_H} - \frac{A_{S1}}{A_{SH} - A_H}\left[\frac{F_{DD}}{F_{SD}}\rho_S\bar{\rho}_{\epsilon D}{}^2\left(\frac{A_\epsilon - A_W}{A_\epsilon}\right)\left(\frac{1}{1 - \rho_S\bar{\rho}_\epsilon\frac{F_{SD} - F_{DD}}{F_{SD}}}\right)\right]\right] + \frac{F_{S1D}[1 - \rho_{HS}\bar{\rho}_{\epsilon D}{}^2\eta'(f_{S-\epsilon})_{S1}]}{\eta\,\bar{\rho}_\epsilon(1 + \frac{F_{S2D}}{F_{S1D}}(0.015))}\left[-\frac{A_H + A_S}{A_{SH} - A_H} + \frac{A_{S1}}{A_{SH} - A_H} \times \left[\frac{F_{DD}}{F_{SD}}\rho_S\bar{\rho}_\epsilon{}^2\left(\frac{A_\epsilon - A_W}{A_\epsilon}\right)\frac{1}{1 - \rho_S\bar{\rho}_\epsilon\frac{F_{SD} - F_{DD}}{F_{SD}}}\right]\right] + \frac{F_{DD}[1 - \rho_{HS}\bar{\rho}_{\epsilon D}{}^2\eta'(f_{S-\epsilon})_D]A_W}{\eta\,\bar{\rho}_\epsilon(1 + \frac{F_{S2D}}{F_{DD}}(0.015))\ A_\epsilon} \tag{48}$$

There are three major unknowns in equation (48). They are as follows:

(1). The efficiencies of the averaging sphere η and η'.

(2). The hemispherical or semi-hemispherical reflectance ρ_{HS} of the sample for the correction to the various terms for the detector ellipsoid interchange.

(3). The reflectance of the sample ρ_S. A good approximation to this is $\rho_S = F_{SD}/F_{1D}$.

The remaining terms of equation (48) are either fixed system parameters, or are obtained from measurements of F_{DD}, F_{SD}, F_{S1D}, and F_{S2D}.

For the absolute measurement of $\rho(7°,\theta)$, the reflectance of the sample (from equations 9 and 48) is equal to

$$\rho_S(7°,\theta) = \frac{F_R}{F_I} \tag{49}$$

Thus, to establish absolute reflectance with the ellipsoidal mirror reflectometer, one needs to have good estimates for η, η', and the various values of ρ_{HS}. This is discussed further in appendix G. It will become clear that the comparison measurement, when a calibrated specular mirror is used for the reference standard eliminates the need for an accurate knowledge of these terms.

Relative Measurement of Reflectance

As in the case of the absolute reflectance measurement, a value for the incident flux is needed so that the reflected flux F_R of equation (48) can be compared to the incident flux to calculate reflectance.

Incident Flux (F_I): In this case a value of flux related to the incident flux is obtained by using a calibrated specular mirror

(appendix B) as the reference sample. The flux F_I that is incident is reflected by the sample so that

$$F_{RM} = F_I \rho_M \tag{50}$$

Of the flux F_{RM} that leaves the sample, an amount $F_{RM} \bar{\rho}_\epsilon$ reaches the entrance port of the detector, where again there is an interchange between the averaging sphere and the ellipsoidal mirror which increases the flux in the averaging sphere so that the flux the detector views is

$$F_{ID} = F_I \rho_M \bar{\rho}_\epsilon \frac{\eta}{(1 - \rho_{HM} \bar{\rho}_{\epsilon D}{}^2 \eta' (f_{S-\epsilon})_I)} \tag{51}$$

where $f_{(S-\epsilon)_I}$ is equal to $f_{(S-\epsilon)_S}$.

From equation (51)

$$F_I = \frac{F_{ID}(1 - \rho_{HM} \bar{\rho}_{\epsilon D}{}^2 \eta' (f_{S-\epsilon})_I)}{\rho_M \bar{\rho}_\epsilon \eta} \tag{52}$$

Therefore, the reflectance $\rho(7°,\theta)$ is equal to F_R, equation (48), divided by F_I, equation (52). Further, the simplifying assumption that all the $(1 - \rho_{HS} \bar{\rho}_\epsilon{}^2 \eta' f_{(S-\epsilon)})$ terms for F_{1D}, F_{SD}, F_{S1D}, and F_{DD} are equal, and the fact that η' and η are identical throughout equations (48) and (52) yields

$$\rho(7°,\theta) = \frac{\rho_M}{F_{ID}} \left(\left[\frac{F_{SD}}{(1 + \frac{F_{S2D}}{F_{SD}} (0.015))} \left[1 + \frac{A_H + A_S}{A_{SH} - A_H} - \frac{A_{S1}}{A_{SH} - A_H} \times \right.\right.\right.$$

$$\left.\left.\left. \left[\frac{F_{DD}}{F_{SD}} \rho_S \bar{\rho}_{\epsilon D}{}^2 \left(\frac{A_\epsilon - A_W}{A_\epsilon}\right) \frac{1}{1 - \rho_S \bar{\rho}_\epsilon \frac{F_{SD} - F_{DD}}{F_{SD}}} \right] \right] + \frac{F_{DD}}{1 + \frac{F_{S2D}}{F_{DD}} (0.015)} \left[\frac{A_W}{A_\epsilon}\right] \right.\right.$$

$$\left.\left. + \frac{F_{S1D}}{(1 + \frac{F_{S2D}}{F_{SD}} (0.015))} \left[- \frac{A_H + A_S}{A_{SH} - A_H} + \frac{A_{S1}}{A_{SH} - A_H} \times \right.\right.\right.$$

$$\left.\left.\left. \left[\frac{F_{DD}}{F_{SD}} \rho_S \bar{\rho}_\epsilon{}^2 \left(\frac{A_\epsilon - A_W}{A_\epsilon}\right) \frac{1}{1 - \rho_S \bar{\rho}_\epsilon \frac{F_{SD} - F_{DD}}{F_{SD}}} \right] \right] \right) \tag{53}$$

where the only remaining unknown is ρ_s, which is the same as $\rho(7°,\theta)$. A very good approximation to ρ_S, as previously stated, is

$$\rho_S = \frac{F_{SD}}{F_{ID}} \tag{54}$$

Even if ρ_S of equation (54) was wrong by five percent, this would have little effect on $\rho(7°,\theta)$, since ρ_S is only found in secondary flux terms. Further, if the need and capability for more accuracy were justified by the other corrections, one could, of course, iterate this process by calculating successively better ρ_S by using $\rho(7°,\theta)$ calculated from ρ_S of equation (54) and then, successively, the $\rho(7°,\theta)$ calculated from equation (53).

Summary

This chapter has presented the general analyses for an ellipsoidal mirror reflectometer, which are based on the supposed ability to measure accurately four defined fluxes. Through the use of the four defined fluxes and an accurate knowledge of system parameters, it is possible to make corrections for system losses based on tacit assumptions about the arbitrary geometric distribution of the flux from the general engineering surface. The lack of knowledge concerning the distribution of reflected flux from common materials has seriously handicapped previous attempts to measure reflectance accurately; however, with the ellipsoidal mirror reflectometer, one is able to establish the important features of the reflected flux's distribution, that is, the required average flux density is established for each correction and the assumptions concerning these corrections appear more realistic than those previously used with other reflectometers. Further, many of the assumptions

leading up to equation (53) can be made more accurate at the cost of further complication of equation (51). With present source-detector limited detection ability, it was felt that more accurate corrections to the system losses were not justified. However, with the advent of infrared continuous wave, many wavelength lasers and more sensitive super-cooled solid state detectors, the ability to account for the system losses will increase and, thus, the assumptions leading up to equation (53) should be reviewed and revised as necessary.

It is also apparent from the analyses presented in this chapter that the relative reflectance measurement requires less knowledge about the system losses than the absolute reflectance measurement. Further, the use of a calibrated mirror as the only reference reflectance standard is very desirable, since they are available and can be individually calibrated by any investigator. All other reflectometers using mirrors to collect hemispherically the reflected flux from the sample require the use of a non-existent diffuse reflectance standard; and even if it did exist, corrections for the hole loss based on the diffuse standard are questionable, due to differences in geometric distribution of the flux reflected by the diffuse standard and that reflected by the sample.

Another point that is of interest is the difference between the absolute method and the relative (comparative) methods discussed in this chapter. In fact, many investigators would denote both these measurements as absolute, since the final answer is given in absolute reflectance units and not compared to some standard (such as MgO). The difference implied in this work between relative and absolute reflectance measurement has to do with how the incidence flux is obtained and not with how the data are reported.

Several losses which were not discussed in this chapter are:

(a) Atmospheric absorption.

(b) Edge loss, due to improper sample leveling in the first focal plane.

(c) The possibility that the detector does not read each signal the same.

However, these are losses that can be largely eliminated by careful attention to experimental technique. Appendices G and H provide an error analysis and some experimental data, and chapter V deals with the summary and conclusions of this dissertation.

TABLE II

FLUX TERMINOLOGY *

F_I = The flux incident on the sample at the first focal point.

F_R = The total flux reflected by the sample (not including inter-reflections).

F_α = The flux effectively absorbed by the ellipsoidal mirror.

F_W = The flux absorbed by the wire divided by $(\bar{\rho}_e)_w$. (i.e., F_w is the flux leaving the sample headed in the direction of the wires).

F_{SP} = The flux that is initially shaded from the detector by the sample divided by $\bar{\rho}_e$.

F_{SR} = The flux that reaches the detector after multiple reflections with the sample divided by $\bar{\rho}_e$.

F_H = The flux lost out the entrance hole.

F_S = The total flux crossing the first focal plane (excluding detector ellipsoid interchanges) divided by $(\bar{\rho}_e)_s$.

F_{S1} = The total flux crossing the first focal plane when shield A_{SH} is used divided by $(\bar{\rho}_e)_{s1}$.

F_{S2} = The total flux crossing the first focal plane when shield A_{S2} is used divided by $(\bar{\rho}_e)_{s2}$.

F_D = The total flux crossing the first focal plane when shield A_D is used divided by $(\bar{\rho}_e)_D$.

---

*All fluxes are defined on the basis of the flux leaving the sample. The subscript D added to the subscript of any of the above fluxes implies the flux actually viewed by the detector when the defined flux is measured by the detector

TABLE II (Cont'd)

REFLECTANCE TERMINOLOGY

ρ_ϵ' = Effective reflectance of a point on the ellipsoidal mirror.

$\bar{\rho}_\epsilon$ = Effective reflectance of the central area of the ellipsoidal mirror.

$(\bar{\rho}_\epsilon)_S$ = Effective reflectance of the ellipsoidal mirror to the flux F_S.

$(\bar{\rho}_\epsilon)_{S1}$ = Effective reflectance of the ellipsoidal mirror to the flux F_{S1}.

$(\bar{\rho}_\epsilon)_{S2}$ = Effective reflectance of the ellipsoidal mirror to the flux F_{S2}.

$(\bar{\rho}_\epsilon)_D$ = Effective reflectance of the ellipsoidal mirror to the flux F_D.

ρ_{HS} = The hemispherical reflectance of the sample.

ρ_{HM} = The hemispherical reflectance of the reference mirror.

ρ_M = The reflectance of the specular reference standard.

ρ_S = The normal hemispherical reflectance, and is approximately equal to $\rho(7°,\theta)$

$(\bar{\rho}_E)_W$ = The effective reflectance of the ellipsoidal mirror to the flux F_W.

$\rho_{\epsilon D}$ = Effective reflectance of the ellipsoidal mirror to diffuse flux from the second focal point.

AREA TERMINOLOGY

A_H = Area of the entrance hole.

A_ϵ = Area of the opening of the ellipsoidal mirror in the first focal plane minus the area of the shield A_D.

A'_{SH} = Area of the shield A_{SH} in the first focal plane.

A'_S = Area of the sample in the first focal plane.

A'_{S1} = First focal plane area of the image of the sphere entrance port at the second focal point.

A_D = Area of the shield used to block the specular component.

TABLE II (Cont'd)

A_{S2} = Represents the shield used to establish the flux distribution for mirror loss corrections.

A_{SH} = Projection of A'_{SH} from the second focal point onto the ellipsoidal mirror.

A_S = Projection of A'_S from the second focal point onto the ellipsoidal mirror.

A_{S1} = Projection of A'_{S1} from the second focal point onto the ellipsoidal mirror.

MISCELLANEOUS TERMINOLOGY

η = Efficiency of the averaging sphere (i.e., the ratio of the flux viewed by the detector to that entering the sphere).

η' = The ratio of flux leaving the entrance port of the sphere to that incident on the entrance port

f_{S-e} = Diffuse configuration factor from the sphere entrance port to the ellipsoidal mirror (corrected for shading effects of the sample and sample support and for the effect of the entrance hole).

CHAPTER V

CONCLUSION

This chapter is composed of three parts, (1) Summary of the development of an ellipsoidal mirror reflectometer, (2) summary of other results obtained during this development, and (3) recommendations.

Main Results

The use of an ellipsoidal mirror, sulfur coated averaging sphere over the detector, and a specular reference standard have allowed the development of a very versatile reflectometer. This versatility includes the ability to measure accurately $\rho(\varphi,\theta)$, $\rho(\varphi,\theta,\varphi',\theta')$, ρ (specular), ρ (non-specular), and ρ(directional annular cone). High accuracy is possible due to the following factors: (1) spatial and angular sensitivity of the detector have been minimized by use of the sulfur coated averaging sphere; (2) a technique for correcting for the entrance and/or exit hole loss has been effectively utilized [12]; (3) the use of the ellipsoidal mirror reduces aberrations in the system and reduces the size of solid angle of the flux incident on the detector; (4) the effective reflectance of the ellipsoidal mirror was measured as a function of position, providing an accurate correction for variations in the mirror's reflectance with position; (5) the reflectometer needs only a specular reference standard which is easy to calibrate; (6) the system losses can be evaluated by establishing the flux involved in each loss through the use of shields placed in the first focal plane.

The actual accuracy of this type of instrument is estimated to be at least two percent and probably better than one percent; however, the present lack of comprehensive data on the goniometric distribution of reflected flux from common engineering materials precludes a positive general statement of accuracy at this time. Indeed, some investigators have questioned whether an accuracy of better than one percent is useful, since it is probable that the variation in reflectance of similar samples may exceed one percent and, further, the condition of the surface while in use (say in space) is never definitely known. In any event, this reflectometer provides more information concerning the reflectance of engineering samples than previous instruments. Further, the separation of the detector and sample permits heating and/or cooling of the sample.

One instrument which seems to be essentially identical in concept to the ellipsoidal reflectometer is the paraboloidal reflectometer shown in figure 28 [30]. If two paraboloids were used and the one that collected the reflected flux and focused it on the detector had a longer focal length than the other, then this reflectometer would seem to possess all of the advantages of the ellipsoidal reflectometer.

Secondary Results

During the development of the ellipsoidal reflectometer the following results were obtained:

(1) The use of the sulfur coated averaging sphere permits the construction of a simple and accurate infrared specular reflectometer.

(2) A method of applying sulfur to a sphere wall was developed. The resulting coating appears to be more durable than standard sphere

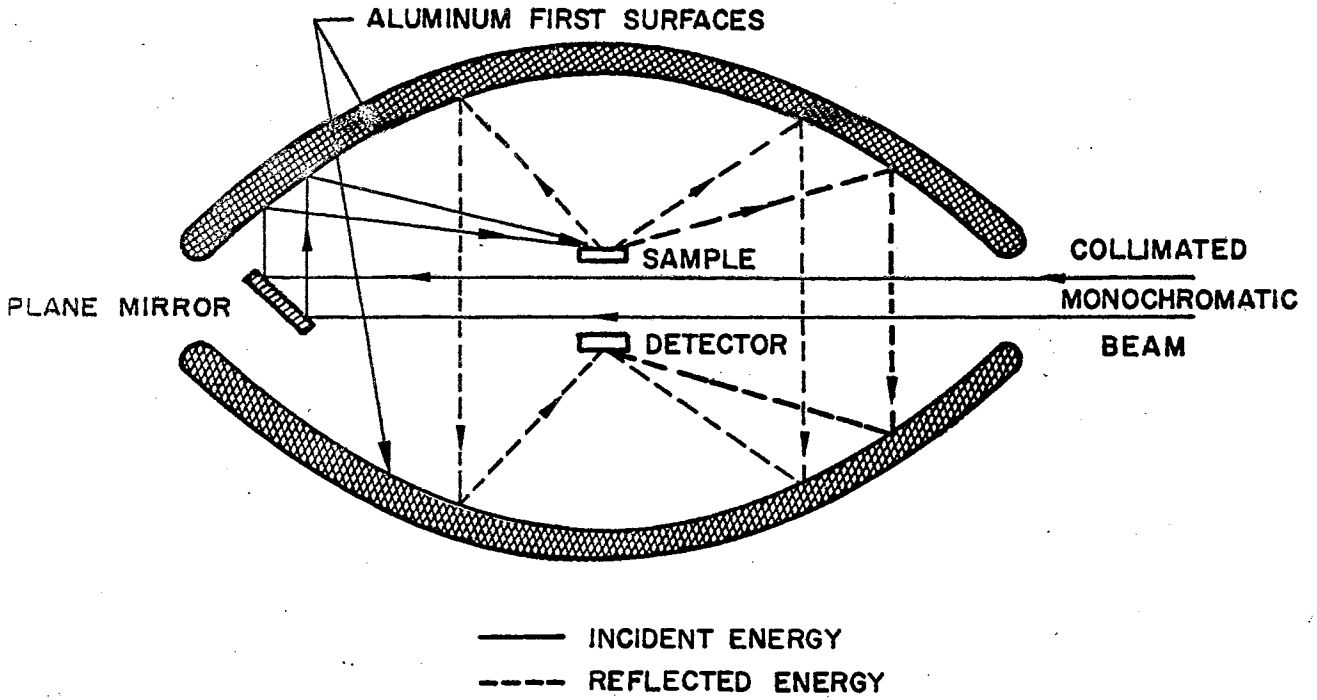

Figure 28. Paraboloidal Reflectometer.
Reprinted from reference 30.

coatings (i.e., MgO or $BaSO_4$) (appendix E).

(3) A simple bench test was proposed for studying sphere coatings for use in the infrared (appendix D).

(4) The directional annular cone reflectance was used to study the diffuseness of several samples (appendix H).

Recommendations

During the course of the development of the ellipsoidal reflectometer several ideas for redesign and/or use of this instrument were generated. They are:

(1) Care should be used in the design of an ellipsoidal reflectometer to keep the specular component of the reflected flux as far away from the sample as is practical.

(2) It is recommended that a more complete ellipsoidal mirror, such as shown in figure 29, be used. This will allow tilting of the sample without flux losses around the edges of the mirror. (It will also be necessary to tilt the detector in some cases).

(3) It is suggested that the continuous wave laser would be a superb source, since it has a high intensity collimated beam. Further, the use of the laser would allow the smallest possible entrance hole and reduce the hole loss to nearly zero.

(4) To use this instrument at its best accuracy, a set of at least 5 specular standards, whose reflectances are evenly distributed between zero and one, should be developed [19].

(5) Figure 30 illustrates a proposed design for a recording spectrometer using a chopped double beam source, where the flux incident on the two samples is the same.

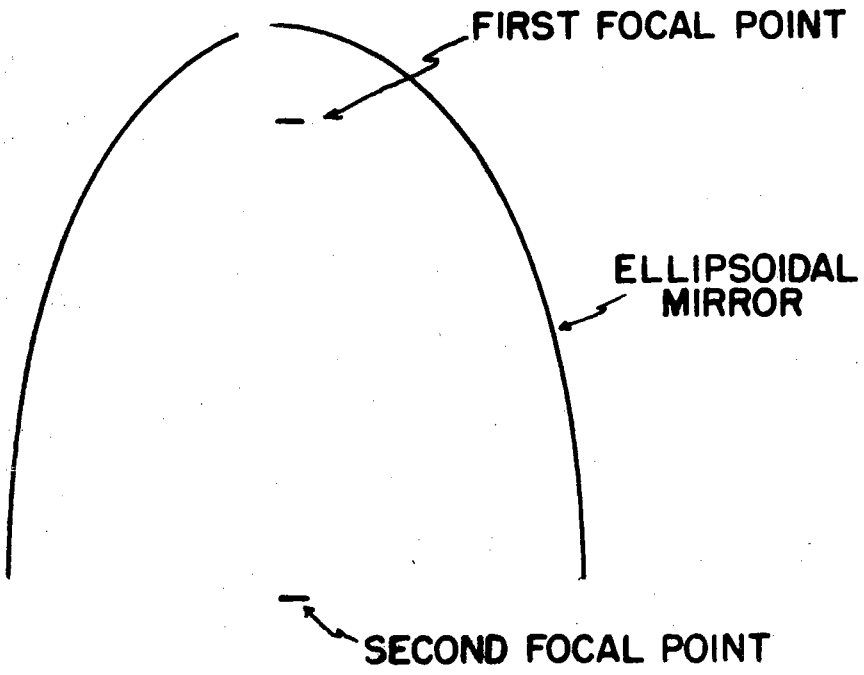

Figure 29. Enlarged Ellipsoidal Mirror

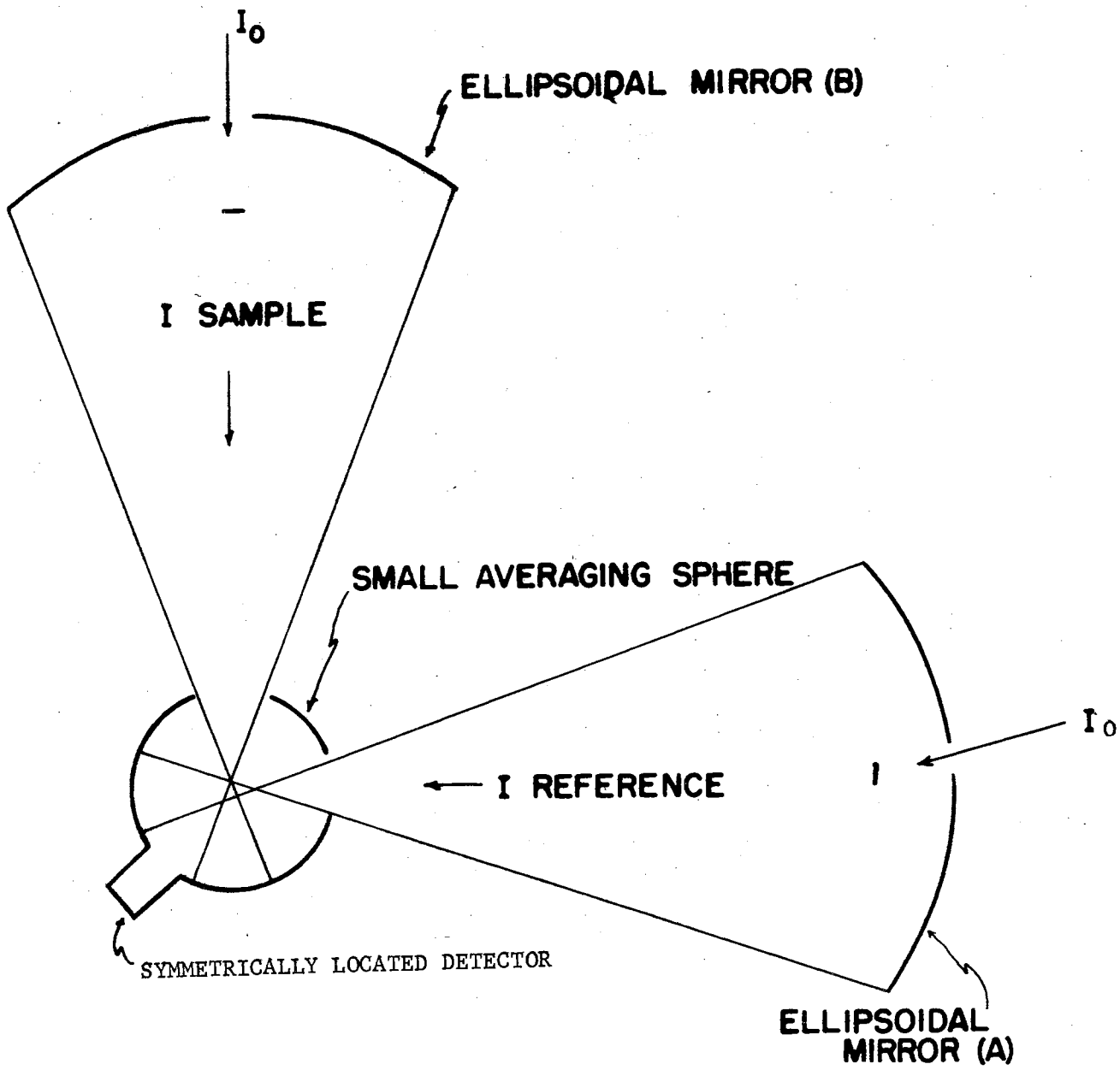

Figure 30. Double Beam Ellipsoidal Reflectometer.

(6) Additional work on controlling the first and second reflections inside a gold-roughened averaging sphere may make this device suitable for use with the reflectometer and extend its range to 10μ.

(7) The instrument is easily convertible to the .4 to 2.0μ range by changing the source, detector, and sphere coating.

(8) A needed experimental study is the effect of the size of the solid angle on the value of the specular component; data of this nature would be valuable to the heat transfer analyst.

(9) Figure 31a illustrates the use of the ellipsoidal mirror optics for transmittance and scattering measurements.

In conclusion, it is felt that the ellipsoidal mirror reflectometer has been shown to be capable of accurate reflectance measurements in the 1.5μ to 7.0μ region. Further, a simple modification will extend this range down to .4μ. In addition, the use of the gold sphere and a helium cooled balometer may well extend the upper wavelength limit to 15μ or more. On the basis of these results the development of integrating spheres for the infrared would seem to be unnecessary.

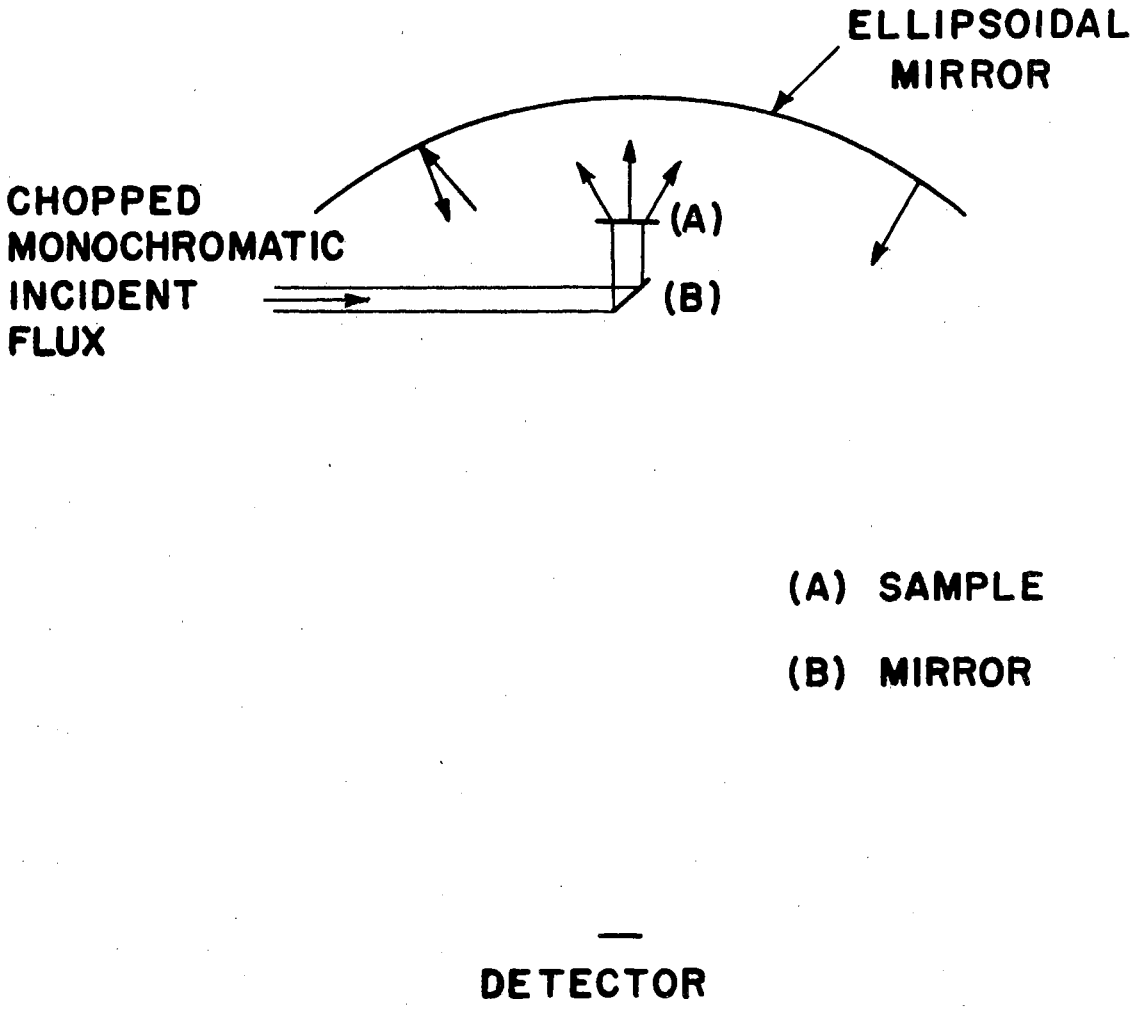

Figure 30a. Transmittance and Scatter Optics
Using An Ellipsoidal Mirror

REFERENCES

1. Parmer, J F., "The Thermal Radiation Characteristics of Specular Walled Grooves in the Solar Space Environment." Ph.D. Thesis, Oklahoma State University, May 1965.

2. Sparrow, E. M., Eckert, E. R. G., and Johsson, V. K., "An Enclosure Theory for Radiative Exchange Between Specularly and Diffusely Reflecting Surfaces." Transactions of ASME, Journal of Heat Transfer, V. 84, 1962, pp. 294-300.

3. Seban, R. A., "Discussion." Transactions of ASME, Journal of Heat Transfer, V. 84, 1962, pp. 299-300.

4. Wiebelt, J. A., Engineering Radiation Heat Transfer, Notes for Oklahoma State University, May 1963.

5. Fragstein, C. V., "On the Formulation of Kirchhoff's Law and Its Use for a Suitable Definition of Diffuse Reflection Factors." Optik, V. 12, 1955, pp. 60-70.

6. Edwards, D. K., Gier, J. T., Nelson, K. E., and Raddick, R. D., "Integrating Sphere for Imperfectly Diffuse Samples." Applied Optics, V. 51, 1961, pp. 1279-1288.

7. Jacques, J. A. and Kuppenheim, H. F., "Theory of the Integrating Sphere." Journal of the Optical Society of America, V. 45, 1955, pp. 460-470.

8. Gates, D. M., Shaw, C. C., and Beaumont, D., "Infrared Reflectance of Evaporated Metal Films." Journal of the Optical Society of America, V. 48, 1958, pp. 88-89.

9. Bennett, H. E. and Koehler, W. F., "Precision Measurement of Absolute Specular Reflectance with Minimized Systematic Errors." Journal of the Optical Society of America, V. 50, 1960, pp. 1-6.

10. Weeks, R. F., "Simple Wide Range Specular Reflectometer." Journal of the Optical Society of America, V. 48, 1958, pp. 775-777.

11. Ramsey, W. Y., "Specular Spectral Reflectance of Paints from .4 to 40.0 Microns." Meteorological Satellite Laboratory Report No. 31, April 1964.

12. Coblentz, W. W., "The Diffuse Reflecting Power of Various Substances." Bulletin of the Bureau of Standards, V. 9, 1913, pp. 283-325.

13. Gier, J. T., Dunkle, R. V., and Bevans, J. T., "Measurement of Absolute Spectral Reflectivity from 1.0 to 15 Microns." Journal of the Optical Society of America, V. 44, 1954, pp. 558-562.

REFERENCES - Cont'd

14. Royds, T., "The Reflective Power of Lamp- and Platinum-Black." Philosophical Magazine, V. 21, 1911, pp. 167-172.

15. Royds, T., "Das Reflexionvermögen schwarzer Flächen." Physikalische Zeit schrift, V. 11, 1910, pp.316-319.

16. Paschen, F., Ber. Berlin Akad. Deut. Wiss., 27(1899).

17. Brandenberg, W. M., "Focusing Properties of Hemispherical and Ellipsoidal Mirror Reflectometers." Journal of the Optical Society of America, V. 54, 1964, pp. 1235-1237.

18. Stair, R. and Schneider, W. E., "Standards, Sources, and Detectors in Radiation Measurements." Symposium on Thermal Radiation of Solids. Editor: Dr. Samuel Katzoff. NASA SP-55. To be published in 1965.

19. Janssen, J. E. and Torborg, R. H., "Measurement of Spectral Reflectance Using an Integrating Hemisphere." Measurement of Thermal Radiation Properties of Solids. Editor: J. C. Richmond. NASA SP-31, 1963, pp. 169-182.

20. White, J. U., "New Method for Measuring Diffuse Reflectance in the Infrared." Journal of the Optical Society of America, V. 54, 1964, pp. 1332-1337.

21. Birkebak, R. C. and Hartnett, J. P., "Measurements of the Total Absorptivity for Solar Radiation of Several Engineering Materials." Transactions of the ASME, V. 80, 1958, pp. 373-378.

22. Kozyrev, B. P. and Vershinin, O. E., "Determination of Spectral Coefficients of Diffuse Reflection of Infrared Radiation from Blackened Surfaces." Optics and Spectroscopy, V. 6, 1959, pp. 345-350.

23. Derksen, W. L., Monahan, T. I., and Lawes, A. J., "Automatic Recording Reflectometer for Measuring Diffuse Reflectance in the Visible and Infrared Regions. " Journal of the Optical Society of America, V. 47, 1957, pp. 995-999.

24. Derksen, W. L. and Monahan, T. I., "A Reflectometer for Measuring Diffuse Reflectance in the Visible and Infrared Regions." Journal of the Optical Society of America, V. 42, 1952, pp. 263-265.

25. Sanderson, J. A., "The Diffuse Spectral Reflectance of Paints in the Near Infrared," Journal of the Optical Society of America, V. 37, 1947, pp. 771-777.

REFERENCES - Cont'd

26. Martin, W. E., "Hemispherical Spectral Reflectance of Solids." Measurement of Thermal Radiation Properties of Solids, Editor: J. C. Richmond, NASA SP-31, 1963, pp. 183-192.

27. Dunkle, R. V., Ehrenburg, F., and Gier, J. T., "Spectral Characteristics of Fabrics From 1 to 23 Microns." Transactions of the ASME Journal of Heat Transfer, V. 82, 1960, pp. 64-70.

28. Streed, E. R., McKellar, L. A., Rollings, R., Jr., and Smith, C. A., "Errors Associated with Hohlraum Radiation Characteristics Determinations." Measurement of Thermal Radiation Properties of Solids. Editor: J. C. Richmond. NASA SP-31, 1963, pp. 237-252.

29. Reid, D. C. and McAlister, E. D., "Measurement of Spectral Emissivity from 2 μ to 15 μ." Journal of the Optical Society of America, V. 49, 1959, pp. 78-82.

30. Dunkle, R. V., "Spectral Reflectance Measurements." Surface Effects on Spacecraft Materials, Wiley & Sons, 1960, pp. 117-137.

31. Clayton, W. A., "Comments on Measurement Techniques." Symposium on Thermal Radiation of Solids. Editor: S. Katzoff. NASA SP-55. To be published in 1965.

32. Shibata, K., "Simple Absolute Method for Measuring Diffuse Reflectance Spectra." Journal of the Optical Society of America, V. 47, 1957, pp. 172-175.

33. Oldham, M. S., "An Infrared Reflectometer." Journal of the Optical Society of America, V. 41, 1951, pp. 673-675.

34. Standard No. D523-62T "Specular Gloss" and Standard No. D1471-57T "Two-Parameter, 60-Deg Specular Gloss." 1964 Book of ASTM Standards, Part 21, published by the American Society for Testing and Materials, Philadelphia 3, Pa., 1964.

35. McNicholas, H. J., "Absolute Methods in Reflectometry." National Bureau of Standards Journal of Research, V. 1, 1928, pp. 29-73.

36. Birkebak, R. C., "Monochromatic Directional Distribution of Reflected Thermal Radiation from Roughened Surfaces." Ph.D. Thesis, University of Minnesota, 1962.

37. Richmond, J. C., DeWitt, D. P., and Hayes, W. D., Jr., "Procedures for Precise Determination of Thermal Radiation Properties, November 1962 to October 1963." National Bureau of Standards Technical Note 252, 1964.

REFERENCES - Cont'd

38. Kronstein, M., Kraushaar, R. J., and Deacle, R. E., "Sulfur as a Standard of Reflectance in the Infrared." Journal of the Optical Society of America, V. 53, 1963, pp. 458-465.

39. Rohzhin, V. V., "A Photomultiplier for Measuring Radiant Flux in Lighted Models with an Absorbing Medium." Iz vestis Vysshikh Uchebnykh Zavedeniy, Priborostroyeniye, No. 1, 1961, pp. 94-98.

40. Agnew, J. T. and McQuistan, R. B., "Experiments Concerning Infrared Diffuse Reflectance Standards in the Range 0.8 to 20.0 Microns." Journal of the Optical Society of America, V. 43, 1953, pp. 999-1007.

41. Bennett, H. E., Silver, M., and Ashley, E. J., "Infrared Reflectance of Aluminum Evaporated in Ultra-High Vacuum." Journal of the Optical Society of America, V. 53, 1963, pp. 1089-1095.

42. Hass, G., Engineer Research and Development Laboratory, Ft. Belvoir, Virginia, Personal Communication.

43. Bennett, H. E., Bennett, Jean M., and Ashley, E. J., "Infrared Reflectance of Evaporated Aluminum Films." Journal of the Optical Society of America, V. 52, 1962, pp. 1245-1250.

44. Bennett, J. M. and Ashley, E. J., "Infrared Reflectance and Emittance of Silver and Gold Evaporated in Ultrahigh Vacuum." Applied Optics, V. 4, 1965, pp. 221-224.

45. Hass, G., Optics Section, American Institute of Physics Handbook Coordinating Editor D. E. Gray, 1957, McGraw-Hill Book Company, Incorporated, New York, pp. 6-19.

46. Hass, G., "Filmed Surfaces for Reflecting Optics." Journal of the Optical Society of America, V. 45, 1955, pp. 945-952.

47. Richmond, J. C., DeWitt, D. P., Hayes, W. D., Jr., and Dunn, S. T., "Procedures for Precise Determination of Thermal Radiation Properties,"November 1963 to October 1964." National Bureau of Standards Technical Note, to be published in 1965.

48. Goebel, D. G., Caldwell, B. P., and Hammond, H. K., III, "Use of an Auxiliary Sphere with a Spectroreflectometer to Obtain Absolute Reflectance." Photometry and Colorimetry Section, National Bureau of Standards, Washington, D. C., October 27, 1964, unpublished.

49. DeWitt, D. P. and Richmond, J. C., "Laser Source Integrating Sphere Reflectometer." Presented at the Annual Meeting of AIAA, January 1965, New York.

50. Jakob, Max, Heat Transfer, John Wiley & Sons, Inc., V. 1, 1949, p. 52.

REFERENCES - Cont'd

51. Richmond, J. C., Harrison, W. N., Shorten, F. J., "An Approach to Thermal Emittance Standards." Measurement of Thermal Radiation Properties of Solids. Editor: J. C. Richmond. NASA SP-31, 1963, pp. 403-424.

APPENDIX A

COMMENTS ON RECIPROCITY

Since the most common condition is that of illumination from a direction and reflection into the hemisphere above the surface, the most useful reflectance to the heat transfer engineer is $\rho(\varphi,\theta)$. As heat transfer calculations become more sophisticated, the specular component of this reflectance will also be needed. In general, most instruments measure $\bar{\rho}(\varphi', \theta')$ (i.e., heated cavity, most recent modifications of the integrating hemisphere, and the integrating sphere as used in reference 36), and only a few instruments measure $\rho(\varphi,\theta)$. Hence, it is important that well-defined relationships between $\rho(\varphi,\theta)$ and $\bar{\rho}(\varphi',\theta')$ be stated. The literature provides two sets of definitions, one which is widely accepted, the other appears only in a very few references.

(1). The most widely accepted statement of the reciprocity between $\rho(\varphi,\theta)$ and $\bar{\rho}(\varphi',\theta')$ is [5, 35]:

If $\rho(\varphi,\theta)$ is measured with constant intensity incident over $d\omega$ from the direction φ,θ, and with collection of the reflected energy over the hemisphere, then the equivalent measurement of $\bar{\rho}(\varphi',\theta')$ is to have constant intensity incident over the hemisphere (i.e., perfectly diffuse illumination), and collection of the reflected energy over the solid angle $d\omega$ in the direction φ,θ.

(2). Reference 36, page 41, indicates that these two reflectances are equivalent if, and only if, the distribution of the incident energy for the $\bar{\rho}(\varphi',\theta')$ measurement is the same as the reflected energy for the $\rho(\varphi,\theta)$ measurement. However this statement does not seem to be consistent

with those from references 5 and 35.

Accepting statement (1), it is apparent that for anisotropic surfaces $\rho(\varphi,\theta) \equiv \bar{\rho}\ (\varphi,\theta')$, that is, the values of θ and θ' are independent when all other given conditions have been met. For isotropic surfaces, θ and θ' must be equal.

With this in mind, then it is critical that the instruments that measure $\bar{\rho}(\varphi',\theta')$ have perfectly diffuse flux incident on the sample, while in instruments measuring $\rho(\varphi,\theta)$, it is only necessary for complete non-selective hemispherical collection. C. V. Fragstein [5] states this in the following manner (his symbols have been converted to the symbols used in this work):

> Consider the surface element dA to be irradiated uniformly from all directions and with the specific radiation intensity I_λ. Then the radiant energy reflected by dA in direction φ,θ into the solid angle $d\omega$ is equal to that energy which is reflected by dA into the hemisphere if dA is irradiated from direction φ,θ over the solid angle $d\omega$ with the same specific radiation intensity I_λ.

These same references [5, 35] discuss the reciprocity relations between the many other kinds of reflectances. Through these reciprocity relationships, it also is possible to relate the non-specular component of reflectance, if the excluded component is identical in both cases and the remaining conditions for $\rho(\varphi,\theta) \equiv \bar{\rho}(\varphi',\theta')$ have been met.

APPENDIX B

DESIGN OF SPECULAR REFLECTOMETER

This section describes a simple, but accurate, infrared specular reflectometer. In previous infrared specular reflectometers, very precise alignment of the optics was necessary to insure that the detector viewed different reflected signals identically [9, 10]. The specular reflectometer used in this work to measure the reflectance of the calibration mirrors (chapter IV) is illustrated in figure 31. The sulfur-coated diffusing sphere developed in chapter III was used to average the monochromatic flux from the Globar for two different signals, one being the flux that is reflected once by each of the sample mirrors, and the other being the unreflected incident flux. The use of the sulfur-coated diffusing sphere reduces the required precision of optical alignment, since the "images" of the two signals need not be the same size, nor on exactly the same area of the sphere wall (figures 18a, and 22).

In the reflectometer, the path length for the two measurements is different, so that it is necessary either to operate in a non-absorbing atmosphere, or at wavelengths where atmospheric absorption does not occur. In this case, the reflectance was measured at the same wavelengths and with the same band passes as were used in the ellipsoidal mirror reflectometer (chapter II, page 26). In chapter III, it was shown that atmospheric absorption did not affect the flux at these wavelengths for changes in path length of six inches and more. Due to the longer path length (approximately 1½ inches longer), the signal reflected by the two sample mirrors has an image area on the sphere wall

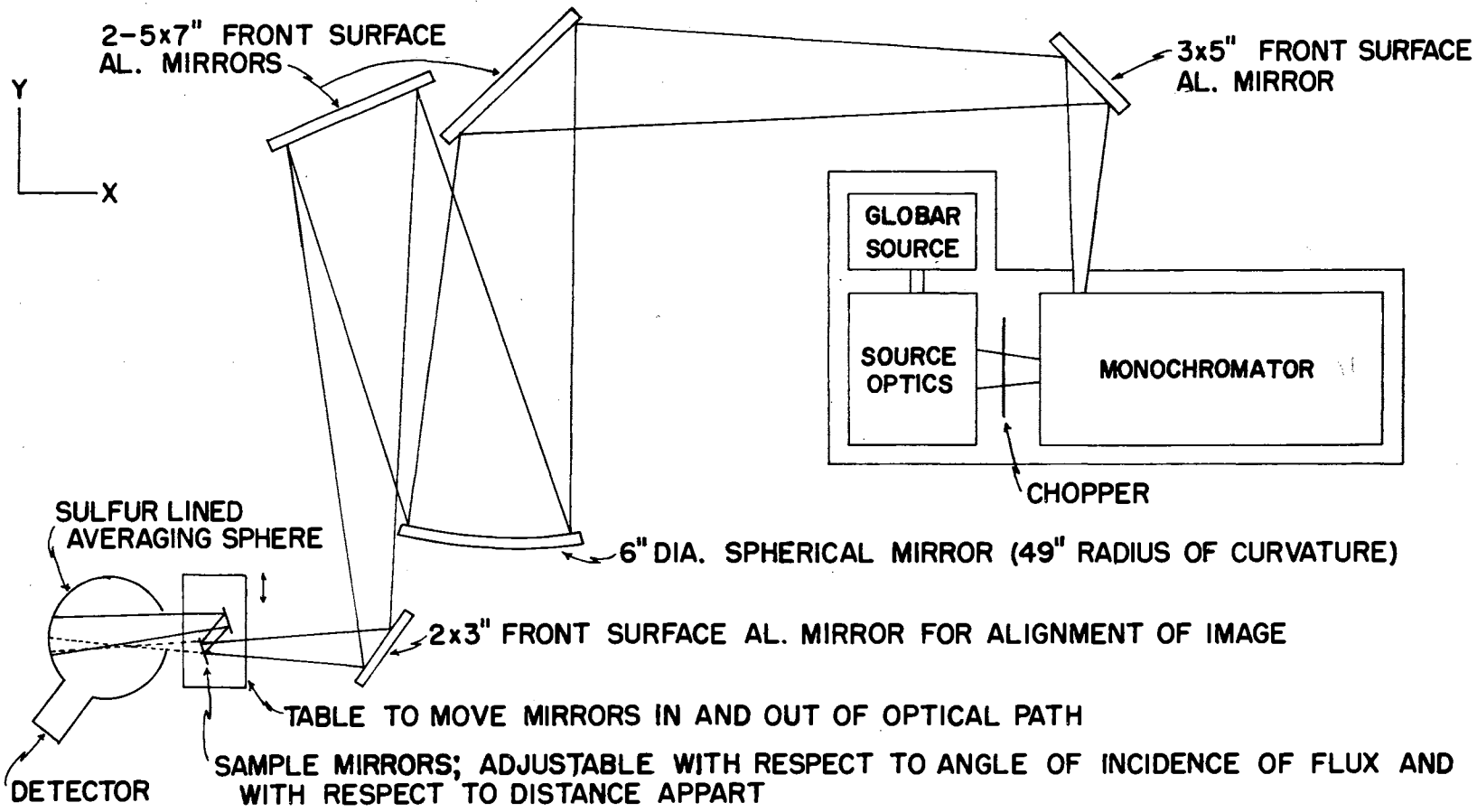

Figure 31. Specular Reflectometer

about 2.1 times that of the unreflected signal. For each measurement, the small unreflected image of the incident flux was visually centered on the large image of the double reflected flux. This insured accurate measurement of both signals (see figures 20 and 22).

The ratio of the twice reflected flux to the incident flux is equal to the product of the reflectances of the two sample mirrors. If the reflectances of the two mirrors can be considered equal, then the ratio is equal to the square of the reflectance of the mirrors. This procedure increases the accuracy of the reflectance measurement, since the expected error in the measured ratio is the same whether one or two reflections are involved (i.e., with two reflections, the final error is approximately the square root of the error in the measurement of the ratio).

The two sets of calibration mirrors were selected as follows:

(1) Aluminum Mirror: A set of 12 optically polished ½-inch by ¼-inch glass samples were prepared. The aluminum coating was then vacuum deposited on all of the samples at the same time, to an opaque thickness, in a time of one second. This should give essentially the same values for reflectance that Bennett, et al. [41] report for their ultra-high vacuum coatings of aluminum. Hass [42] indicates that the fast evaporation times at normal vacuums yield the same reflectance values as those measured for the ultra-high vacuum coatings. The aluminum used for the coatings was 99.999% pure.

(2) Gold Mirrors: A set of 12 optically polished ½-inch by ¼-inch glass samples were prepared. The gold was vapor-plated on all of the samples at the same time, over a chromium substrate (to increase its mechanical durability), in accordance with standard procedures. At the

time of the coating, it was not known that the infrared reflectance of gold (like aluminum) varies significantly with evaporation techniques [44]; thus, no effort was made to control the evaporation time to ensure a coating of the highest possible reflectance.

Four of these mirrors were then visually selected from each of the sets of 12 to form the two sets of calibration mirrors, as follows:

(1) They were examined with an 8-power microscope with grazing illumination for surface irregularities, and

(2) They were examined for opacity and scatter when illuminated by the 0.632 μ line of a helium-neon laser.

The aluminum and gold mirrors both exhibited no visible surface irregularities under examination with the microscope, and they were both opaque to the 0.632 μ laser line. Qualitatively, the aluminum and gold mirrors both seem to scatter the 0.632μ laser beam about the same. No quantitative value of scatter was obtained.

The reflectance of the two sets of calibration mirrors was then measured in the following manner:

Six reflectance measurements were made; 2 each of three combinations of pairs from each set of the mirrors. This does not exhaust the six unique pairs from a set of four, but does allow inter-comparison of all of the mirrors to establish that their reflectances are indeed equal, as would be expected for samples prepared at the same time.

Table 3 gives the results for aluminum. Each reflectance value is the square root of the ratio of the two signals. Further, each of the six readings represents a completely separate measurement, taken on different days and after realignment of the optics and repositioning of the samples; therefore, these measurements should be independent and

TABLE 3

REFLECTANCE OF ALUMINUM

λ	ρ_{1-2}*	ρ_{1-2}	ρ_{1-3}	ρ_{1-3}	ρ_{2-4}	ρ_{2-4}	Average	Standard Deviation	Best Literature Values [41]
1.5	0.961^{+}	0.961^{-}	0.962	0.960^{-}	0.962	0.959	0.9608	0.0012	0.9742
2.0	.975	$.975^{+}$	.972	$.975^{-}$	.976	.972	.9742	.0017	.9779
2.5	$.977^{-}$	$.976^{+}$	.974	.976	.975	.976	.9757	.0010	.9794
3.5	$.985^{+}$	.983	.984	.981	.982	.982	.9828	.0005	.9816
4.5	.985	$.985^{+}$	.982	$.984^{-}$	$.984^{-}$	.984	.9840	.0011	.9835
5.5	.985	.986	.983	$.985^{+}$	$.986^{-}$	$.986^{+}$	.9852	.0012	.9850
6.5	.985	.985	.983	.985	.986	$.987^{+}$	.9852	.0013	.9861
7.0	.988	$.988^{-}$	.984	$.985^{+}$	.986	$.987^{+}$	.9863	.0017	.9866

* The subscripts on the symbol "ρ" for reflectance indicate the particular mirrors used for the measurement.

$$\text{Average} = \frac{\sum_{1}^{n} \rho}{n}$$

$$\text{Standard deviation} = \frac{\sum_{1}^{n} (\rho - \bar{\rho})^2}{(n-1)}$$

errors should be random. The results for reflectance of the different pairs of mirrors indicate that, within the precision of measurement, there does not appear to be any variation in reflectance among the samples in this set. The arithmetic average and the standard deviation of the measurements are reported in table 3 and are compared to the data (accurate to ±.001 reflectance units) reported by Bennet, et al. [41]. The agreement is excellent beyond three microns; the tendency of the reflectance to be lower than comparable values at the shorter wavelengths is attributed to differences in optical finish and oxide formation on or in the coating. The reflectance values reported in this work are higher than the reflectance values reported for standard aluminum coatings throughout the 1.5 to 7.0 micron range [43]. Further, when comparing these values to other values in the literature, the band width of flux at 1.5 microns is very important, since aluminum's reflectance is changing quite rapidly below 2.0 microns. Due to this, the wide band (about 0.18 microns in width) values reported for 1.5 microns in this work will be lower than narrow band literature values for a coating with the same spectral reflectance

The results for the gold mirrors shown in table 4 are qualitatively similar to the results for aluminum mirrors. That is, the reflectances of all four gold mirrors are equal, and the reported reflectances tend to be lower than the best literature values at the shorter wavelengths. Since the gold mirrors were prepared without special attention being paid to the evaporation time or the level of vacuum, exact agreement with the literature was not expected. The recent work of J. Bennett [44] indicates ultra high vacuum techniques increase the reflectance of gold by about 1 percent in the infrared.

TABLE 4

REFLECTANCE OF GOLD

λ	ρ_{1-2}*	ρ_{1-2}	ρ_{2-3}	ρ_{2-3}	ρ_{3-4}	ρ_{3-4}	ρ_{3-4}	Average	Standard Deviation	Literature Values [45]	Best Literature Values [44]
1.5	0.980	0.981	0.980	0.981	0.982	0.983	0.979	0.9809	0.0014	0.982	0.9806
2.0	.984	$.984^{+}$	.984	.983	.983	$.983^{+}$	.981	.9833	.0010	.983	.9914
2.5	.984	$.986^{+}$	.986	.982	.984	.984	$.984^{+}$	.9843	.0014	.983	.9922
3.5	.987	.987	.988	.987	.986	.987	.988	.9870	.0005	.983	.9934
4.5	$.986^{+}$	.988	$.987^{+}$	.988	.987	$.986^{+}$	$.987^{+}$	.9874	.0008	.983	.9938
5.5	.987	.989	$.988^{+}$	.986	.985	$.986^{-}$	.988	.9870	.0014	.983	.9938
6.5	$.988^{-}$	$.987^{+}$	.988	.987	$.988^{+}$	.988		.9878	.0005	.983	.9939
7.0	.988	$.987^{+}$	.988	.992	.989	.989		.9890	.0017	.984	.9939

*The subscripts on the symbol "ρ" for reflectance indicate the particular mirrors used for the measurements.

Table 5 gives the average value of reflectance for a set of 4 rhodium mirrors purchased from Evaporated Metal Films Corp., Ithaca, N. Y. These mirrors are also ½ inch by ¼ inch, and exhibit reflectances very close to literature values for the longer wavelengths and much lower for the shorter wavelengths. Visual examination of these samples with the 0.632 μ laser line qualitatively indicated considerably more scatter than for the aluminum or gold mirrors.

It is not believed that the lower values for the short wavelength reflectances reported in this work represent an instrumental error, since there is every reason to expect an increase in accuracy at the shorter wavelengths, where more energy is available for detection and the required precision of optical alignment is at a minimum (chapter 3).

Since in the calibration of the ellipsoidal reflectometer, these mirrors are used with several different angles of incidence (from 0° from the normal to 52° from the normal), the effect of changing the angle of incidence was studied. Within the accuracy of the measurements, no change of reflectance with angle of incidence was observed for the gold and aluminum mirrors (for incident angles up to 50°).

Summary

The mirrors used for calibrating the ellipsoidal reflectometer, and later to be used as a reference reflectance standard, have a reflectance known to ±0.0015 reflectance units and do not vary in reflectance by more than -0.000 and +0.003 reflectance units with angle of incidence up to incident angles of 50°.

TABLE 5

REFLECTANCE OF RHODIUM

λ	Average	Literature Values [46]
1.5	0.8383	0.882
2.0	.8850	.905
2.5	.9104	.915
3.5	.9339	.932
4.5	.9428	.942
5.5	.9470	.946
6.5	.9474	.950
7.0	.9510	.953

Further, this section illustrates the design of very simple and accurate infrared specular reflectometers, with an accuracy of at least ±0.0015 reflectance units. The use of the sulfur-coated diffusing sphere in front of the detector considerably reduces the inherent problems of optical alignment, and detector spatial sensitivity. It should be indicated that the design illustrated in figure 31 is not the best design, but the most convenient for this work. It would be a berter instrument if an odd number of reflections were used and the path length kept the same. The sulfur sphere (with a thermocouple detector and Globar source) should easily extend the use of the Bennett and Koehler [41] specular reflectometer to 8 microns.

APPENDIX C

OTHER FLUX-AVERAGING DEVICES

In the course of this work, several flux-averaging devices were tested for use with the ellipsoidal mirror reflectometer. Essentially, there are two workable solutions to the problems imposed by the use of large area detectors that are spatially sensitive.

(1) The absolute averaging device reads the flux correctly regardless of image configuration. The sulfur-coated sphere discussed in chapter 3 is such a device. So is the roughened gold-plated sphere. With the absolute device, no correction is made for either small area signals or large area signals.

(2) The averaging device that can be calibrated consistently reads the small area signal and the large area signal in known different factions. That is, the values can be corrected by using a calibration procedure to correlate the magnitude of a large area signal to that of a small area signal. Some devices of this nature are reported in this section.

The absolute method was preferred in this work, since calibration procedures for all other devices would have reduced the over-all accuracy of the measurements in the ellipsoidal reflectometer. If accuracies of the order of only five percent are required, the averaging device that can be calibrated is very useful. The results for several averaging devices are reported in the following discussion.

Diffusing Windows

The first device tested was a roughened sodium chloride window. The data in figure 32 are from the same types of tests as reported

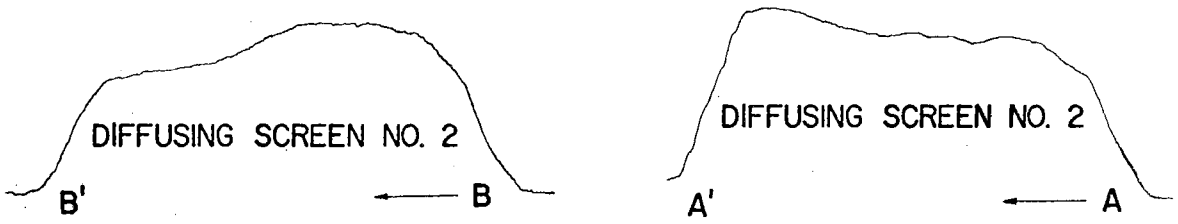

Results of scans across the sensitive area of the thermopile detector in the A-A' and B-B' directions, with unchopped tungsten incident flux. The A-A' direction is across five rows of plates, and the B-B' direction is across two columns of plates.

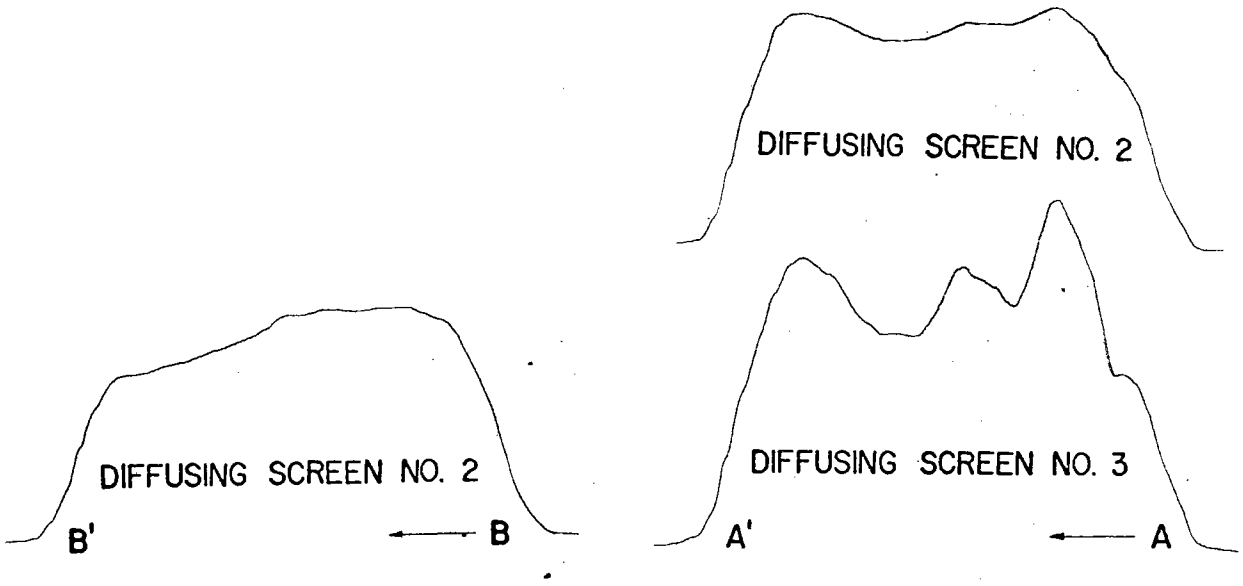

Results of scans across the sensitive area of the thermopile detector in the A-A' and B-B' directions, with chopped tungsten incident flux. The A-A' direction is across five rows of plates, and the B-B' direction is across two columns of plates.

Figure 32. Results of Spatial Sensitivity Test for NaCl Diffusing Screen. Reprinted from reference 47.

for figures 12 and 13, except that the diffusing screen holder* now held the diffusing screens. Diffusing screen No. 2 was 5 mm thick, and one surface had been ground with a 9.5 μ abrasive. Screen No. 3 was 2.5 mm thick, and one surface had been ground with a 50 μ abrasive.

In figure 32, it can be seen that diffusing screen No. 3 had only a slight effect in smoothing out the peaks, but diffusing screen No. 2 was quite effective, and produced a relatively uniform response across the sensitive area of the detector in both the a-c and d-c scans. The use of a roughened window would be suitable only for signals that are small relative to the detector area, since the roughened window would scatter energy away from the sensitive elements for larger area signals.

Diffusing Elbows

The second effort was to construct a diffusing elbow, shown in figure 33. This elbow greatly reduced the spatial sensitivity when the flux was incident on one end of the elbow, and the detector was placed at the other end. However, figure 34 indicates that the sensitivity of the elbow-detector combination varied radically with angle of incidence across the diffusing surfaces, while figure 35 shows relatively little angular sensitivity in the plane of incidence perpendicular to the mirror surfaces. Figure 36 is an improved design, in which the walls are all mirrors, except for the diffuse 45° surface used to reflect the incoming radiation toward the detector. The diffusely reflecting surface used with this device consists of a series of spherical depressions in

---

*The screen holder is used to hold the diffusing screens, to be tested, in front of the detector window.

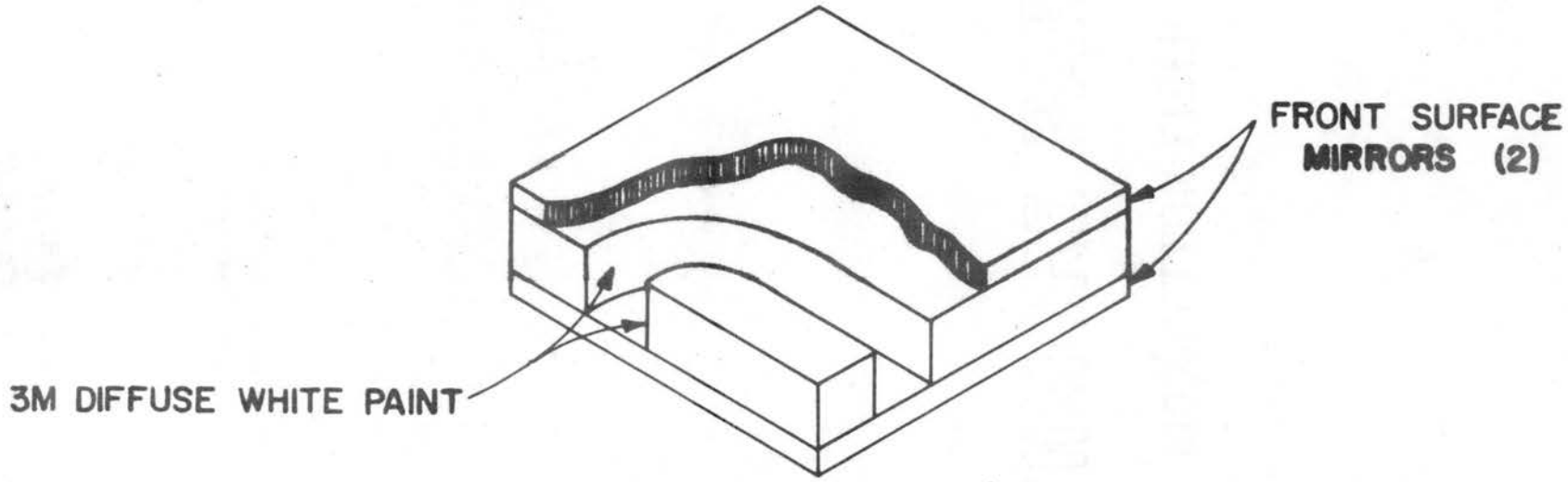

Figure 33. Diffusing Elbow

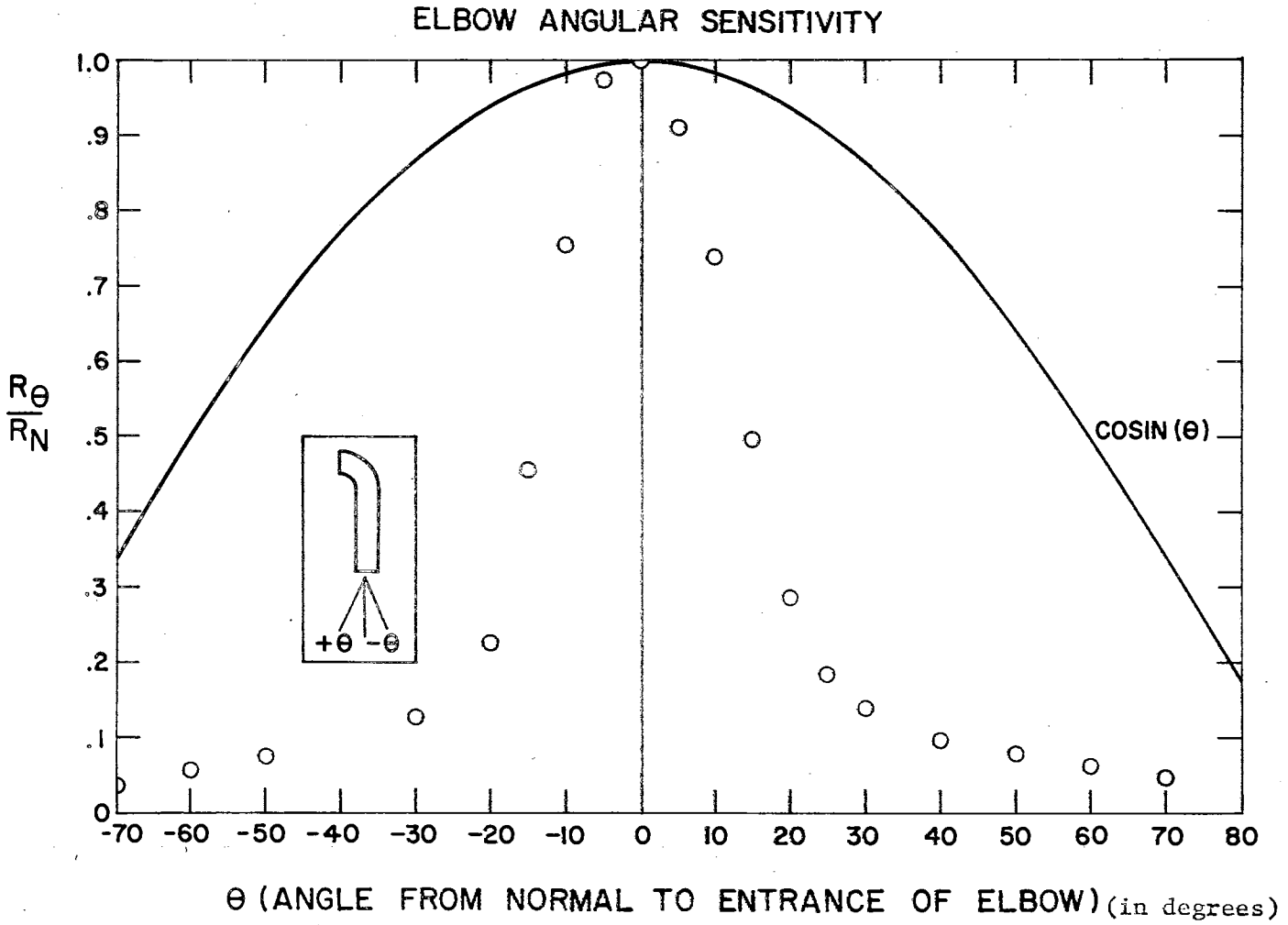

Figure 34. Angular Sensitivity of Diffusing Elbow

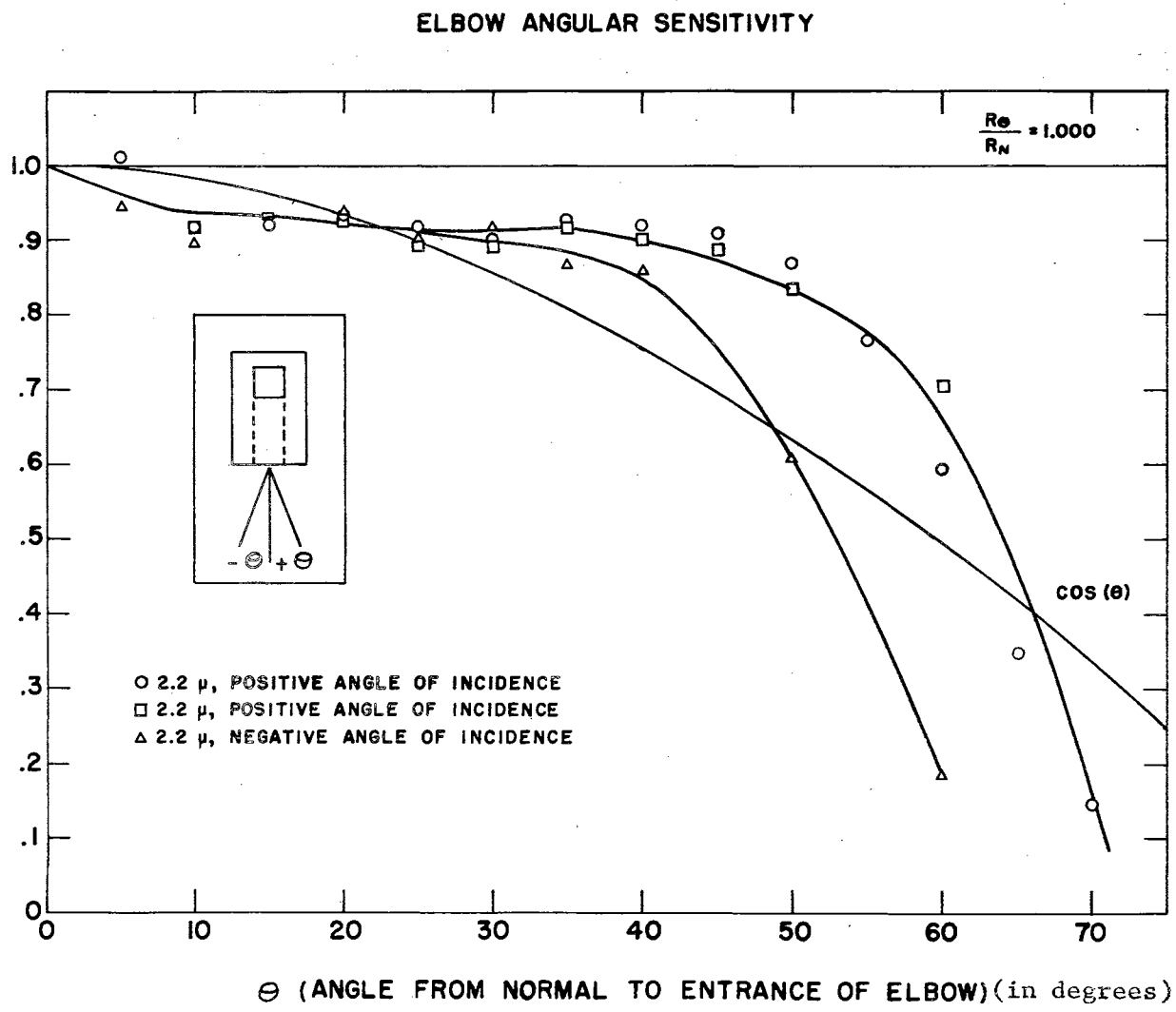

Figure 35. Angular Sensitivity of Diffusing Elbow (B)

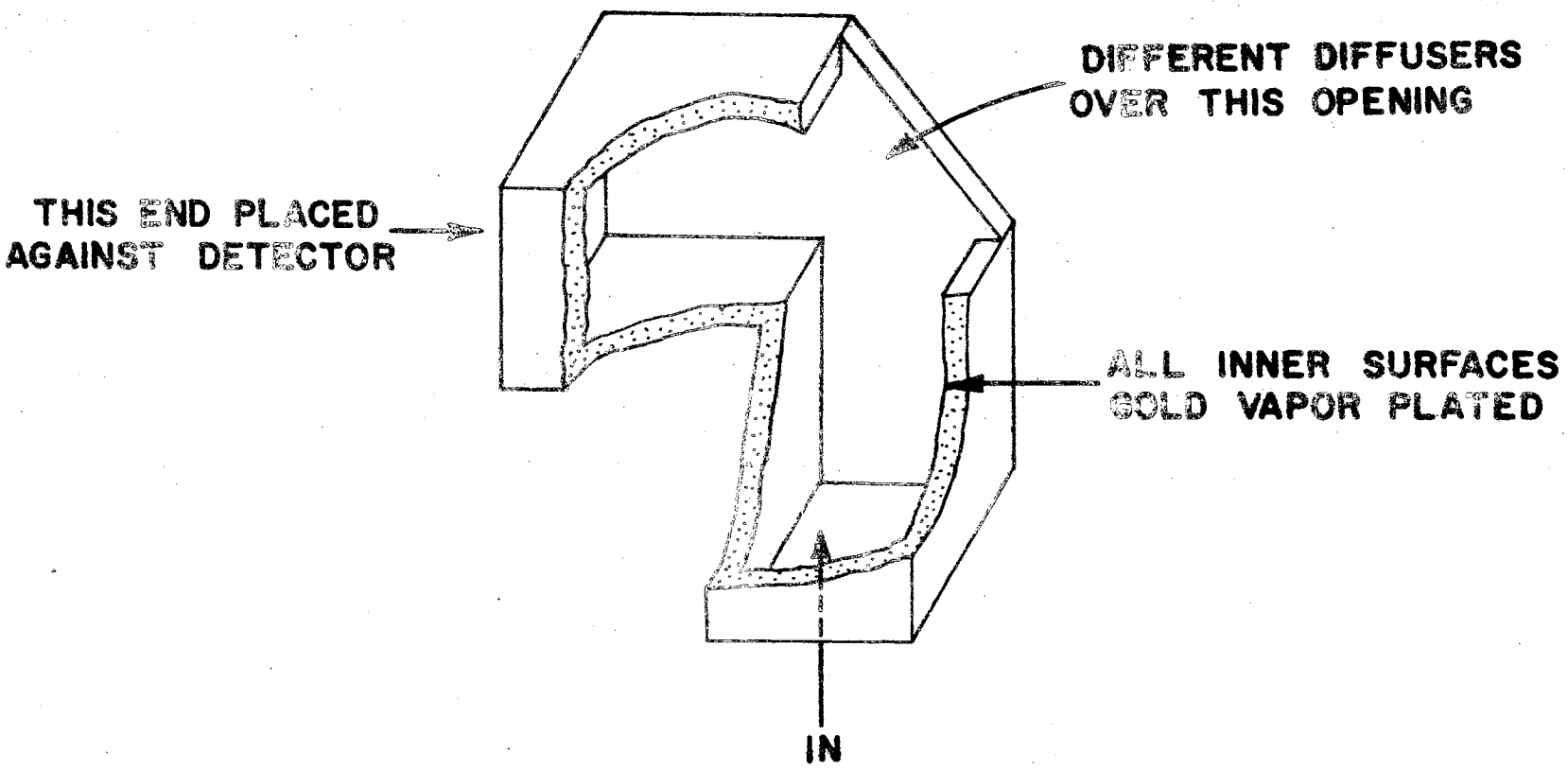

Figure 36. 45° Diffusing Elbow

aluminum, each of 1/16-inch radius, spaced 0.088 inch apart in a hexagonal, close pack array. Goniophotometric reflectance curves for this surface for white light incident at 45° are shown in figure 37. This surface has since been liquid honed, and then gold plated. The liquid honing gives a diffusing surface of small roughness, which, in combination with the large roughness of the spherical depressions, should reduce the height of the specular peak at 45°, seen in figure 37.

Figure 38 represents the spatial sensitivity (chapter III) of this elbow as a small image is traversed across the entrance port. It is apparent that a small area signal can be reproduced by positioning the elbow to yield a maximum signal for each case. Figure 39 represents the area sensitivity test (chapter III) for the case when for A/A(minimum) = 1 the elbow is moved until a maximum reading is obtained (figure 38) and then the area sensitivity of the elbow is measured. Figure 39 indicates that the decrease in signal for the large areas is calibratable; that is, the device senses the large area signal about 20 percent lower than the small area signal of the same flux. Thus, careful calibration and measuring techniques would allow use of a device of this nature for reducing spatial sensitivity for large area detectors.

Some devices that were not tested in this work, but appear to be qualitatively similar in nature to the above approaches, are:

(1) Condensing specular cones [39].

(2) A four-walled specular duct with a diffusing window at one end and the detector at the other, similar to the detector viewing configuration in reference 47.

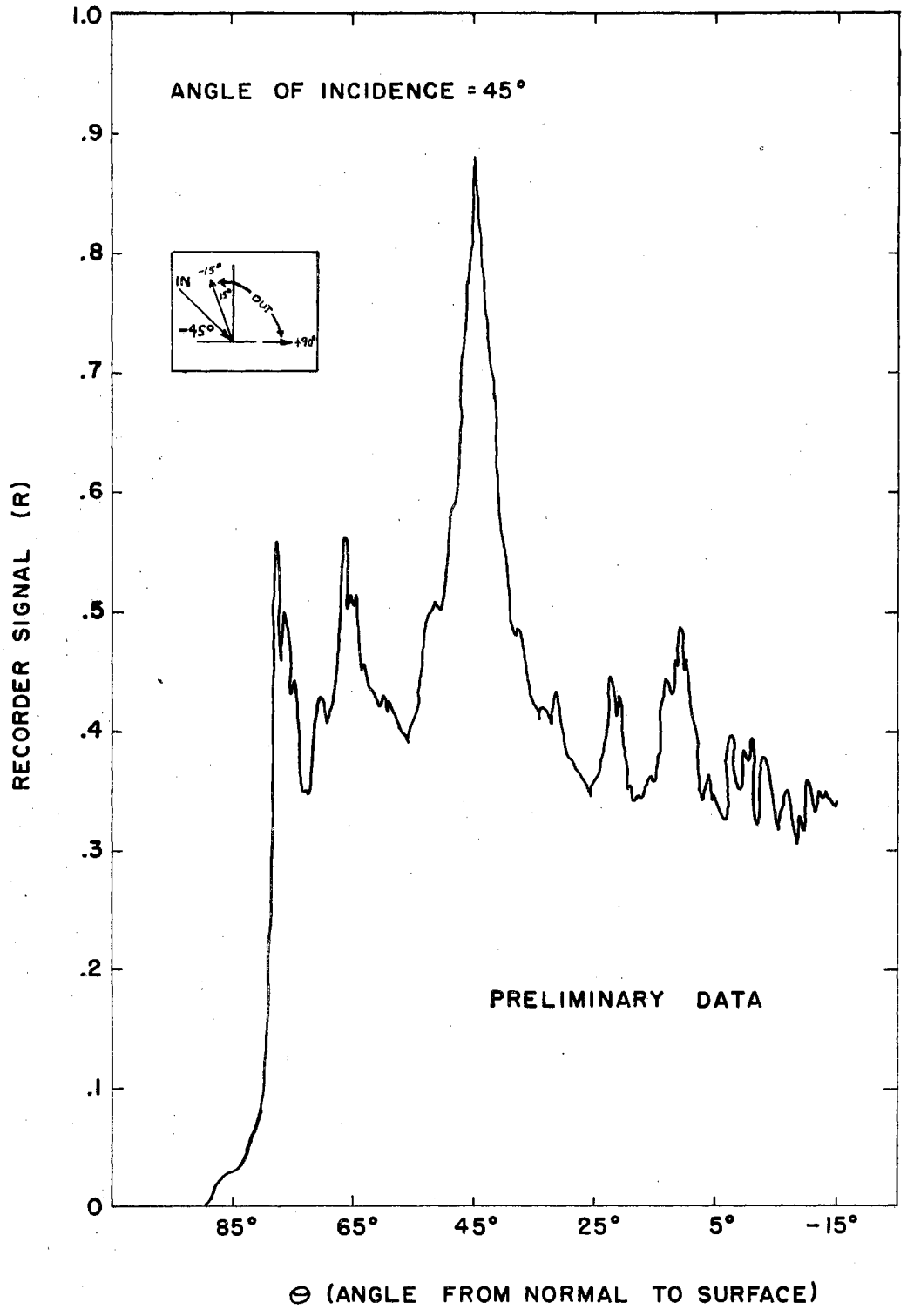

Figure 37. Goniophotometric Data of Spherical Impression Surface

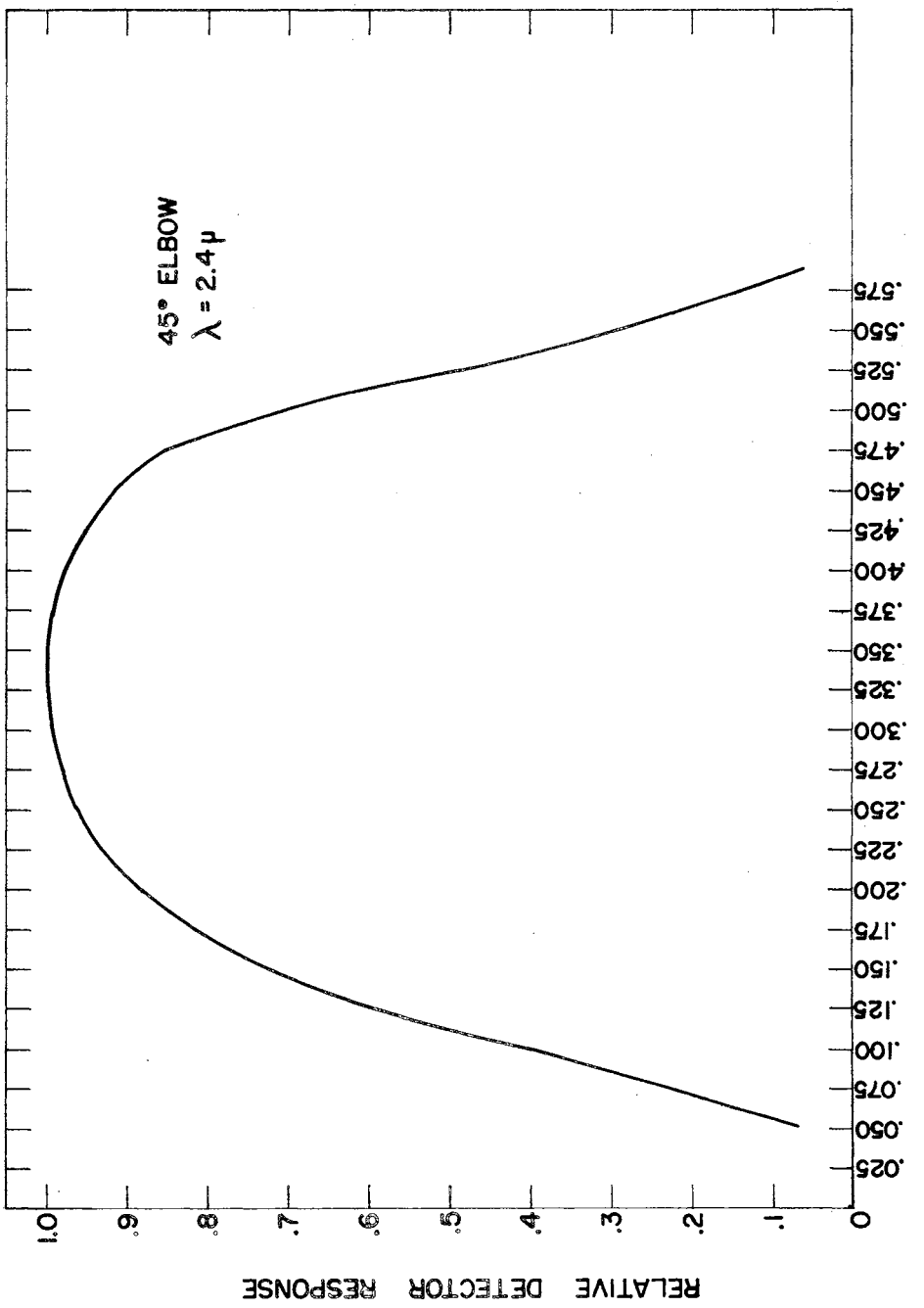

Figure 38. Spatial Sensitivity of 45° Diffusing Elbow

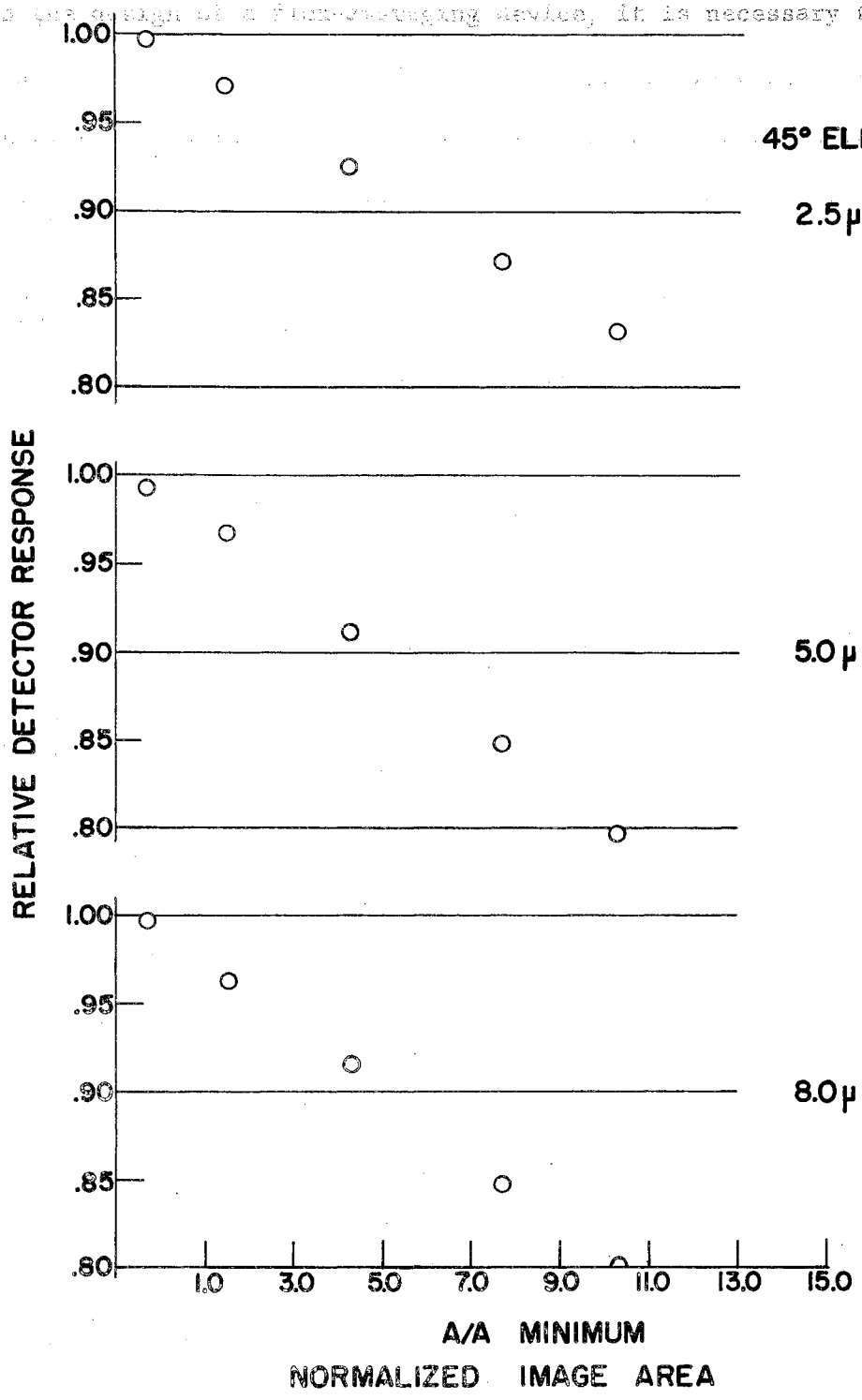

Figure 39. Area Sensitivity Test of 45° Diffusing Elbow

In the design of a flux-averaging device, it is necessary to decide what end accuracy is desired and to accept the fact that extremely good absolute averaging devices, available with present technology, very seriously limit the energy available for detection. Thus it is necessary to make a compromise between averaging ability and efficiency of energy detection. All the calibratable devices were in general more efficient by an order of magnitude than the absolute devices tested.

APPENDIX D

TEST FOR INTEGRATING SPHERE COATING

Although this dissertation is not specifically concerned with integrating sphere reflectometers, some of the measurements made while investigating diffusing spheres appeared to provide a practical test for the usability of a given sphere coating in an integrating sphere reflectometer. Tests of this nature are necessary, since perfect diffusers of unit reflectance are not available for sphere coatings. In each case, a sphere coating is a combination of a high reflector and a good diffuser; i.e., the higher reflectance coatings can be poorer diffusers and still perform acceptably in an integrating-sphere reflectometer.

To date, despite the very extensive use of integrating spheres for the past 40 years, there are only two accurate tests to compare the performance of the actual integrating sphere reflectometer to the theoretical model used for reducing the data from the actual reflectometer.

The first of these tests is quite old but, for reasons unknown, its use has not been reported in the literature. Goebel, et al. [48], have expressed the theoretical basis for the "appended sphere" approach and have gathered preliminary data. The "appended sphere" technique utilizes the theory of integrating spheres to compare theoretically and experimentally the efficiency of a small sphere with a diffusing coating and one opening to the reflectance of a flat sample of the same diffusing material. Both the efficiency of the small sphere and the reflectance of the flat sample are measured with a standard integrating sphere.

The second of these tests is the relatively new approach of the "First Reflection Cavity," which was utilized by Dewitt and Richmond [49]. This approach utilizes a cavity of a varying depth with a "perfectly" diffusing bottom and "perfectly" absorbing side walls. By varying the depth of the cavity and measuring the effective reflectance of the cavity and comparing this to the diffuse configuration factor from the image centered on the bottom of the cavity to the opening at the top of the cavity, one then establishes how well the integrating sphere reflectometer measures flux of differing geometric distribution in the sphere.

Both of these tests are quite elaborate and depend on very exacting experimental conditions, including the availability of a complete integrating sphere reflectometer. The test proposed below provides a quick easy way to establish at least a necessary condition for an integrating sphere coating.

Qualitative Description of Test

The general optical system for these tests is shown schematically in figure 10. In this test, the sphere was mounted with its entrance port at the center of rotation of the milling head, and the incident beam was centered on the entrance port. The sphere was then rotated, and the response of the detector was recorded as a function of the angular position of the sphere measured as the angle between the axial ray of the incident beam and the normal to the sphere entrance port.

If a perfect integrating sphere were tested in this way, and the detector viewed only a portion of the sphere wall, as illustrated in figure 40, then the signal from the detector would change as the

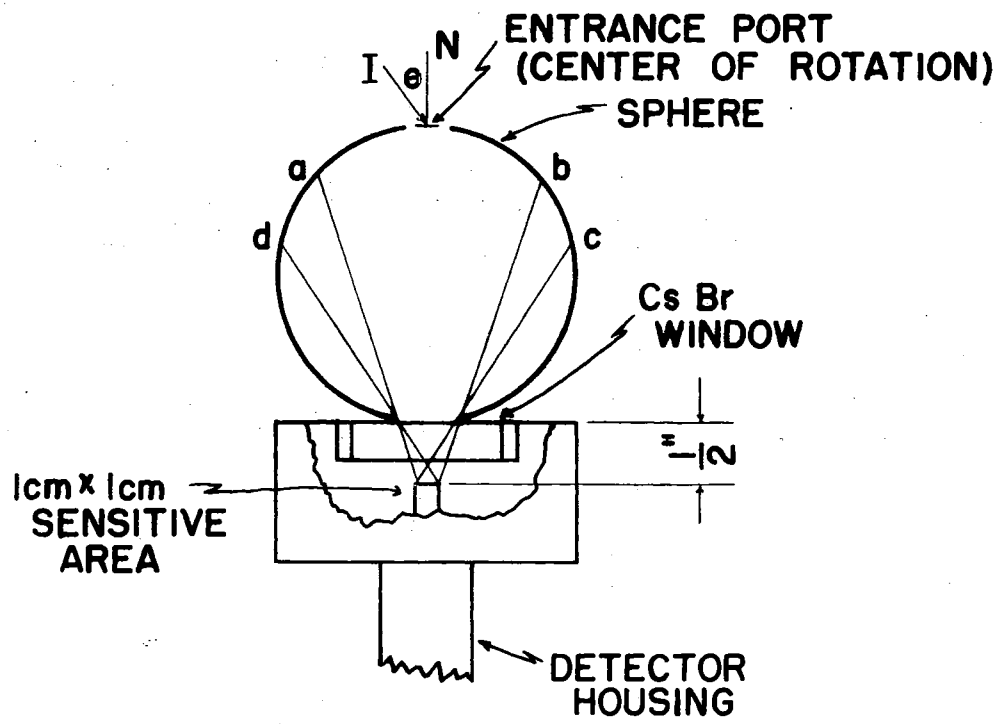

GENERAL DETECTOR VIEWING CONFIGURATION

Figure 40. Model for Sphere Test

illuminated spot moves around the sphere, by an amount proportional to the difference in brightness of areas on the sphere wall that are and are not illuminated by the incident flux. If the area illuminated by the incident beam is not viewed by the detector, no flux will be received by the detector on the first reflection of the incident flux. Thus, for a surface that approaches an ideal integrating sphere coating, the curve of response as a function of angle should show two ranges of constant response with a smooth monotonic transition between the two ranges. The lower range would represent those angles at which the detector views none of the illuminated area, and the higher level would represent those angles at which it views the entire illuminated area, and the transition would represent those angles at which the detector views an increasing fraction of the illuminated area.

Theory for Tests of Integrating Sphere Coatings

Figure 40 illustrates the theoretical model to be studied. The flux from the first reflection will be considered separately from that due to multiple reflections in the sphere. To get a quantitative value for the ratio of the two flat regions discussed above, it is necessary to account for the flux getting to the detector in each case.

Case 1. The detector does not view the first reflection of the incident flux (F). The incident flux (F) is reflected by the sphere wall (with a reflectance of ρ_S).

$$R = F \rho_S \tag{55}$$

and none of this reflected flux impinges directly on the detector. This flux is then rereflected by the entire sphere (except for the portion lost out the entrance and exit ports).

$$R = F \rho_S^2 \frac{A_{SH}}{A_S} \tag{56}$$

Where A_S is the total area of the sphere ($A_S = 4\pi R^2$) and $A_{SH} = A_S - A_{H1} - A_{H2}$ (A_{H1} and A_{H2} are the areas of the exit and entrance ports, respectively). Of the flux R_1', only R_2' reaches the detector sensing element.

$$R_2' = F \rho_S^2 \frac{A_{SH}}{A_S}\left[\frac{A_{DV} - A_{H2}}{A_S}\right] f_1 \tag{57}$$

where A_{DV} is the area of the sphere fully viewed by the detector, $(A_{DV} - A_{H2}/A_S)$ is the proportion of the twice-reflected flux in the area viewed by the detector, and f_1 is the diffuse configuration factor from $(A_{DV} - A_{H2})$ to the sensing element of the detector.

Similarly, on the third reflection the amount of flux R_3' reaches the detector

$$R_3' = F \rho_S^3 \left(\frac{A_{SH}}{A_S}\right)^2 \left[\frac{A_{DV} - A_{H2}}{A_S}\right] f_1 \tag{58}$$

and on the n'th reflection

$$R_n' = F \rho_S^n \left(\frac{A_{SH}}{A_S}\right)^{n-1} \left[\frac{A_{DV} - A_{H2}}{A_S}\right] f_1 \tag{59}$$

The sum of the quantities of flux that reaches the detector is easily summed to

$$E_1 = F \rho_S^2 \frac{A_{SH}}{A_S} \left[\frac{A_{DV} - A_{H2}}{A_S} \right] f_1 \left[\frac{1}{1 - \rho_S \frac{A_{SH}}{A_S}} \right] \tag{60}$$

Thus, the flux reaching the detector for the case where the detector does not view the first reflection is E_1.

Case 2. The detector views the first reflection. In this case, the only additional flux impinging on the detector is that due to the first reflection. From equation (55), this is

$$R_1''' = F\ \rho_S\ f_2 \tag{61}$$

where f_2 is the configuration factor from the area illuminated by the beam to the detector sensing element. Since this is the only additional flux impinging on the detector, the total flux reaching the detector for this case is

$$E_2 = E_1 + F\ \rho_S\ f_2 \tag{62}$$

The ratio of the flux reaching the detector for these two cases is

$$\frac{E_1}{E_2} = \frac{E_1}{E_1 + F\ \rho_S\ f_2} = \frac{1}{1 - \dfrac{F\ \rho_S\ f_2}{E_1}} \tag{63}$$

which upon substitution from equation 60 becomes

$$\frac{E_1}{E_2} = \frac{1}{1 + \dfrac{(f_2/f_1)\left[A_S - \rho_S A_{SH}\right]A_S}{\rho_S (A_{SH})(A_{DV} - A_{H2})}} \tag{64}$$

Therefore, the ratio of the detector readings when it does and does not view the illuminated area is known for a completely diffuse sphere coating.

Thus, an easily performed test can illustrate the quality of a given sphere coating with regard to its reflectance-diffuseness combination, the uniformity of coating reflectance throughout the sphere, and whether the cavity used is close enough to a sphere in shape.

Preliminary Data

Two types of possible infrared sphere coatings were tested with the configuration illustrated in figure 40. These were the roughened gold-plated coating and the "Crystex" sulfur coating; both are described more completely in appendix E.

Gold Roughened Spheres

Figure 41 shows results obtained with the gold-plated S-460 shot, 2-inch diameter sphere, at wavelengths of 2.2, 5, and 8 μ. In this case, the detector port is in the plane of incidence, and is diametrically opposite the entrance port. The curves indicate that there is a large specular component to the reflected flux at 50°, and that the reflectance characteristics do not change appreciably with wavelength. The S-460 shot surface has a roughness of about 150 μ in rms; hence, no effect of wavelength would be expected in this range. This sphere coating does not follow the integrating sphere model in any respect; thus, it does not appear promising as a true integrating sphere coating.

Sulfur Sphere Coatings

The sulfur sphere coating outlined in chapter III also was tested in this manner. Figure 42 illustrates the results for sulfur at 1.5, 2.2, 5.0, and 10.0 μ. Each of these curves illustrates two flat regions with a smooth monotonic transition between the regions. These results gave a qualitative indication of the utility of sulfur surface as an integrating sphere coating. However, the values for the ratio of the reading when the illuminated area was not viewed directly by the detector (area c-d in figure 40, i.e., the low flat portion of the curves in figure 42),

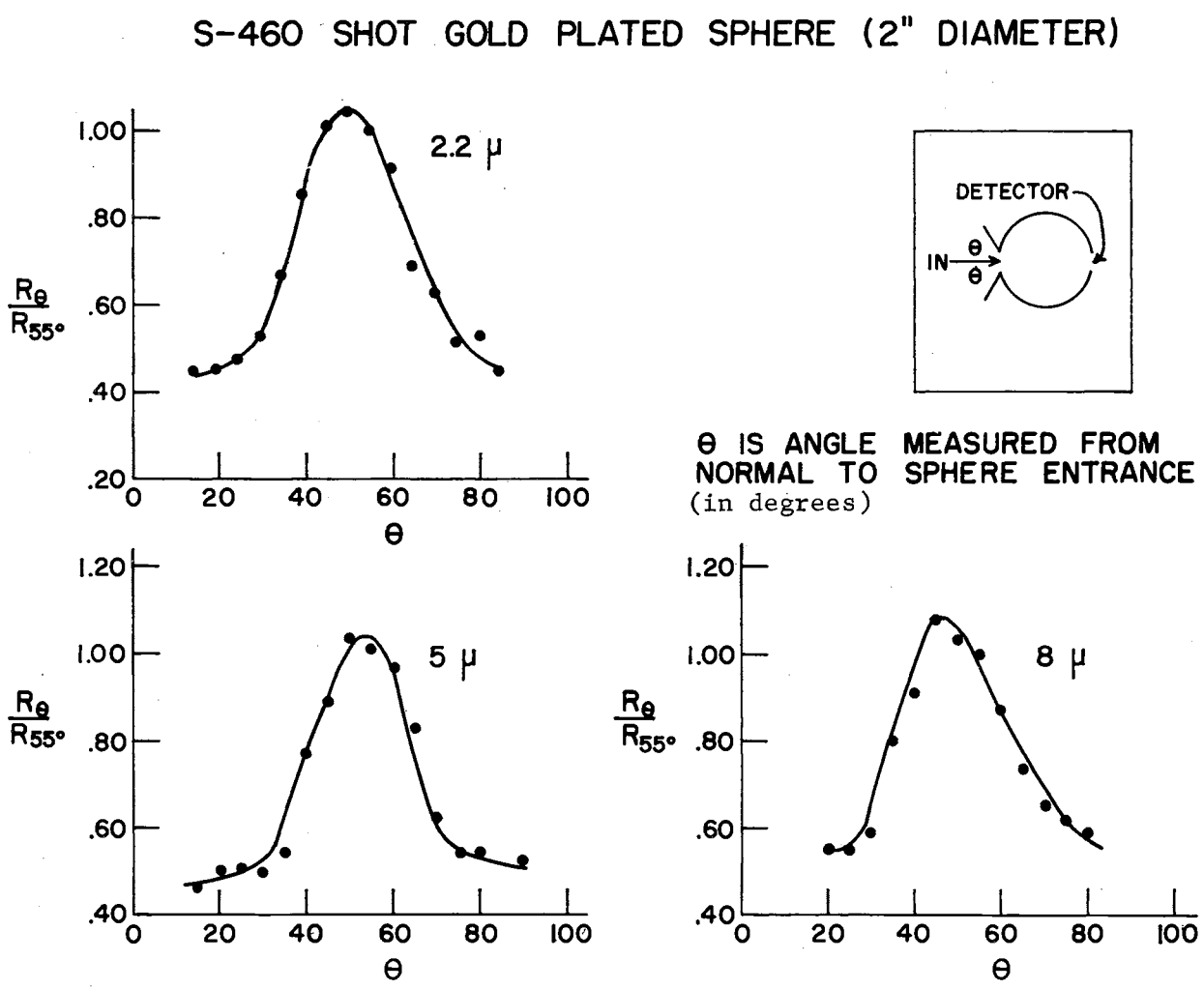

Figure 41. Sphere Test for Gold Roughened Sphere

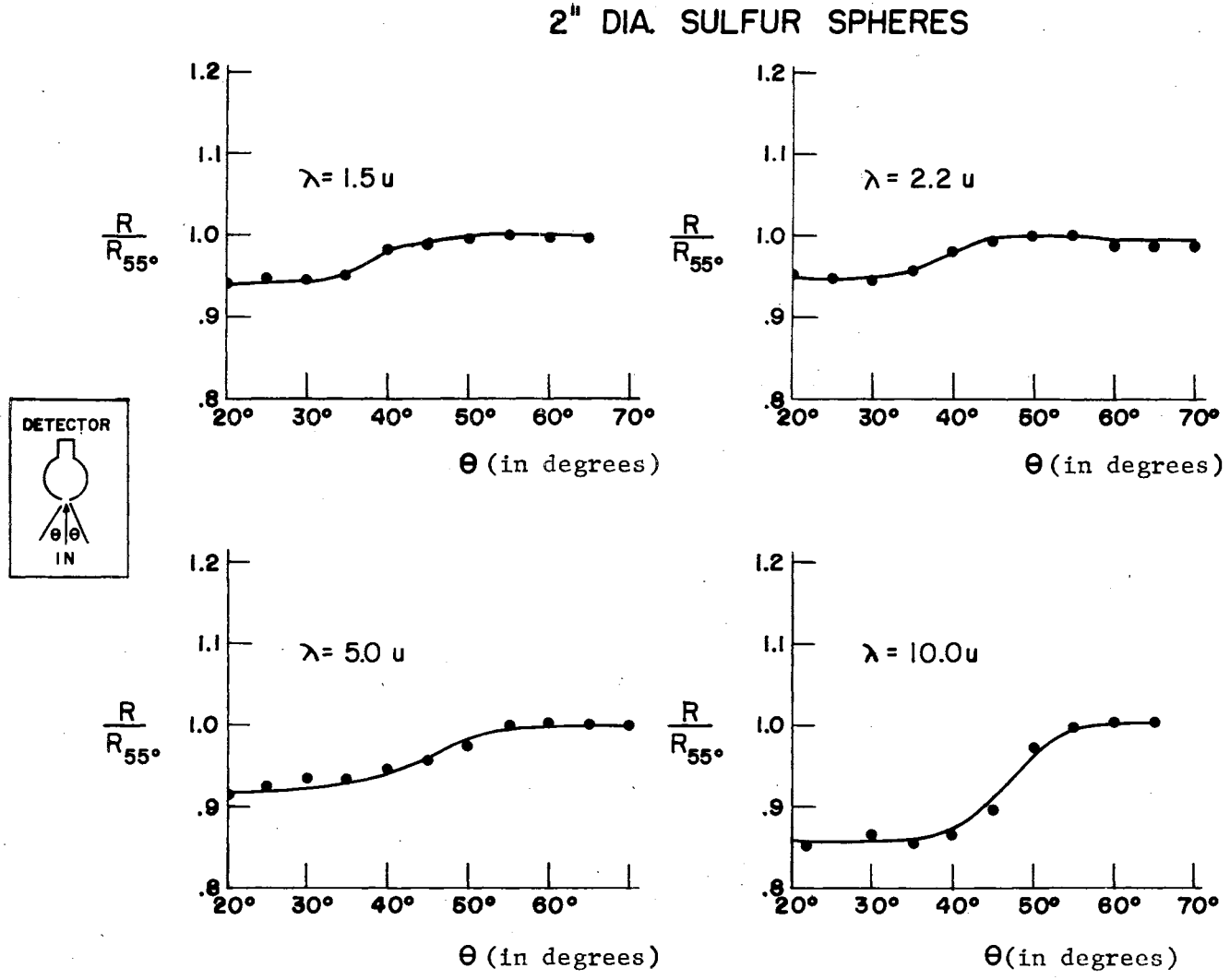

Figure 42. Sphere Test for Sulfur Coated Sphere

and the reading when it was viewed directly by the detector (area a-b in figure 40, high flat portion of the curves in figure 42) were lower by a factor of 2-3 than would be predicted by theory (equation (64)). Apparently, the experimental set-up did not fit the theoretical model. The following may contribute to the failure of quantitative theoretical and experimental agreement.

(1). The flux from the illuminated area when it is not directly viewed by the detector (i.e., when the incident flux is in area c-d in figure 40) could reach the detector by paths other than by being multiply reflected from the d-a-b-c area viewed by the detector, by (a) hitting the lip of the detector port and being reflected to the detector, and (b) being diffused to the detector by scratches on the CsBr window. The net effect would be to increase the height of the low flat portion of the curves in figure 42.

(2). The illumination in the a-b area of figure 40 is incident at high angles of incidence, where even the best diffusers tend to become somewhat specular. Thus, the flux tends to be specularly reflected around the sphere wall into the area c-d, which is not viewed by the detector, instead of being diffusely reflected to the detector. The net effect would be to reduce the value of the high flat portion of the curves in figure 42.

(3). Using the wrong value for A_{DV} in equation 64.

(4). Using the wrong value for the reflectance of the sulfur coating.

(5). Improper evaluation of f_1 and f_2.

Undoubtedly, the first two effects are largely responsible for the low ratio of the two signals, as compared to the theoretical model.

Detector and beam configurations for a proposed new test are given in figure 43. In this test, both beams are incident at angles near normal, and flux from areas not viewed by the detector can no longer reach it by indirect paths. Equation (64) will still be valid, except that $A_{SH} = A_S - A_{H1} - A_{H2} - A_{H3}$.

This procedure should provide a convenient bench test for investigating the quality of individual sphere coatings. As such, it could be utilized in studying the many proposed coatings for infrared integrating spheres.

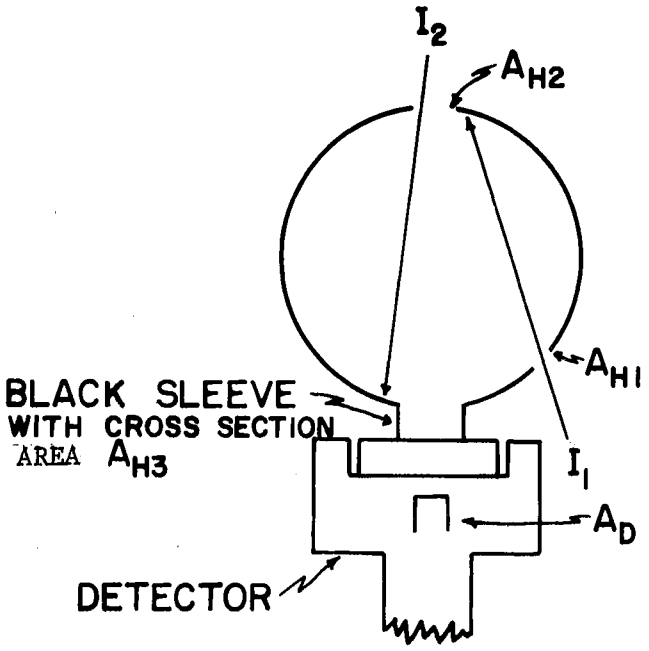

Figure 43. Sphere Configuration for Integrating Coating Tests

APPENDIX E

Several types of sphere coatings were prepared for use as described in chapter III and appendices C and D. This section briefly outlines the methods used in preparation of these surfaces. In each case, two hemispheres were coated and then joined to form the sphere.

Sulfur

All sulfur used in this work was Crystex brand sulfur; however, reference 38 indicates that ordinary flowers of sulfur has about the same reflectance as Crystex brand sulfur through the infrared. No effort was made to establish the usefulness of this or other forms of sulfur other than Crystex brand sulfur. It should also be noted that Stauffer Chemical Co., also supplies Crystex brand sulfur which contains 20 percent by weight of oil and which has excellent mechanical properties. However, information on the reflectance is not available. Several different techniques were used to apply sulfur to the sphere walls, as follows:

Hand Pressed: Initially, sulfur was applied to the sphere over a thin coat of rubber cement by hand pressing (with the fingers). The sulfur was built up to a thickness of about 1/8 inch, and contoured to roughly conform to the outline of the two hemispheres. The surface was then smoothed with an artist's brush. This surface had a fairly uniform appearance but it was extremely fragile.

Sulfur-Alcohol Slurry: To increase the uniformity of the coating over the surface of the sphere and the reproducibility from one sphere to

another, a spraying application technique was investigated. One part sulfur was mixed with about two parts alcohol by volume to form a slurry which was sprayed from a BVl Model VS-850 Electric Sprayer.* The slurry was sprayed so that most of the alcohol evaporated before the spray hit the roughened (approx. 50 μ in. rms) sphere wall. To insure rapid evaporation of the remaining alcohol, the hemispheres were heated to 170 °F before spraying. About ten spray applications were necessary to obtain a 1/8-inch coating. The hemispheres were reheated to 170 °F and the sulfur surface was smoothed with an artist's brush between applications. The resulting coating was very uniform in appearance, but it tended to crack with time, and its adherence to the metal hemisphere was poor. The sulfur itself formed a quite hard surface.

Benzene-Sulfur Slurry: To alleviate the problems experienced with the sulfur-alcohol slurry, the alcohol was replaced by benzene. This slurry was applied to the roughened hemisphere wall over a thin coat of a benzene-soluble contact cement. During the first few seconds of spraying, the spray gun was held very close to the surface so that the benzene dissolved the contact cement, which migrated slightly into the sulfur coating. The thin coating was then dried, leaving the sulfur bonded to the sphere wall. For the subsequent spraying operation, the spray gun was moved further away from the sphere wall, the temperature of which was maintained at about 150 °F by heat from two infrared lamps. This, and the fact that benzene is more volatile than alcohol, permitted the slurry to be sprayed continuously until a coating thickness of about 1/8 inch was obtained. The surface was then smoothed with an artist's

*Burgess Vibrocrafters, Inc., Grayslake, Illinois.

brush. The surface produced by this technique was very uniform in appearance and mechanically strong enough to withstand normal laboratory handling. The surface hardened considerably with age.

$BaSO_4$ Surfaces

A $BaSO_4$-Benzene slurry was sprayed in the same manner as the sulfur-benzene slurry to coat spheres with $BaSO_4$.

Gold-Roughened Surfaces

Several spheres were roughened with glass and steel spherical shot by the Pangborn Company, using a Roto-blast process. The glass shot (Pangborn No. L) are -200+325 mesh SAE and yield a surface roughness on the aluminum sphere of about 25 μ inch rms. The steel shot (Pangborn No. S-460) are 10 mesh SAE and yield a surface roughness on the aluminum spheres of about 150 μ inch rms. After the hemispheres had been uniformly roughened with one of the above shots they were cleaned and gold was vapor-deposited onto the surface.

APPENDIX F

EFFECTIVE REFLECTANCE OF THE ELLIPSOIDAL MIRROR

The reflectance measured in this section is the effective reflectance defined in chapter IV. The effective reflectance accounts not only for mirror absorptance and transmittance, but also for scattering due to surface roughness and aberrations due to improper construction of the ellipsoidal mirror.

The effective reflectances of various areas of the ellipsoidal mirror were measured because (1) in the absolute reflectance measurement (chapter IV) it was necessary to know the reflectance of the ellipsoidal mirror, and (2) in the relative reflectance measurement it was necessary to know the change of reflectance with position of the reflected sample flux on the mirror.

Figure 44 illustrates the 13 areas of the mirror that were examined. First, the reflectance of area 1 was measured using one of the calibrated mirrors described in appendix B, and then the reflectances of the remaining 12 areas were compared to that of area No. 3 by using two of the calibrated mirrors described in appendix B. These two calibrated mirrors were used to compare, for one pair of areas at a time, the flux reflected from one of the outer areas (areas 2 - 13) to the flux reflected by area No. 1. All of the areas on the mirror were larger than ½ inch square, so that each reflected flux represented an average sampling of the reflectance over the particular region of the ellipsoidal mirror.

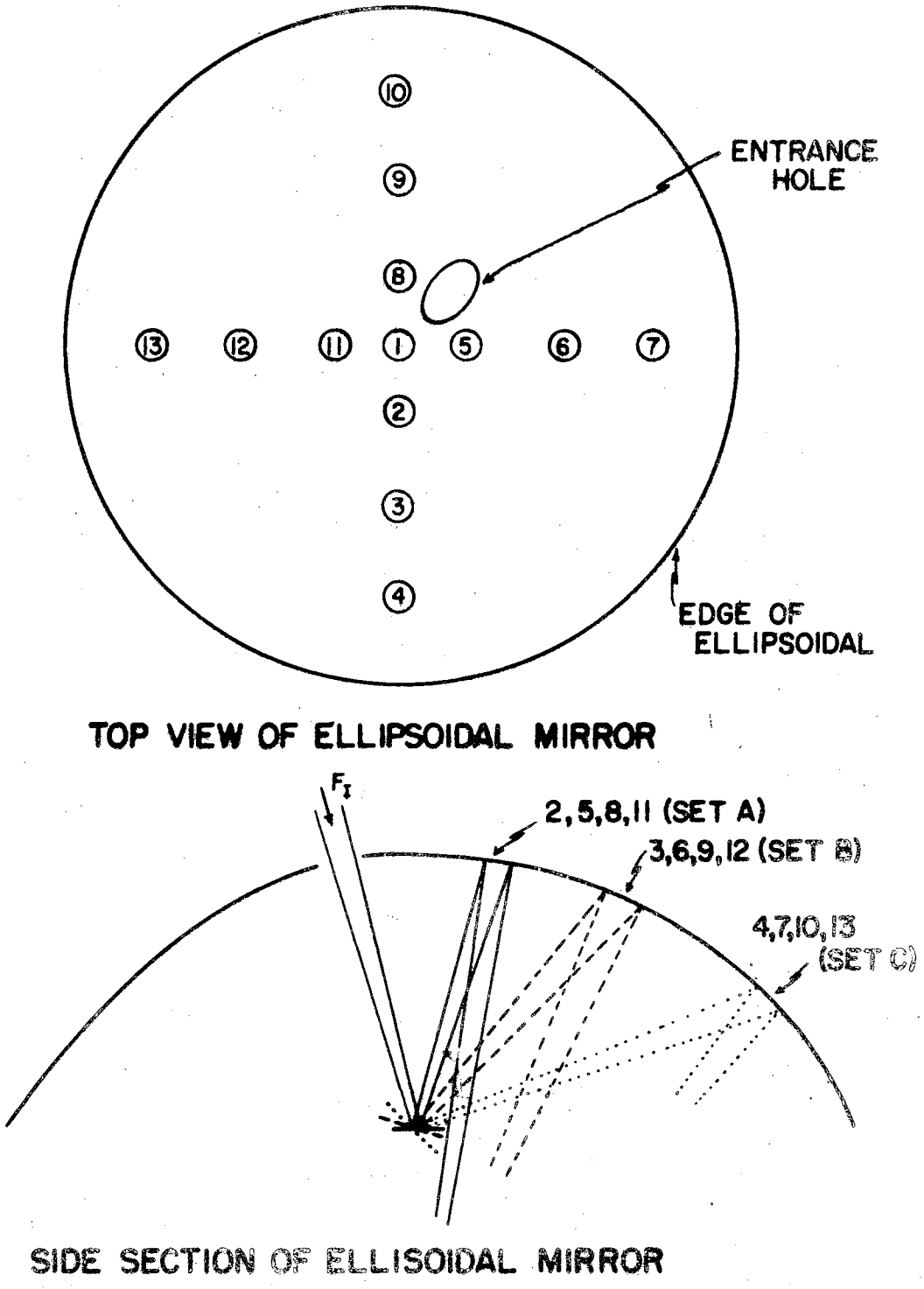

Figure 44. Areas Used in Effective Reflectance Measurement

Reflectance Measurement

The reflectance of area 1 was evaluated by taking two measurements; one with the averaging sphere-detector combination at the first focal point, to measure the incident flux F_I, and the other with a calibrated aluminum mirror at the first focal point and the detector at the second conjugate focal point, to measure the flux F_1 reflected by the sample and the ellipsoidal mirror. In both measurements the image of the flux to be measured was positioned on the same place in the averaging sphere, so that a very accurate comparison of the two fluxes could be made (see chapter III). Also, in both measurements, the sphere entrance was shielded to allow entrance of only the flux to be measured, eliminating any flux interchange between the sphere and the ellipsoidal mirror (see chapter IV). Since this is essentially an absolute reflectance measurement, the analysis of chapter IV can be used. Equation (9) of chapter IV yields

$$F_{ID} = F_I \eta \tag{65}$$

and equation (51) yields

$$F_{RD} = F_I \eta \rho_m \rho_\epsilon \tag{66}$$

where the terms for the interchange between the ellipsoidal mirror and the sphere entrance are eliminated by the shielding described above. Therefore

$$\bar{\rho}_\epsilon = \frac{F_{RD}}{F_{ID}\ \rho_m} \tag{67}$$

where ρ_m is given in Table 3 of appendix B. The values obtained from four sets of these measurements are listed in table 6. The arithmetic average

of ρ_ϵ for area No. 1 for these four sets was used in computing the reflectance of the other areas of the mirror.

TABLE VI

ELLIPSOIDAL MIRROR REFLECTANCE

	Set #1	Set #2	Set #3	Set #4	Average
1.5μ	0.951	0.949	0.951	0.948	0.950
2.0μ	.964	.963	.959	.961	.962
2.5μ	.965	.969	.967	.963	.966
3.5μ	.969	.971	.969	.971	.970
4.5μ	.969	.971	.970	.973	.971
5.5μ	.970	.971	.973	.970	.971
6.5μ	.971	.973	.973	.974	.972
7.0μ	.972	.972	.974	.973	.972

Variation of Reflectance with Position

The change of reflectance as a function of position was measured by use of two of the calibrated mirrors. These mirrors were placed on sample holders set at different angles to the first focal plane of the ellipsoidal mirror (figure 44). Four measurements for each pair of areas were made. One of each pair of measurements was made with area No. 1 in the optical path. The detector was again shielded to prevent interchange between the averaging sphere and the ellipsoidal mirror. The flux viewed by the detector was

$$F_{ID} = \eta\, F_I\, \rho_{m1}\, \rho_{\epsilon 1} \tag{68}$$

where $\rho_{\epsilon 1}$ is the reflectance of area No. 1 and ρ_{m1} is the reflectance of the particular sample mirror. The second measurement was made with sample mirror 2 placed on another sample holder such that one of the remaining areas was in the optical path (areas No. 2-13). Again the averaging

sphere was shielded to prevent interchange with the ellipsoidal mirror. The flux viewed by the detector was

$$F_{nD} = \eta\, F_I\, \rho_{m2}\, \rho_{en} \tag{69}$$

where n represents one of the areas No. 2 through 13. Since the efficiency of the averaging sphere (η) is the same for equations (68) and (69), the ratio of these fluxes is

$$\left(\frac{F_{nD}}{F_{1D}}\right)_{21} = \frac{\rho_{m2}}{\rho_{m1}} \frac{\rho_{en}}{\rho_{e1}} \tag{70}$$

To eliminate the effect of a possible difference in reflectance between ρ_{m2} and ρ_{m1}, the mirror samples were interchanged and measurements taken again to yield

$$\left(\frac{F_{nD}}{F_{1D}}\right)_{12} = \frac{\rho_{m1}}{\rho_{m2}} \frac{\rho_{en}}{\rho_{e1}} \tag{71}$$

From equations (70) and (71), the ratio of the two reflectances is given by

$$\frac{\rho_{en}}{\rho_{e1}} = \sqrt{\left(\frac{F_{nD}}{F_{1D}}\right)_{21} \left(\frac{F_{nD}}{F_{1D}}\right)_{12}} \tag{72}$$

Table 7 presents the values obtained in this manner for the 13 positions and for the 8 wavelengths used in this work. The results indicate that ρ_{en}/ρ_{e1} does not vary with wavelength and that ρ_{en}/ρ_{e1} increases as one moves away from the apex of the ellipsoidal mirror. Thus, it is apparent that the reflectance of the outermost parts of the mirror is about 1.5 percent higher than that of the apex at all wavelengths. Therefore, the flux from a diffusing sample when measured with the ellipsoidal mirror reflectometer should be corrected for mirror reflectance depending on what part of the mirror is used to refocus the flux at the second focal point (see chapter IV).

TABLE VII

THE CHANGE IN REFLECTANCE OF THE ELLIPSOIDAL MIRROR AS A FUNCTION OF POSITION. VALUES ARE ALL REFERRED TO AREA NO. 1. FOR LOCATION OF THE AREAS ON THE ELLIPSOID, SEE FIGURE 44.

Wavelengths → / Areas↓	1.5 μ	2.0 μ	2.5 μ	3.5 μ	4.5 μ	5.5 μ	6.5 μ	7.0 μ
1	1.000	1.000	1.000	1.000	1.000	1.000	1.000	1.000
2	1.001	1.001	1.000	1.000	1.000	1.000	1.001	1.000
3	1.002	1.002	1.001	1.000	1.001	1.001	1.001	1.002
4	1.013	1.010	1.012	1.016	1.016	1.015	1.015	1.013
5	1.000	1.001	1.002	1.001	1.000	1.001	1.000	1.000
6	1.002	1.002	1.003	1.001	1.002	1.002	1.002	1.001
7	1.015	1.013	1.015	1.015	1.014	1.014	1.015	1.013
8	1.001	1.001	1.001	1.000	1.002	1.001	1.001	1.001
9	1.002	1.002	1.003	1.002	1.003	1.002	1.003	1.002
10	1.014	1.015	1.014	1.016	1.015	1.015	1.015	1.014
11	1.001	1.002	1.001	1.000	1.000	1.001	1.001	1.002
12	1.002	1.002	1.001	1.002	1.001	1.002	1.002	1.002
13	1.013	1.014	1.014	1.016	1.014	1.014	1.015	1.014
Average Values of Areas Equal Distance From the Apex of the Ellipsoid								
Set A*	1.001	1.001	1.001	1.000	1.001	1.001	1.001	1.001
Set B*	1.002	1.002	1.002	1.001	1.002	1.002	1.002	1.002
Set C*	1.014	1.013	1.014	1.016	1.015	1.015	1.015	1.014

*Set A is composed of areas 2, 5, 8, and 11; set B is composed of areas 3, 6, 9, and 12; and set C is composed of areas 4, 7, 10, and 13.

To increase the accuracy of this measurement, a scale expansion technique (provided for on the Brower Model 129 amplifier) was used. With this technique, the scale is expanded by a factor of 5 by suppressing the zero by 400 percent. Hence, the error in reading the data from the recorded curve is reduced by about a factor of 5. This permits small changes in large signals to be measured with increased precision. The precision of these measurements is expected to be greater than that reported for the measurements in appendix B. This scale expansion technique could be used to increase the precision and accuracy of the values reported in appendix B.

APPENDIX G

ERROR ANALYSIS OF THE ELLIPSOIDAL MIRROR REFLECTOMETER

This section deals with estimating the errors involved in the various corrections discussed in chapter IV, which are required to establish $\rho(7°,\theta)$.* The estimated error is used because most of the corrections depend on an unknown quantity, the geometric distribution of the reflected flux. Thus, this particular error analysis is based on an estimate of the effects of various changes in the geometric distribution of the fluxes on the individual losses. In this section the various parameters will be considered to vary over ranges that are larger than the expected ranges for engineering surfaces. This should permit a conservative estimate of the accuracy of an ellipsoidal reflectometer measurement. This analysis does not distinguish between the errors caused by imprecision and the errors caused by uncertainties in measured parameters (random error and bias).

The error analysis will concern equation (53), chapter IV, which is the equation used to determine the absolute reflectance of the sample. The additional errors present in the direct measurement of absolute reflectances are discussed at the end of this section. In the error analysis of the relative reflectance measurement, the following types of errors are considered.

*Throughout this section ρ_s and $\rho(7°,\theta)$ are used interchangeably.

(1). Errors due to the flux interchange between the ellipsoidal mirror and the averaging sphere.

(2). Errors due to incomplete knowledge of system parameters.

(3). Errors due to uncertainty in the measurement of F_{SD}, F_{S1D}, F_{S2D}, and F_{DD}.

(4). Errors due to faulty assumptions concerning the geometric distribution of the reflected flux.

(5). Errors caused by the uncertainty in the reflectance of the specular reflectance standard.

(6). Other sources of error.

First, the errors associated with the flux interchange between the averaging sphere and the ellipsoidal mirror are analyzed, then the effect of the uncertainty in the reflectance of the specular reflectance standard and the effect of the uncertainty of reading the various fluxes are discussed. Next, the effect of variation in the reflectance of the ellipsoidal mirror are analyzed. The remaining errors are discussed in connection with the specific corrections for the hole loss, wire loss, mirror loss, and the sample shading effect. For the analysis of these corrections a set of assumptions is made concerning the distribution of the reflected flux in order to establish an over-all estimate of accuracy. Since the magnitudes and interdependance of the various fluxes used in equation 53 are unknown, standard error propagation formulas are not used in this error analysis. It is felt that continued usage of this instrument will provide the massive amount of data needed to justify a more accurate error analysis. Until that time, this section offers an estimated accuracy of data which is at least partially supported by the precision of measurement indicated in appendix H, Table XI.

Sphere-Ellipsoid Interchange

The error associated with the interchange of flux between the averaging sphere and the ellipsoidal mirror is caused by the assumption that (in derivation of equation 53, chapter VI)

$$\frac{\left[1 - \rho_{HS}\, \bar{\rho}^{\approx}_{\epsilon D}\, \eta'\, f_{(S-\epsilon)S}\right]}{\left[1 - \rho_{HM}\, \bar{\rho}^{\approx}_{\epsilon D}\, \eta'\, f_{(S-\epsilon)I}\right]} \equiv 1 \tag{73}$$

$$\frac{\left[1 - \rho_{HS}\, \bar{\rho}^{\approx}_{\epsilon D}\, \eta'\, f_{(S-\epsilon)S1}\right]}{\left[1 - \rho_{HM}\, \bar{\rho}^{\approx}_{\epsilon D}\, \eta'\, f_{(S-\epsilon)I}\right]} \equiv 1 \tag{74}$$

$$\frac{\left[1 - \rho_{HS}\, \bar{\rho}^{\approx}_{\epsilon D}\, \eta'\, f_{(S-\epsilon)D}\right]}{\left[1 - \rho_{HM}\, \bar{\rho}^{\approx}_{\epsilon D}\, \eta'\, f_{(S-\epsilon)I}\right]} \equiv 1 \tag{75}$$

and

$$\frac{\left[1 - \rho_{HS}\, \bar{\rho}^{\approx}_{\epsilon D}\, \eta' \left(\frac{F_{SD} - F_{S^{\approx}D}}{F_{S2D}}\right) f_{(S-\epsilon)S2}\right]}{\left[1 - \rho_{HM}\, \bar{\rho}^{\approx}_{\epsilon D}\, \eta' f_{(S-\epsilon)I}\right]} \equiv 1 \tag{76}$$

The error arises from the fact that $\rho_{HS} \neq \rho_{HM}$ and the various $f_{S-\epsilon}$ are not equal. However, in equations 73, 74 and 75 the differences among these three configuration factors are insignificant since the use of small shields in the first focal plane (17 in. from the sphere entrance port) does not appreciably change the flux reflected back to the ellipsoidal mirror by the averaging sphere. Further, the left hand side of equation 76 is a term that is only used to establish the mirror absorption F_{α}, therefore it is possible to simply factor out a single

term from the entire equation (53) and study the effect of setting this term equal to one. The resulting equation is

$$\rho_S = \frac{[1 - \rho_{HS}\, \bar{\rho}^{\circ}_{\epsilon D}\, \eta'\, f_{(S-\epsilon)}]}{[1 - \rho_{HM}\, \bar{\rho}^{\circ}_{\epsilon D}\, \eta'\, f_{S-\epsilon}]}\, \rho_S' \tag{77}$$

where ρ_S is the true reflectance and ρ_S' is the reflectance for the assumption that the multiplying term is one. Thus the error in ρ_S caused by the assumptions of equations 73, 74, 75, and 76 is

$$\frac{\rho_S - \rho_S'}{\rho_S} = \frac{[\rho_{HM} - \rho_{HS}]\, \bar{\rho}^{\circ}_{\epsilon D}\, \eta'\, f_{S-\epsilon}}{1 - \rho_{HS}\, \bar{\rho}^{\circ}_{\epsilon D}\, \eta'\, f_{S-\epsilon}} \tag{78}$$

Experimental measurements indicate that the term $\bar{\rho}^{\circ}_{\epsilon D}\, \eta'\, f_{S-\epsilon}$ has a maximum value of 0.04. These measurements were made with a specular mirror sample with and without a shield in the first focal plane that completely eliminated this interchange (see appendix H). Thus equation 78 becomes

$$\frac{\rho_S - \rho_S'}{\rho_S} = \frac{[\rho_{HM} - \rho_{HS}]\,(0.04)}{1 - \rho_{HS}(0.04)} \tag{79}$$

It remains then to establish the values for ρ_{HS} and ρ_{HM}. Jakob [50] indicates that for conductors $(1 - \rho_N)/(1 - \rho_H)$ lies between 1.00 and 1.33, while for insulators he indicates the limiting values to lie between approximately .935 and 1.05, where ρ_N is essentially the $\rho(7^{\circ},\theta)$ measured by the ellipsoidal mirror reflectometer. Thus, by letting $\rho_{HM} = \rho_M$ and $\rho_{HS} = \rho_S$, the error caused by this term can be graphed as a function of ρ_S with ρ_M as a parameter. Figure 45 illustrates such a graph and indicates that accurate reflectance measurements are possible either

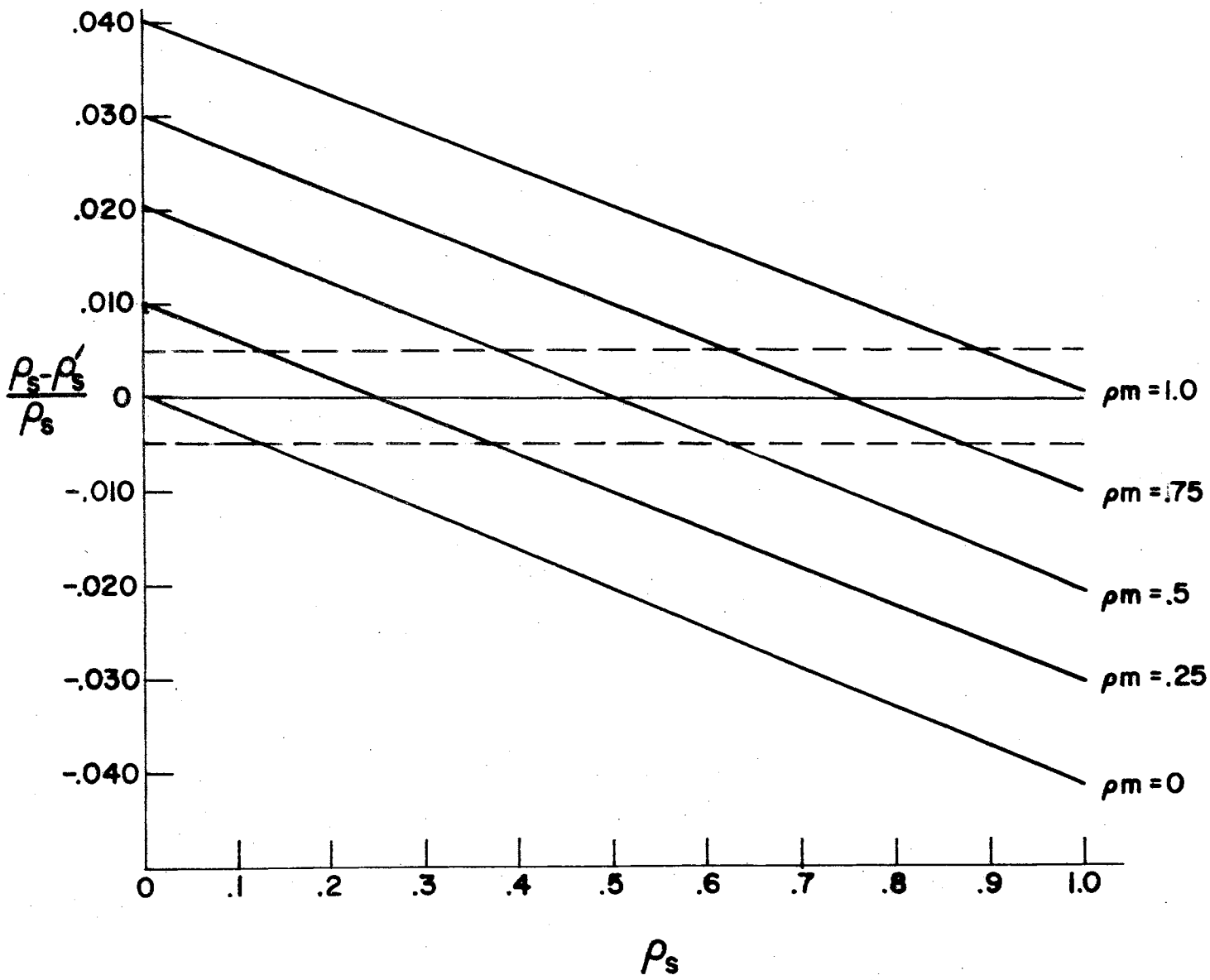

Figure 45. Error Caused by Sphere-Ellipsoid Interchange.

(1) when $\rho_{HM} \approx \rho_{HS}$ or (2) when the terms in equations 73 through 76 can be accurately evaluated and the appropriate corrections made to the terms in equation 48, chapter IV.

Reflectance Standard

The error caused by the uncertainty in the reflectance of the specular reflectance standard is (from appendix B) $\pm.0015/\rho_M$ which for the case of the aluminum and gold standards is (on the average) $\pm.0017$. Since ρ_M is multiplied by all the terms of equation 53, the uncertainty of ρ_M carries over directly as an uncertainty in ρ_S.

Flux Measurement

The effect on $\rho(7^\circ,\theta)$ of the uncertainty in the measurement of the various fluxes F_{SD}, F_{S1D}, F_{S2D}, F_{DD}, and F_{1D} is discussed in this section. Examination of equation 53 indicates that the flux ratios F_{SD}/F_{1D}, F_{DD}/F_{1D}, F_{S2D}/F_{1D} and F_{S1D}/F_{1D} are the only terms involving measured fluxes that could appreciably affect $\rho(7^\circ,\theta)$. Further, it is apparent that the measurement of each of these fluxes involves about the same uncertainties, so that in effect the uncertainty of measurement of the fluxes can be converted (as a first order approximation) to the uncertainty in F_R/F_I where

$$\rho_S = \frac{F_R}{F_I} \tag{80}$$

All other flux ratios in equation 53 are in secondary terms so that no significant error is caused by uncertainty in measurement of these ratios. The uncertainty of measurements in this case involves several variables, (1) the actual mechanics of reading signals from a 10 in. strip chart

recorder, (2) the lack of linearity of the detector-electronics system, (3) the instability of the entire system between measurements and (4) the effects of spatial sensitivity of the detector as present in chapter III. The strip chart recorder has an accuracy of ±0.2 percent of full scale deflection. The linearity of the system is accounted for in appendix H by an independent check on the linearity of the complete system. The effects noted in chapter III are minimized in the relative measurement by careful placement of all beams on the same part of the averaging sphere's wall. Thus the total uncertainty of careful measurements of fluxes is estimated to be less than ± 0.5 percent. This percision could be increased by the use of a mechanical digital voltmeter, which gives one additional significant figure, and by a statistical analysis of repeated readings of these fluxes.

Variation in Mirror's Reflectance

Appendix F indicated that the edges of the ellipsoidal mirror reflected about 1.5 percent more of the incident flux than the central portions of the mirror. In chapter IV a correction for the effect was established. In equation 53 of chapter IV, each term is multiplied by this correction and since the corrections to each term are very nearly equal, the total effect of the correction can be studied by assuming this term to factor out of equation 53 so that

$$\rho_S = \frac{1}{1 + \frac{F_{S2D}}{F_{SD}} (0.015)} \quad [F_{53}] \tag{81}$$

where F_{53} represents the remaining terms in equation 53. The factor (0.015) is the increased reflectance of the edges of the ellipsoidal

mirror and is estimated to have uncertainty of less than ±0.003. The effect of this uncertainty on ρ_S is

$$\frac{\rho_S - \rho_S'}{\rho_S} = 1 - \frac{1 + \frac{F_{S2D}}{F_{SD}}(0.015 \pm 0.003)}{1 + \frac{F_{S2D}}{F_{SD}}(0.015)} \qquad (82)$$

where $F_{S2D}/F_{SD} = 0.20$ for the case of the perfect diffuser. This yields an uncertainty in ρ_S of less than ±0.0009. From this it is also apparent that variation in F_{S2D}/F_{SD} will not affect this term; further, the value for F_{S2D}/F_{SD} will in general be less than 0.2, so that this uncertainty will generally be smaller than ±0.0009.

Flux and System Assumptions

In order to establish the effects of the remaining factors involved in an estimate of the uncertainty, the following assumptions are made about the geometric distribution of the flux.

(1) $\frac{F_{SD}}{F_{1D}} = 0.95\ \rho_S$

(2) $\frac{F_{S1D}}{F_{1D}} = 0.7\rho_S$

(3) $\frac{F_{S2D}}{F_{1D}} = 0.15\rho_S$

(4) $\frac{F_{DD}}{F_{1D}} = 0.90\ \rho_S$

(5) $\frac{F_{S2D}}{F_{SD}} = 0.16$

(6) $\frac{F_{S2D}}{F_{S1D}} = 0.21$

(7) $\frac{F_{S2D}}{F_{DD}} = 0.17$

The following values for system constants are approximately those used in this work.

(1) $\bar{\rho}_{\varepsilon} = 0.97$ (3) $\frac{A_H}{A_{SH} - A_H} = \frac{1}{3}$

(2) $\rho_M = 0.98$ (4) $\frac{A_{S1}}{A_{SH} - A_H} = \frac{1}{12}$

(5) $\frac{A_{\varepsilon}}{A_w} = 0.0021$

The above values for the flux ratios and the system parameters are used in the following analyses.

Hole Correction

From chapter IV the hole correction is given as

$$\frac{F_H}{F_R} = \frac{A_H}{A_{SH} - A_H} \left(\frac{\rho_M}{\rho_S F_{1D}}\right)\left(\frac{F_{SD}}{1 + \frac{F_{S2D}}{F_{SD}}(0.015)} - \frac{F_{S1D}}{1 + \frac{S2D}{F_{S1D}}(0.015)}\right) \qquad (86)$$

The value for F_H/F_R under the previous assumptions is 0.0816. There remain two sources of error in this correction which have not yet been discussed; these are the uncertainty in area ratios and in the average flux density assumption of chapter IV, equation 19. The area ratio was measured with an accuracy of ±0.01 sq in., which generates by calculation similar to equation 82 an uncertainty in equation 86 of ±0.0015.

In equation 19, chapter IV, it was assumed that $(F_S - F_{S1})/(A_{SH} - A_H)$ was the flux density on the area of the ellipsoidal mirror immediately surrounding the entrance hole in the mirror. The maximum error* for this correction could occur if instead of being distributed evenly about the shield A_{SH} the flux was distributed such that no flux left through the

---

* Again excluding the case of a diffraction grating.

entrance hole while 25 percent of the reflected flux was absorbed by the shield. In this case there would be no hole correction, but equation 19 would indicate that 8.33 percent of the flux was lost out the hole. This error is very large; no known engineering surface has a distribution of this nature; further, experimental techniques are available that will warn the investigator of this problem, such as tilting the sample with respect to the first focal plane and observing the variation in F_{S1D}. On the whole, an uncertainty of less than ±0.003 is expected from this correction. With the availability of more goniometric reflectance data in the next few years, this loss can be more accurately studied.

Wire Correction

From chapter IV the wire correction is given by

$$\frac{F_W}{F_R} = \frac{A_W}{A_\epsilon} \frac{\rho_M}{\rho_S F_{1D}} \left[\frac{F_{DD}}{1 + \frac{F_{S2D}}{F_{DD}} (0.015)} \right] \tag{87}$$

which under the previous assumptions is equal to 0.0018 . The uncertainty of the area ratio is ±0.005 when the uncertainty in A_W is ±0.005 and the uncertainty in A_ϵ is ±.05. This affects the value of ρ_S by less than ±0.0005.

The assumption that the flux density over A_W is the same as the flux density over A_ϵ is probably the most accurate assumption of all, for the case where the specular component is not incident on the wires; as such, no uncertainty is attributed to this assumption.

Sample Shading Correction

From chapter IV the two sample shading correction terms are

$$\frac{F_{SP}}{F_R} = \frac{\rho_M}{\rho_S F_{1D}} \left[\frac{F_{SD}}{1 + \frac{F_{S2D}}{F_{SD}}(0.015)} - \frac{F_{S1D}}{1 + \frac{F_{S2D}}{F_{S1D}}(0.015)} \right] \frac{A_S}{A_{SH} - A_H} \qquad (88)$$

and

$$\frac{F_{SR}}{F_R} = \frac{\rho_M}{\rho_S F_{1D}} \left[\frac{F_{SD}}{1 + \frac{F_{S2D}}{F_{SD}}(0.015)} - \frac{F_{S1D}}{1 + \frac{F_{S2D}}{F_{S1D}}(0.015)} \right] x$$

$$\left[\frac{A_{S1}}{A_{SH} - A_H} \right] \left[\frac{F_{DD}}{F_{SD}} \rho_S \bar{\rho}_e^2 \left(\frac{A_\epsilon - A_W}{A_\epsilon} \right) \frac{1}{1 - \rho_S \bar{\rho}_e \left(\frac{F_{SD} - F_{DD}}{F_{SD}} \right)} \right] \qquad (89)$$

First F_{SP} is analyzed for the remaining unaccounted for uncertainty due to the uncertainty in $A_S/(A_{SH}-A_H)$. The value of F_{SP}/F_R under the original assumptions is 0.020 and the uncertainty in $A_S/(A_{SH}-A_H)$ is $\pm.001$ which yields an uncertainty in F_{SP}/F_{1R} that is less than ± 0.0002.

In equation 89 the value of F_{SR}/F_R is 0.0008 (for $\rho_S = 1.0$) and the effect of the uncertainty in $A_{S1}/(A_{SH} - A_H)$ and $(A_\epsilon - A_W)/A_\epsilon$ is negligible, for even if these terms were 50 percent in error they would influence ρ_S by only $\pm.0003$, thus no uncertainty is attached to this term, in fact it will almost always be neglected; it is included in the analysis so that its magnitude can be checked for each sample and used whenever it is significant.

Edge Loss

If the sample is placed slightly below the first focal plane, the ellipsoidal mirror no longer collects flux over the entire hemisphere.

In the experimental measurements reported in appendix H, care was exercised to insure that the sample was at or above the first focal point. The effect of being below the first focal plane is easily studied for the case of the perfect diffuser. That is, the flux reflected by the perfect diffuser is

$$F_R = \pi I' \tag{90}$$

where I' is the outgoing intensity and is constant over the hemisphere. If the sample is slightly below the focal plane then the flux reflected by the ellipsoid is

$$F_E = I' \int_0^{2\pi} \int_0^{\varphi'} \cos \varphi' \sin \varphi' \, d\varphi' d\theta' \tag{91}$$

The fraction of the total reflected flux lost is

$$\frac{F_R - F_E}{F_R} = 1 - \frac{2\pi \left[1 - \cos^2 \varphi'\right]}{(2)\pi} = \cos^2 \varphi' \tag{92}$$

where the $\cos \varphi'$ is (as function of the distance (h) below the first focal plane and radius (r_e) of the opening of the ellipsoidal mirror).

$$\cos \varphi = \sqrt{\frac{h^2}{h^2 + r_e^2}} \tag{93}$$

or

$$\frac{F_R - F_E}{F_R} = \frac{h^2}{h^2 + r_e^2} \tag{94}$$

The quantity expressed in equation 94 is graphically illustrated in figure 46. Further, if the instrument were deliberately operated with the sample a fixed distance below the first focal plane, the S2 shield could be used to establish the average flux density on the edges of the mirror, then a correction, similar to the entrance hole correction, could be used.

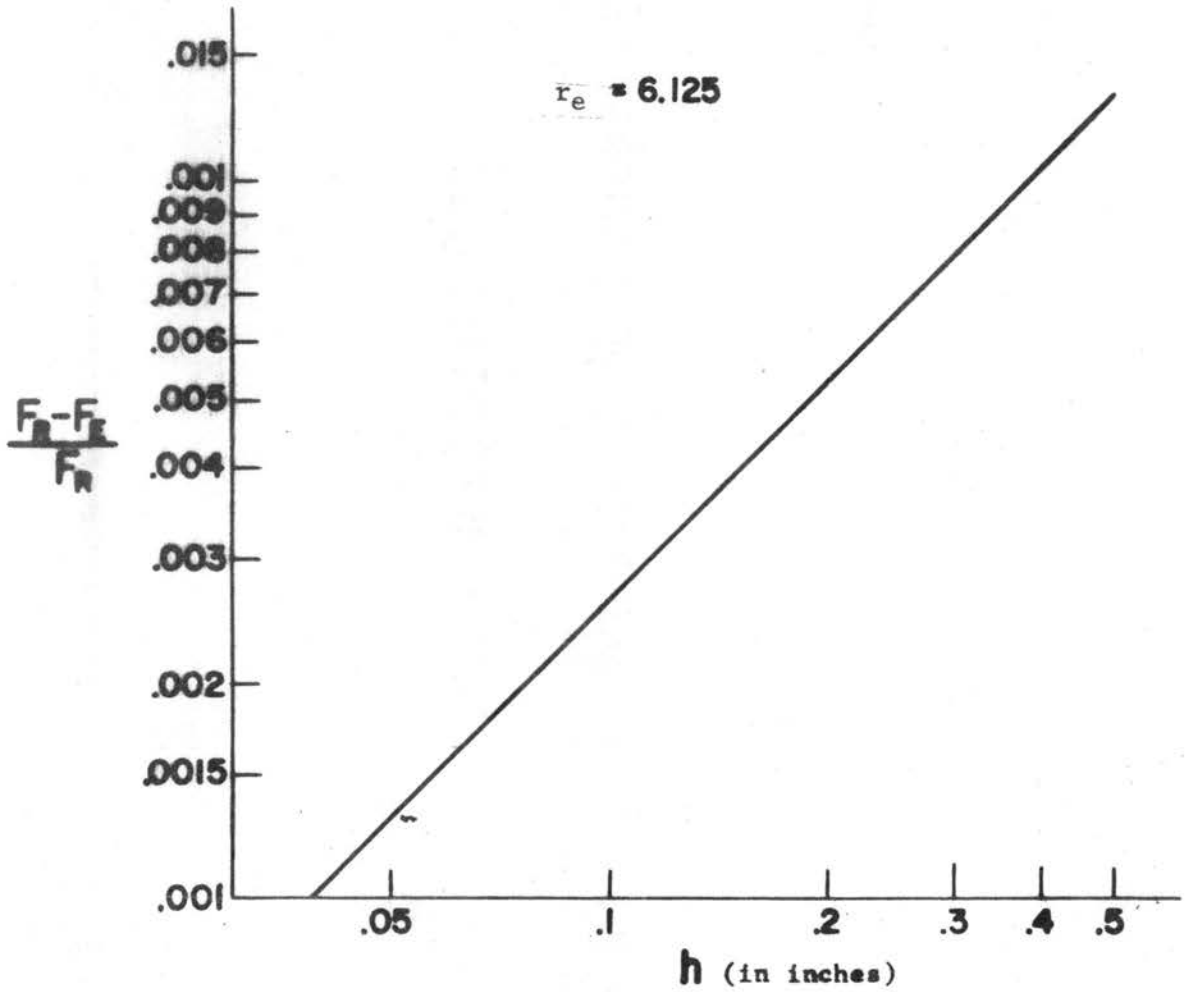

Figure 46. Edge Loss for Perfect Diffuser

Absolute Measurement

The major additional uncertainty arises from the fact that the sphere-ellipsoid interchange is present only in the reflected flux measurement, thus the error caused by this interchange is essentially shown by the $\rho_M = 0$ curve in figure 45. That means that a good knowledge of this interchange is needed to provide accurate data with the absolute measurement technique.

In addition, a better knowledge of the ellipsoidal mirror's reflectance is needed, since for the absolute measurement the reflectance $\bar{\rho}_e$ doesn't cancel out as in the relative measurement.

Summary

Since only fragmentary data are presently available for use in an error analysis, no effort was made to establish accurately the relation between the various uncertainties calculated in this section. Table VIII lists the percentage uncertainties. It should be noted that most of the uncertainties will also depend on the difference between the reflectances of the standard and the sample.

From table VIII it appears that the ellipsoidal mirror reflectometer is capable of accuracies of better than two percent. However, only continued reevaluation can establish unequivocally the overall accuracy of this instrument. Further, figures 45 and 46 indicate specific nonrandom errors which must be corrected for or eliminated if highly accurate measurements of reflectance are desired.

TABLE VIII

EXPECTED UNCERTAINTIES

Uncertainty Due To	Term Involved	Expected Uncertainty in ρ_S^*
Reflectance Standard	ρ_S^*	±.17%
Flux Measurement	ρ_S	±.50%
Variation in Mirror Reflectance	ρ_S	±.09%
Area Ratio	F_H/F_R	±.15%
Average Flux Density	F_H/F_R	±.30%
Area Ratio	F_W/F_R	±.05%
Area Ratio	F_{SP}/F_R	±.02%
Area Ratio	F_{SR}/F_R	±.01%

* $\rho_S = \rho(7^\circ, \theta)$

APPENDIX H

EXPERIMENTAL DATA

This section presents experimental data taken with an ellipsoidal mirror reflectometer. There are four main parts to this appendix: (1) System parameter and alignment, (2) directional hemispherical reflectance, (3) specular component of reflectance, and (4) directional annular cone reflectance.

System Parameters and Alignment

Alignment: Optical alignment of the ellipsoidal mirror reflectometer was accomplished by setting the monochromator so that the visible part of the spectrum was focused on the exit slits. The image of the exit slits* was visually focused (by the 49-in. radius of curvature spherical mirror through the entrance hole in the ellipsoidal mirror) onto the center of a diffuse sample. The sample holder and mirror holder were adjusted to give an image of minimum size and maximum sharpness at the second focal point. To ascertain that all of the beam of reflected flux was passing through the entrance port of the averaging spere at the second focal point, a Polaroid Land camera back was placed at the second focal point so that the plane of the film was at the position where the sphere entrance port would be placed.** Two different samples were used

---

* The exit slits were masked to a height of 2 mm.
** The film was Polaroid type 47 - a 3000 speed film.

at the first focal point, (1) an aluminum mirror and (2) a diffuse porcelain enamel reflectance standard. Figure 47 displays the images formed at the second focal point for the two different samples and for different exposure times. The black area around each image is the approximate size and shape of the entrance port of the averaging sphere.

The image formed when the aluminum mirror was used in the first focal plane is quite clear and well defined. The image formed when the mirror was inclined 25° with respect to the first focal plane shows light gray areas surrounding the white image, which indicate that the scatter and aberration of the ellipsoidal mirror increase with distance from the apex. The image formed at the second focal point when the porcelain enamel (a fairly good diffuser) was placed at the first focal point is enlarged and indicated that careful position of the image on the sphere entrance port is required if one expects to collect all of the flux represented by these images. The increased image size for the diffuser is indicative of the total scatter and aberrations for this particular ellipsoidal mirror. In all cases, increased time of exposure yielded slightly enlarged images, indicating that a small amount of flux surrounds the visual image. This poor image definition is due to aberrations and scatter caused by the ellipsoidal mirror. The conclusion drawn from the results displayed in figure 47 is that flux at the second focal point does pass through the sphere entrance when care is taken to center the visual image on the entrance to the sphere.

Linearity: A set of five sector discs was constructed to provide an independent check of the linearity of the entire detector-electronics system. These discs were made by machining out equally spaced radial

Aluminum Mirror
0° Sample Holder
2-Second Exposure

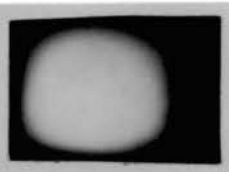

Enamel
0° Sample Holder
2-Second Exposure

Aluminum Mirror
0° Sample Holder
1-Minute Exposure

Enamel
0° Sample Holder
15-Second Exposure

Aluminum Mirror
25° Sample Holder
5-Second Exposure

Enamel
0° Sample Holder
45-Second Exposure

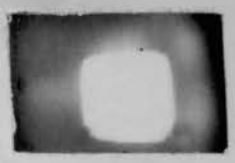

Aluminum Mirror
25° Sample Holder
1.5-Minute Exposure

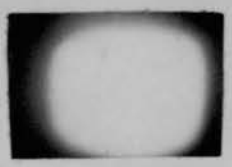

Enamel
0° Sample Holder
2-Minute Exposure

Figure 47. Image configurations at the second focal plane. The black area surrounding each image is approximately the area of the sphere entrance port.

sections of an aluminum disc, leaving a multiple bladed disc. The transmittance of these rotating discs is equal to the ratio of the open area on the disc to the total area of the disc. These areas were very accurately measured by the Engineering Metrology Section of the National Bureau of Standards.

Reference 51 contains a more complete description of these sector discs. The discs (rotating at about 1300 rpm) were used to attenuate the incident flux when an aluminum mirror was at the first focal point and the averaging sphere-detector at the second focal point. The output of the amplifier was read on a 10 in. strip chart recorder. The unattenuated signal was then divided into the five attenuated signals to give the ratios that the system yields for the five separate known transmittances. These results, along with the measured area ratios for each disc, are presented in table IX. The values are reported for each of the wavelengths used in this work.

TABLE IX

LINEARITY CHECK

Disc	Calculated Transmission	Standard Deviation of Calculated Transmission	Signal Attenuation (average of 4 tests) 1.5μ	2.0μ	2.5μ	3.5μ	4.5μ	5.5μ	6.5μ	7.5μ
A	.7510	±.002	.748	.749	.749	.748	.751	.752	.751	.746
B	.5000	±.0002	.498	.497	.499	.500	.503	.500	.502	.496
C	.2528	±.0014	.252	.250	.254	.253	.250	.254	.251	.251
D	.1273	±.001	.126	.126	.127	.127	.130	.126	.125	.124
E	.0507	±.0003	.050	.049	.046	.049	.049	.047	.050	.046

From table IX it is apparent that, within the precision of reading a 10 in. strip chart recorder, no corrections for linearity are necessary.

Sphere-Ellipsoidal Interchange: The interchange of flux between the averaging sphere and the ellipsoidal mirror was measured by using the aluminum mirror and a shield just below the first focal plane that only passed the specularly reflected beam from the mirror. By comparing the detector signal when the shield was in the system and when it was not in the system it was possible to calculate $\bar{\rho}_{\epsilon D}{}^{2}\eta' f_{S-\epsilon}$ from equations in chapter IV and appendix B. The values for this term are given in table X.

TABLE X

MEASURED VALUES OF $\bar{\rho}^{2}_{\epsilon D}\ \eta' f_{S-\epsilon}$

λ	$\bar{\rho}^{2}_{\epsilon D}\ \eta' f_{S-\epsilon}$
1.5	0.039
2.0	.039
2.5	.040
3.5	.036
4.5	.031
5.5	.026
6.5	.018
7.0	.013

Shields: To enable measurement of F_{S1D}, F_{DD}, and F_{S2D} two shields were constructed. (1) A small shield shaped as depicted in figure 26, chapter IV, and (2) a circular disc which only allows flux from the central part of the ellipsoidal mirror to reach the second focal point.

The same small shield was used for both the F_{S1D} and F_{DD} measurements. The shield was placed on opposite sides of the sample for the two measurements. No effort was made to design a specific shield to block out only the specular component, since this is a study in itself. The area of this shield projected onto the ellipsoidal mirror is 1.905 sq. in. The other shield (for F_{S2D}) was constructed so that it blocked the

flux from the outer 2 in. of the mirror. Then to get the flux on this area of the mirror the signal read with the shield in the system is subtracted from the signal for the system with no shield (F_{SD}).

The area of the entrance hole was measured to be 0.339 sq. in. and the projected area of the sample is 0.146 sq. in. Thus

$$\frac{A_S + A_H}{A_{SH} - A_H} = 0.310 \tag{95}$$

Area A_{S1} is 0.05 ±0.01 so that

$$\frac{A_{S1}}{A_{SH} - A_H} = 0.032 \tag{96}$$

The Platinum-13% Rhodium sample was a ½-in. diameter disc which yields (after correcting for the overlap of the image of the hole and the sample)

$$\frac{A_S + A_H}{A_{SH} - A_H} = 0.331 \tag{97}$$

The value of the left hand side of equation (96) is unaffected in either case.

Directional Hemispherical Reflectance

Several samples were chosen for reflectance measurement with the ellipsoidal mirror reflectometer (1) Platinum-13% Rhodium, (2) Gold Mesh, (3) a porcelain enamel, (4) oxidized Kanthal, and (5) Crystex brand sulfur. Samples (1) and (4) are high temperature emittance standards provided by the National Bureau of Standards and described by Richmond, et. al. [51]. Sample (2) was provided by Bernd Linder of the Missile and Space Division, General Electric Co., Philadelphia, Pa., and is 2 mil. stainless steel wire

screen (135 mesh) backed by .015 mil mylar with vapor deposited gold coating. Sample (3) is one of the standards of luminous daylight reflectance provided by the National Bureau of Standards. Sample (4) is the same sulfur that has been used throughout this work.

Platinum-13% Rhodium: The average value of six determinations of the reflectance of two samples is shown in figure 48. Table XI gives the individual reflectances and the standard deviation of their average. The six reflectances reported in table XI were measured by two different operators over a period of one week. Further, determinations 1a and 2a were made on samples tilted 10° to the first focal plane to eliminate the hole and sample corrections. This is possible because, as the specular component in table XI indicates, the reflected flux is concentrated around the specular peak and tilting the sample does not result in an edge loss. The data for the case where the samples were tilted shows no significant difference from the data for the samples in the first focal plane, thus the hole and sample corrections apparently were correct. Further examination of the values given in table XI indicates that there may be a slight difference in reflectance between the two samples. The specular component presented in table XI will be discussed later in this section.

Gold Mesh: The data for the Gold Mesh are presented in figure 49 where each data point is the average of three determinations. The data are self-explanatory.

Enamel: The data for the porcelain enamel reflectance standard are presented in figure 50. No effort was made to correct the low reflectances for the sphere ellipsoidal mirror interchange (see appendix G).

Oxidized Kanthal: The data for the oxidized Kanthal are graphed in figure 51. These data were taken by attenuating the flux for the reference

TABLE XI

REFLECTANCE OF PLATINUM - 13% RHODIUM **

Wave length	# 1a	# 1b	# 1c	# 2a	# 2b	# 2c	Average	Standard Deviation	Specular Component*
1.5	0.610	0.597	0.591	0.566	0.574	0.603	0.596	±0.005	69%
2.0	.701	.691	.692	.694	.686	.696	.693	.002	82%
2.5	.823	.813	.821	.826	.827	.820	.822	.002	83%
3.5	.919	.905	.921	.924	.930	.913	.919	.005	86%
4.5	.933	.926	.937	.935	.940	.929	.933	.004	87%
5.5	.942	.936	.940	.946	.947	.932	.941	.005	88%
6.5	.945	.938	.940	.947	.949	.942	.944	.005	90%
7.0	.947	.940	.942	.946	.953	.943	.945	.005	92%

*This is an approximation of the specular component by using $[(F_{SD} - F_{DD}) / F_{SD}] \times 100\%$, and includes the diffuse component of flux in the solid angle about the specular direction.

** Two samples are represented in this table, sample 1 and sample 2. 1a and 2a were made with the sample tilted 10° to the first focal plane.

NBS Reflectance for Pt. 13% Rh. reference 37.
(various sample temperatures)

λ	800°K	1100°K	1300°K
1.5μ	74.8%	78.7%	77.4%
2.0	80.8	81.5	80.3
2.5	83.5	83.2	82.0
3.5	87.4	85.7	84.5
4.5	89.1	87.4	86.5
5.5	90.4	88.9	87.3
6.5	91.4	89.9	88.7
7.0	91.6	90.4	89.2

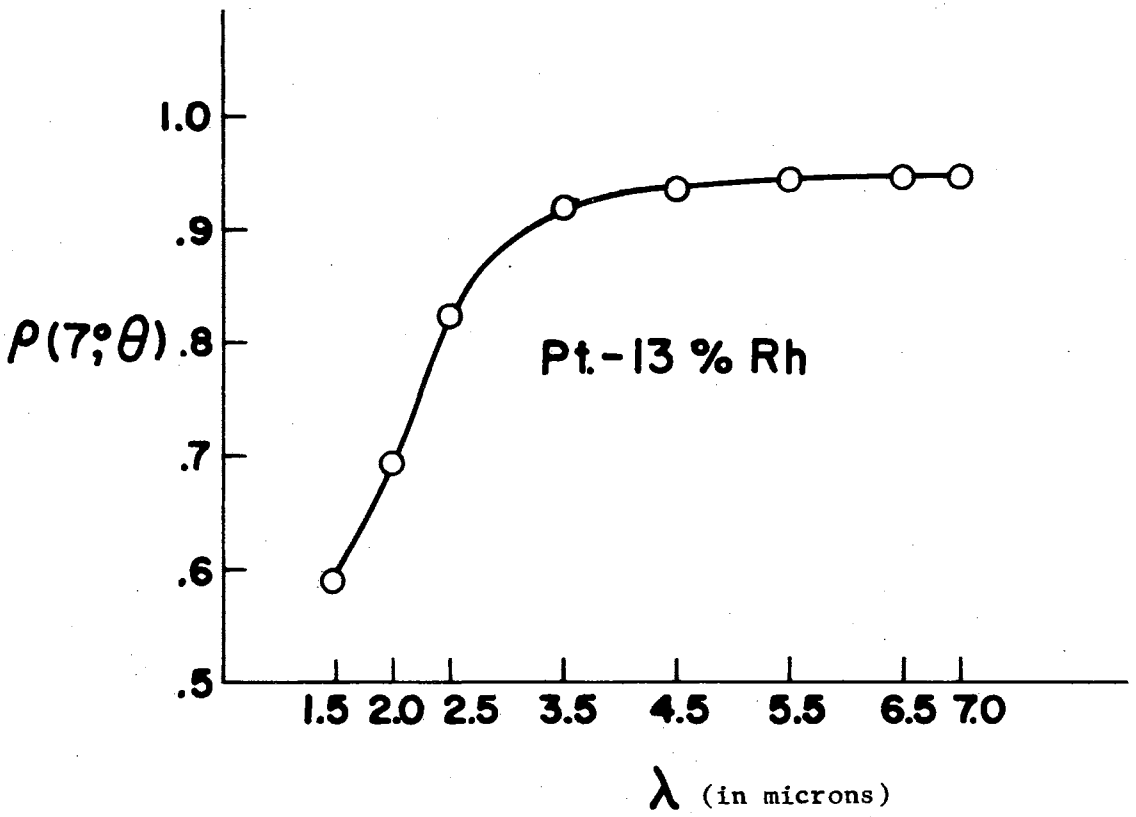

Figure 48. Reflectance of Platinum-13% Rhodium.

λ	Specular Component
1.5μ	13%
2.0	13%
2.5	13%
3.5	13%
4.5	13%
5.5	13%
6.5	13%
7.0	13%

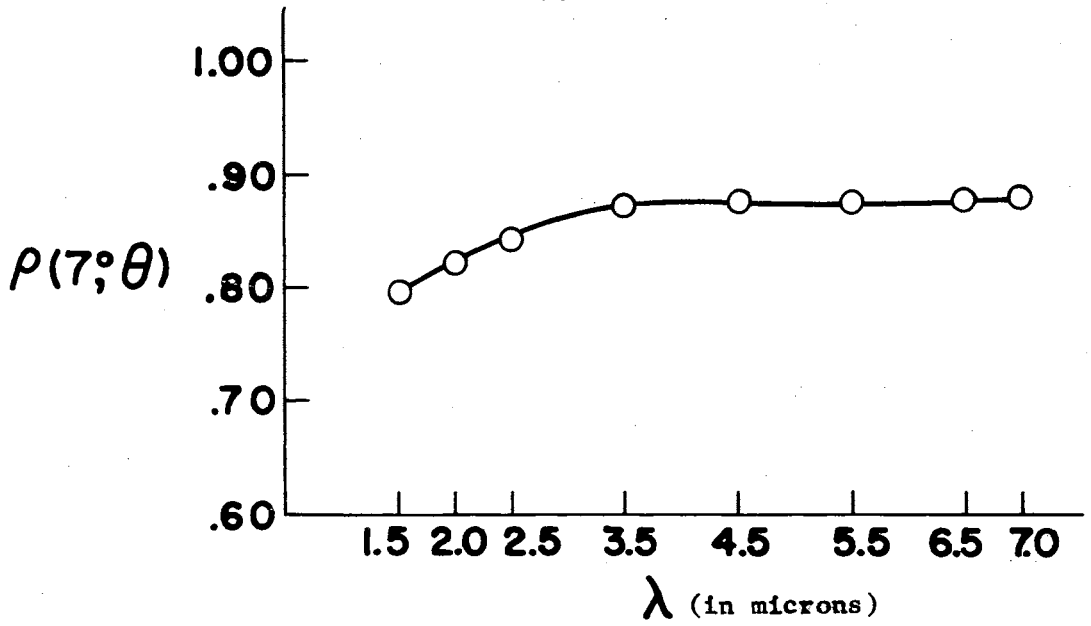

Figure 49. Reflectance of Gold Mesh.

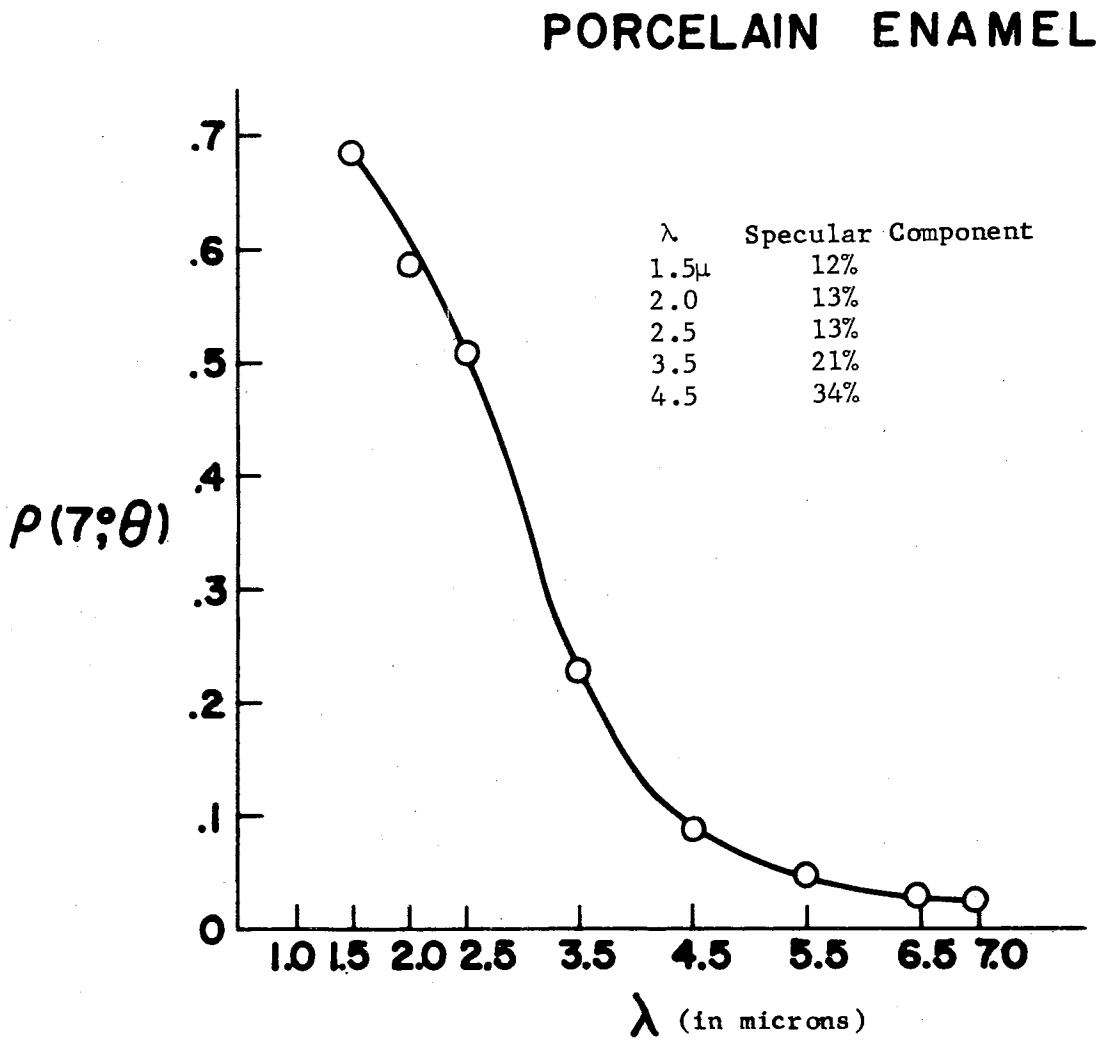

Figure 50. Reflectance of Porcelain Enamel.

λ	Specular Component
1.5μ	6%
2.0	7%
2.5	8%
3.5	8%
4.5	8%
5.5	8%
6.5	8%
7.0	8%

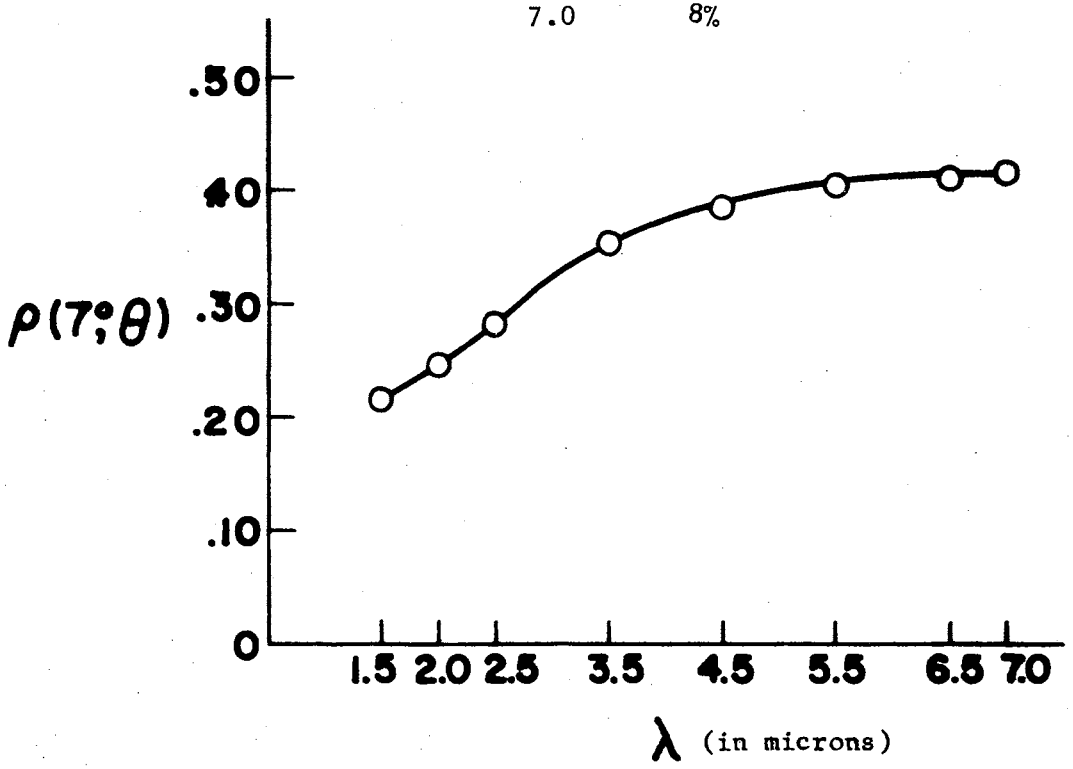

Figure 51. Reflectance of Oxidzed Kanthal

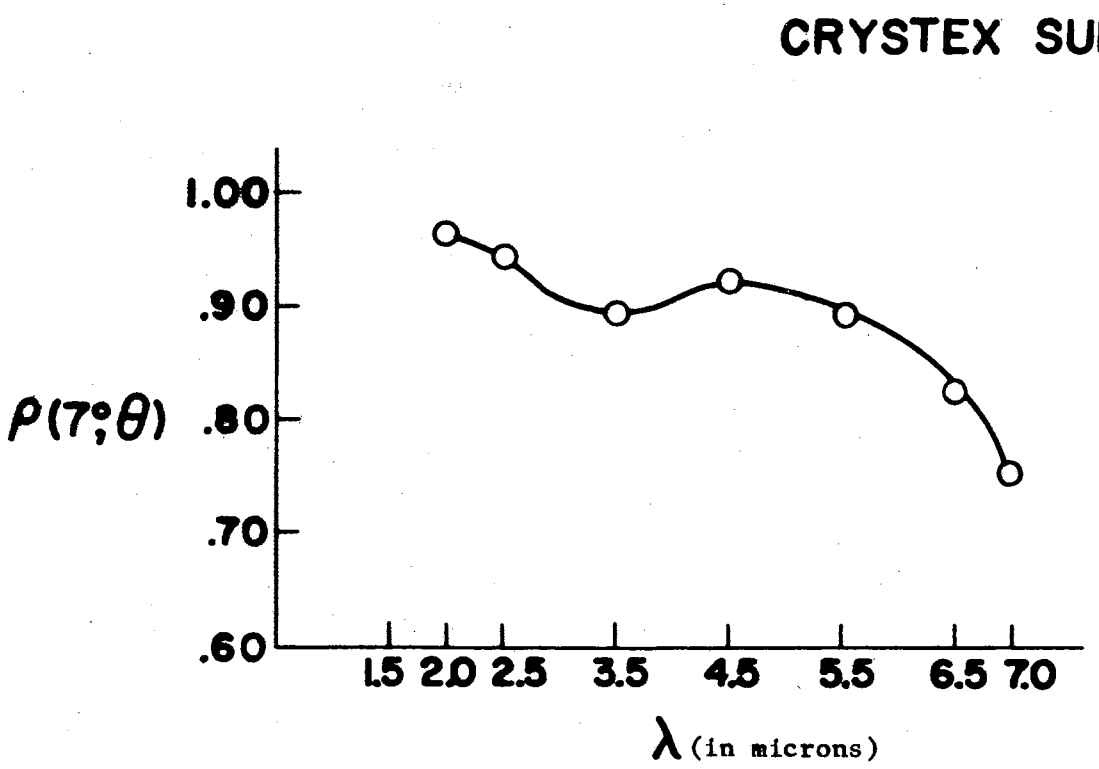

λ	Specular Component
1.5μ	9%
2.0	9%
2.5	9%
3.5	9%
4.5	9%
5.5	9%
6.5	9%
7.0	9%

Figure 52. Reflectance of Crystex Sulfur

measurement by 50 percent, by use of one of the previously described sector discs. No attenuation was used for the sample measurement. In addition, the data were corrected for the sphere-ellipsoid interchange through use of table X in this appendix and equation 78 of appendix G.

Sulfur: The directional hemispherical reflectance for "Crystex" brand sulfur is presented in figure 52. The dip in reflectance at about 3.5μ indicates an absorption band that could be caused by an organic contaminate in the sulfur. It is not known whether this absorption occurs in the sulfur coated averaging sphere.

Specular Component of Reflectance

The data in table XI, and figures 49, 50, 51 and 52 include the specular component of the reflected flux. No effort was made to study the size of shield that would yield the most useful conponent; instead a convenient shield (the A_{SH} shield) was used. The specular components reported were calculated as follows:

$$\% \text{ specular component} = \frac{F_{SD} - F_{DD}}{F_{SD}} (100) \qquad (97)$$

Thus the experimental specular component for the diffuser (assuming sulfur to be a near perfect diffuser) is 9 percent. The specular component defined by equation 97 minus the specular component for sulfur is the "true" specular component and is shown in table XII for the samples reported in this work.

TABLE XII

"TRUE" SPECULAR COMPONENT

λ	Sample	Pt-13% Rh	Gold Mesh	Porcelain Enamel	Oxidized Kanthal	Sulfur
1.5		60.%	4.%	3 %	- 3. %	0.0 %
2.0		73.%	4.%	4 %	- 2. %	0.0
2.5		74.%	4.%	4 %	- 1. %	0.0
3.5		77.%	4.%	12 %	- 1. %	0.0
4.5		78.%	4.%	25 %	- 1. %	0.0
5.5		79.%	4.%	--	- 1. %	0.0
6.5		81.%	4.%	--	- 1. %	0.0

Directional - Annular Cone Reflectance

Various directional annular cone reflectances of three samples were measured and compared to the values expected for the "perfect" diffuser. The reflectance measured for this section was

$$\rho(\text{directional annular cone}) = \frac{\int_0^{2\pi} \int_{\varphi'}^{\pi/2} I'(\varphi',\theta') \cos\varphi' \sin\varphi' d\varphi' d\theta'}{I\,(7^\circ,\theta)\cos 7^\circ\,(\Delta\omega)} \qquad (98)$$

where the flux reaching the detector was restricted to the annular solid angle between φ' and $\pi/2$ by use of a circular disc centered on the sample and placed just below the first focal plane. Five shields providing different φ's were used. Then the detector signals for each of the five shields were divided by F_R and compared to resulting values calculated for the perfect diffuser, which is

$$\frac{\rho(\text{directional annular cone})}{\rho(\text{directional hemispherical})} = \cos^2\varphi' \qquad (99)$$

The angle φ' was measured for each of the shields and table XIII illustrates the data for three samples at 2.5μ. They are sulfur, $BaSO_4$, and the gold mesh.

TABLE XIII

RATIO OF DIRECTIONAL ANNULAR CONE REFLECTANCE TO THE DIRECTIONAL HEMISPHERICAL REFLECTANCE FOR SUSPECTED DIFFUSERS.*

φ'	Perfect Diffuser	Crystex Sulfur	$BaSO_4$	Gold Mesh
79.5°	0.033	0.035	0.035	0.033
62.8°	.210	.207	.207	.194
43.7°	.522	.523	.520	.480
34.3°	.683	.692	.680	.641
14.5°	.936	.935	.934	.917

*Data taken at 2.5μ

VITA

Stuart Thomas Dunn

Candidate for the Degree of

Doctor of Philosophy

Thesis: DESIGN AND ANALYSIS OF AN ELLIPSOIDAL MIRROR REFLECTOMETER

Major Field: Mechanical Engineering

Biographical:

Personal Data: Born in Rock Island, Illinois, August 27, 1940, the son of Paul T. and Margaret Dunn.

Education: Attended grade school in St. Louis and Florissant, Missouri; graduated from Ferguson-Florissant High School in 1958; received the Bachelor of Science degree from the University of Missouri at Rolla, Missouri, with major in Mechanical Engineering, in May 1962; received the Master of Science degree from Oklahoma State University, with a major in Mechanical Engineering, in May 1963; completed requirements for Doctor of Philosophy degree in May 1965.

Professional Experience: Have been employed at the National Bureau of Standards since May 1964. Presently working in the area of thermal radiation properties. Honor Societies: Tau Beta Pi, Phi Kappa Phi, Pi Tau Sigma, and Kappa Mu Epsilon.